UNIVERSITY OF
KWAZULU-NATAL

INYUVESI
YAKWAZULU-NATALI

Development of a Design Methodology of a Composite Monocoque Chassis

Jason Denny

Submitted in fulfilment of the academic requirements for the degree of Master of Science in Mechanical Engineering, College of Agriculture, Engineering and Science, University of KwaZulu-Natal.

Supervisor: Ms. Kirsty Veale

Co-Supervisor: Ms. Fiona Leverone

Co-Supervisor: Prof. Sarp Adali

August 2018

DECLARATION 1 - PLAGIARISM

I, Jason Denny, declare that

1. The research reported in this thesis, except where otherwise indicated, is my original research.
2. This thesis has not been submitted for any degree or examination at any other university.
3. This thesis does not contain other persons' data, pictures, graphs or other information, unless specifically acknowledged as being sourced from other persons.
4. This thesis does not contain other persons' writing, unless specifically acknowledged as being sourced from other researchers. Where other written sources have been quoted, then:

a. Their words have been re-written but the general information attributed to them has been referenced

b. Where their exact words have been used, then their writing has been placed in italics and inside quotation marks, and referenced.

5. This thesis does not contain text, graphics or tables copied and pasted from the Internet, unless specifically acknowledged, and the source being detailed in the thesis and in the References sections.

Signed _____ Date _____

Mr. Jason Denny

As the candidate's supervisor I have approved this dissertation for submission.

Signed _____ Date _____

Ms KirstyVeale

As the candidates co-supervisor I have approved this dissertation for submission.

Signed _____ Date _____

Ms Fiona Leverone

As the candidates co-supervisor I have approved this dissertation for submission.

Signed _____ Date _____

Prof. Sarp Adali

DECLARATION 2 - PUBLICATIONS

Denny, J.A.; Veale, K. L.; Adali, S. and Leverone, F. K., 2018. Conceptual Design and Numerical Validation of a Composite Monocoque Solar Passenger Vehicle Chassis. *Engineering Science and Technology, an International Journal.* Accepted. Article in press.

Denny, J.A.; Veale, K. L.; Leverone, F. K. and Adali, S., 2017. Development of a Composite Monocoque Solar Passenger Vehicle Chassis. To be presented at *20th International Conference on Composite Structures (ICCS20)*, Paris, France, 4-7 September.

Signed _____ Date _____

Jason Denny

Acknowledgements

I would like to thank my primary supervisor, Ms. Kirsty Veale for her extraordinary effort in co-ordinating and supporting this project; and who together with Ms. Fiona Leverone and Prof. Sarp Adali, provided invaluable technical guidance.

A special thanks to David Woods at *Stealth* for his assistance and expertise in manufacturing and preparing test specimens.

This Research was funded by *Armscor*.

I would also like to thank my parents for their love, support and sacrifices made that enabled me to attend University.

Abstract

The concept of the composite monocoque chassis has been implemented in many vehicle designs; however, there is little open-access literature defining the primary considerations when simulating one. The purpose of this research is to develop a methodology for determining the structural integrity of a composite monocoque chassis, through finite element analysis, with the intention of developing a lightweight solar powered vehicle. Factors that influence this methodology include; the definition of the vehicle loading conditions, failure criteria, and important design parameters, chief among which is the torsional stiffness. Chassis design specifications were developed from the *2017 Bridgestone World Solar Challenge* rules and regulations as these are the most common and complete specifications for this particular type of vehicle.

The primary design criteria considered is the torsional stiffness, which was determined from the application requirements and literature, and resulted in a suitable value of 4000 Nm/deg. *Siemens NX Nastran* was used to develop a torsional stiffness model, which uses the torsional loading condition, to determine the torsional stiffness value. The design methodology then follows an iterative process where various geometry and layup modifications were considered, under the same loading conditions, with the aim of increasing the torsional stiffness to achieve the required value. Aerodynamic properties were adapted from existing UKZN solar vehicle knowledge; however, this research does not consider the optimisation of the aerodynamic properties of a monocoque chassis. Only a structural simulation was conducted. The ultimate strength of the material was also considered throughout the simulation process, however in all cases the model failed to meet the required torsional stiffness parameter before material failure modes. The door recesses had the most significant effect on the torsional stiffness. By compacting the door recesses the torsional stiffness was increased by 29.04 %. A final torsional stiffness was of 4097 Nm/deg was attained with the implementation of an aluminium honeycomb core.

Additionally; an analysis of the mounting points was conducted to ensure that the layup can withstand the concentrated loads at the suspension mounts. This analysis is concerned with the principal stresses, where the principal stresses give insight into the most suitable orientation of the layup. The torsional stiffness model resulted in a maximum principal stress of 81.68 MPa, below the 464.4 MPa tensile strength of the reinforcement material orientated in the direction of the fibres.

To verify the significance of the torsional stiffness failure criterion, vertical and lateral bending analyses were conducted. A vertical bending model was developed where the chassis is modelled as a simply supported beam, simulating the squatting and diving of a chassis under acceleration and deceleration respectively. The maximum deflection was 5.28 mm, which is below the

maximum allowable deflection of 12.29 mm, determined from a maximum deflection ratio of $1/360^{th}$ of chassis length. A lateral bending model modelled the chassis as a simply supported beam with the maximum stress being analysed. The maximum stress experienced by the chassis under this loading condition was 18.73 MPa, which was 75.8 % less when compared to the maximum stress exhibited by the chassis under the torsional loading condition.

Flexural bending tests were conducted on various laminate sandwich structures used in the finite element analysis to validate the simulation material properties. The peak load and mid-span deflection of each specimen was recorded to determine the maximum flexural stress and flexural modulus of elasticity. The flexural stress at specific midspan deflections was compared, under the same loading conditions, to that of the bending stress exhibited by a flexural bend test model finite element analysis conducted in *Siemen's NX Nastran*. Graphs of the stress versus midspan deflection were plotted for each specimen layup type and the curves of the simulated and experimental results were compared. In each laminate sandwich structure case, the simulation curve exhibited a linear relationship between the midspan deflection and flexural bend stress and the experimental curve exhibited a linear relationship until the elastic limit of the specimens was reached. Thereafter the curve exhibited an exponential relationship as plastic deformation occurs until the specimen failure.

An iterative finite element analysis design methodology was used to develop a composite monocoque chassis. The design process of a composite monocoque chassis is simplified by using finite element analysis to iterate through many different configurations, such as core thicknesses, layup orientations, and geometry features, to customise the properties of the structure. With these properties, it is possible to determine chassis performance. The finite element analysis results illustrated that geometry modifications, such as compacting door recesses, and applying strategic layup orientations, such as implementing a honeycomb core, significantly affected the torsional stiffness of a chassis. In addition, a chassis with sufficient torsional stiffness exhibits sufficient bending stiffness. The methodology presented in this research stands to be supportive in designing a fully composite monocoque chassis for lightweight race vehicle applications.

Table of Contents

List of Figures

List of Tables

Nomenclature

φ	Angular Deflection
F	Applied Force
P	Applied Specimen Load
T	Applied Torque
L	Characteristic Length of Cross Section
ρ	Density
E_f^{secant}	Flexural Secant Modulus of Elasticity
G	Material Shear Modulus of Elasticity
σ_f	Material Strength
δ	Mid-span Deflection
NU	Poisson's Ratio
J	Polar Moment of Inertia
L	Specimen Span
h	Specimen Thickness
b	Specimen Width
ϵ	Strain
σ	Stress on Specimen Outer Surface
K_T	Torsional Stiffness
v	Vertical Deflection
E	Young's Modulus

Abbreviations

1-D	One Dimensional
2-D	Two Dimensional
CAD	Computer Aided Design
CFRP	Carbon Fibre Reinforced Polymer
deg	Degree
FEA	Finite Element Analysis
FEM	Finite Element Modelling
GPa	Gigapascal
kg	Kilogram
KPI	Key Performance Indicator
m	Meter
mm	Millimetre
MPa	Megapascal
N	Newton
PEI	Polyethermide
PS	Polystyrene
PU	Polyurethane
PVC	Polyvinyl Chloride
SAN	Styreneacrylonitrile
UKZN	University of Kwa-Zulu Natal
UNSW	University of New South Wales
UV	Ultraviolet
WSC	World Solar Challenge

Chapter 1. Introduction

The chassis is the supporting frame or structure of a vehicle. It is the structure that supports the suspension system, steering system, the motor, and other components. Maintaining rigidity in bending and torsion, providing efficient load absorption and reducing the overall weight of the chassis are key to ensuring satisfactory chassis performance. There exists little open-access literature defining the primary considerations when simulating a composite monocoque chassis. This research aims to design a composite monocoque chassis for solar powered applications and, in doing so, develop a procedure for future chassis designs. It must be noted that the purpose of this research is to develop a methodology for analysing a chassis under operating conditions and to determine a structurally sound chassis, through finite element analysis. All functional and aerodynamic considerations will be assessed where possible; however, they are not the objectives of this research and therefore no additional computational analyses were conducted. Complexities involved in this specific type of analysis include composite layup orientation, determining smart geometries for structural enhancement, and general motor vehicle safety requirements. Traditionally, due to their monocoque chassis design and low weight requirements, composite materials are the materials of choice for the manufacture of solar vehicles. In addition to maintaining rigidity in torsion and bending, a solar vehicle chassis must be able to accommodate an appropriate solar array.

The objectives of the research are as follows:

- To develop a procedure for modelling a composite monocoque chassis for future solar vehicle development.
- To design a composite solar vehicle chassis that will serve as an alternative environmental friendly means of transport for public use.
- To minimise the mass of the design to reduce the effects of rolling resistance.
- To investigate various composite materials suitable for the manufacture of the vehicle chassis.
- To experimentally determine the flexural properties of various composite sandwich structures to validate simulation material properties.

1.1 Methodical Approach

A methodical approach is the application of a project management arrangement to an engineering design project. With complex multidisciplinary projects, like a solar vehicle, the design procedure must be divided into sub-categories, whereby the workload is split amongst the design team. The team must work together to ensure that their resulting designs are compatible. Any large

engineering design plan must employ basic management measures to keep the project within the allotted period and budget.

There are specific considerations for each step of the design procedure when applied to solar vehicle chassis design. It must be noted that this dissertation only covers the design process of the composite monocoque chassis, with particular attention given to the generation of a finite element analysis procedure. Essentially, the design of a solar passenger vehicle has been divided into subsections, of which the chassis design is one.

The first step is to analyse existing chassis design. There exists a variety of effective composite chassis designs, including vehicles such as the *McLaren F1*. It is important to analyse the design and manufacturing techniques in the production of these vehicles. This gives insight into the research and allows for a better understanding of the topic. Researching top solar car teams, such as *Solar Team Eindhoven*, to determine what makes them so successful is also significant. Analysing existing methods used to simulate a monocoque chassis, such as constraints and loads, assists in determining the procedure to conduct the finite element analysis.

The next step is to define the design specifications. Design decisions, such as the number of vehicle occupants and dimension limitations, need to be considered prior to any concept generation. These decisions were based on which race class the vehicle was intended for in the *2017 Bridgestone World Solar* Challenge. There were the *Challenger Class*, for one occupant, or the *Cruiser Class*, for two or more occupants. To satisfy the design requirement of public use as well as competitive use, the *Cruiser Class* was selected. This is considered a more practical design for public use, which coincides with the purpose of the *Bridgestone World Solar Challenge* to develop alternative energy powered means of transport for the city of the future. The design specifications were adopted from the *2017 Bridgestone World Solar Challenge*, regarding chassis design, and are detailed in section 1.3.

Conceptual design generation is the phase where the shape of the chassis is the primary consideration. Existing designs indicate that the monocoque design is the most suitable chassis type for a solar vehicle. When designing the vehicle chassis, it is important to consider the placement of the occupants, battery box, solar array, suspension mounts, and other functional components. Vehicle stability is also greatly affected by the body design. The torsional stiffness parameter has a strong correlation to vehicle stability, and chassis geometry largely affects the torsional stiffness. Aerodynamic properties are another important vehicle body consideration. Many competitive solar vehicles exhibit exceptional aerodynamic properties. This is due to calculated geometry alterations, such as frontal area reductions and smooth geometry transitions. Once several concepts are developed, they must be compared to one another and scored on a

points system considering relevant design attributes. The concept with the greatest score must be implemented as the final design.

Once the most suitable concept has been selected, the finer details, such as the curvature of the roof, of the chassis must be developed. These details ensure that the chassis adheres to the design specifications. In this phase the material layup, type of material, suspension systems, and steering systems are all considered. Through an iterative finite element analysis process, the weight and layup optimisation of the structure was determined. The torsional stiffness requirement was first achieved by optimising the laminate layup and geometry. Next, the laminates were altered to adhere to the strength requirements of the design without compromising the torsional stiffness. This corresponds to the local loading conditions of the suspension mounting points.

The design manufacture and testing does not form part of this research. This is because the vehicle will not be manufactured at this stage, due to lack of funding, however, it is possible that in the future the design will be manufactured to compete in the *2018 Sasol Solar Challenge* and the *2019 Bridgestone World Solar Challenge*. Therefore, it is important to consider manufacturing techniques and testing to ensure that a manufacturable design is generated. Once the vehicle has been manufactured, as per the detailed design, and assembled, testing can commence. Generally, when testing is conducted, design flaws arise. These could include that the vehicle does not meet certain regulations and criteria that it was intended to be designed to adhere to and design alterations must commence.

1.2 Design Specifications

The specified characteristics and design criteria that are required to be met are defined in section 1.2. For the purposes of this research, the design specifications were developed from the *2017 Bridgestone World Solar Challenge* cruiser class rules and regulations. This includes conforming to the roadworthiness and safety requirements, however, the design of the safety components, such as the anti-roll bar, are not part of this project. The primary *2017 Bridgestone World Solar Challenge* requirements for the chassis design are as follows:

- The vehicle must fit inside a rectangular prism 5000 mm long, 2200 mm wide, and 1600 mm high.
- The vehicle must be supported by four wheels, two in the front and two in the rear.
- The distance between the front and rear wheel centers must be more than half the width of the vehicle.
- Cruiser class solar vehicles must have two or more seats. They must accommodate a minimum of two or more occupants, each with their respective seat.
- Cruiser class solar vehicles must have doors or access points that can be secured and released from both the inside and outside of the vehicle.

1.3 Key Performance Indicators

A key performance indicator is a quantitative or qualitative value that evaluates the performance of a product or service. Key performance indicators regarding chassis design, detailed in section 2.3, are rigidity in torsion and bending, torsional stiffness, low weight and aerodynamic considerations. For the chassis to achieve its performance requirements these key performance indicators must be a central part of the design process. Some key performance indicators are of greater significance than others, and identifying them is important to accurately measure performance during the design process. These key performance indicators serve as the performance measurement tools of the analysis and modelling phase.

1.4 Analysis and Design

The torsional stiffness parameter is used as the chief key performance indicator when analysing the chassis and dictates the geometry and layup orientation of the design. A CAD model was developed and modelled using *Siemens NX Nastran* software. The design was optimised through an iterative design process, detailed in section 4.7 to satisfy the torsional stiffness requirement. The maximum principal stress was analysed to ensure that the chassis withstands the subjected torsional loading conditions.

In the chapters to follow in this research, Chapter 2 will summarise existing literature regarding chassis design. This includes investigating existing chassis designs of solar vehicles, material selection, design parameters and modelling techniques. Chapter 3 illustrates the developed conceptual designs and the selection of the most suitable concept. Chapter 4 details finite element analysis process and the results thereof. Chapter 5 shows the results of the flexural bending tests conducted on the material test specimens and compares these results to simulated flexural bending test results to verify the simulation material properties.

Chapter 2. Literature Review

An in-depth knowledge of the different chassis types and their history, materials used, different load cases and failure criteria are important to effectively address the aim of this research. Key factors, such as rigidity in bending and torsion, efficient load absorption, and low weight, are imperative for an effective design (Reddy & Kumar, 2013). Chapter 2 is a detailed review of the literature that is relevant to chassis design. This includes investigating existing solar vehicle chassis designs, what materials are used in the construction of a monocoque chassis, the design parameters that govern chassis performance and design simulation and modelling techniques.

2.1 Chassis Design

In the past, a vehicle's chassis was separate from its body, known as the body-on-frame design, with the frame being responsible for the vehicle's rigidity and strength. Although cheap and easy to build, this chassis design resulted in a heavy chassis with low rigidity. To address this issue, a new method for chassis design was developed. Modern vehicles utilize a unibody design, where the body has become part of the supporting structure, to reduce weight and improve chassis performance, particularly rigidity (Happian-Smith, 2001). Although sometimes referred to as a monocoque, because the body panels form part of the load bearing structure, there are also sections that reinforce the body, making the unibody design more of a semi-monocoque. There exist many different chassis types, with the spaceframe and unibody chassis being the selection of choice for most vehicle manufacturers.

Space frames and monocoque chassis designs are currently the preferred types for race vehicles (Bolles, 2010). Each exhibit advantages but the intended application is key in selecting the appropriate chassis type. A space frame chassis involves the assembly of components onto a skeleton-like structure constructed from rods of the selected material, Figure 2.1 (Walker, 2012). The body panels are attached to this structure and do not form part of the load bearing members. The frame rods are welded together at nodes, and utilize the concept of triangulation, which ensures that the beams are mostly loaded in tension or compression. There are multiple rods connected at a single node such that stress is transferred along each of the connecting rods in various directions. This eliminates bending stresses, which improves the rigidity of the structure.

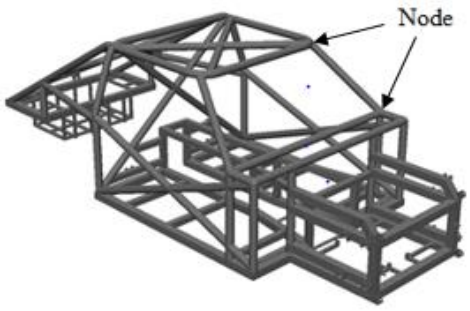

Figure 2.1: Spaceframe chassis (Walker, 2012)

The principle of the space frame design is to utilize the strength of triangulation to distribute the stresses that the chassis experiences among the tubes or bars. This creates a more rigid structure. A nontriangulated box offers little resistance to deformation in the direction of the force represented by the arrow in Figure 2.2.

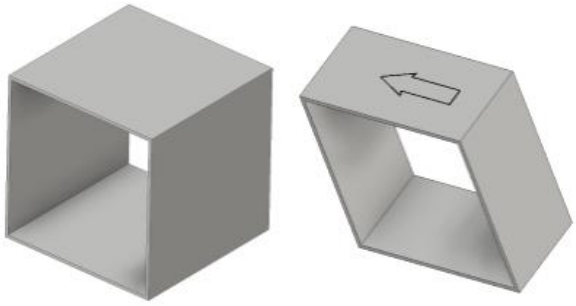

Figure 2.2: Reaction of nontriangulated box when loaded

To increase the ability of a box to resist deformation, a support beam is attached from one corner to the diagonally opposite corner. This forms two triangles within the box and is known as the concept of triangulation. This triangulation distributes the load through the diagonal beam. When the load is applied in the direction as illustrated in Figure 2.3, it loads the beam in tension. This is favourable as beams are stronger in tension than in compression, as buckling cannot occur.

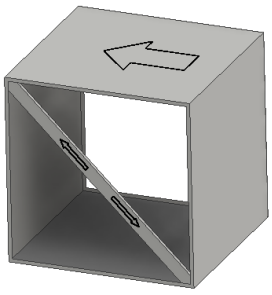

Figure 2.3: Triangulated box in tension

The monocoque chassis, Figure 2.4, is essentially a single bodied, or unibody, frame where the body also forms the supporting structure. The most common materials used in the production of

a monocoque chassis are composites (Davies, 2012), such as carbon fibre reinforced polymers (CFRP) and Kevlar, because they exhibit high stiffness and strength to weight properties. The composite monocoque is favourable due to its low weight and high rigidity properties. However, there are some disadvantages, such as intricate design procedures, expensive materials and complex manufacturing processes.

Figure 2.4: Monocoque chassis (GT-R Life, 2012)

A monocoque chassis does not need to capitalise on the strength properties of triangulation, as the chassis is a single piece structure. Therefore, the loads are distributed throughout the entire chassis. From a structural perspective, the monocoque is an improvement of the space frame chassis. A simple example of how the monocoque chassis, shown in Figure 2.5 (a), reacts to a load is similar to that of a triangulated spaceframe, Figure 2.5 (b).

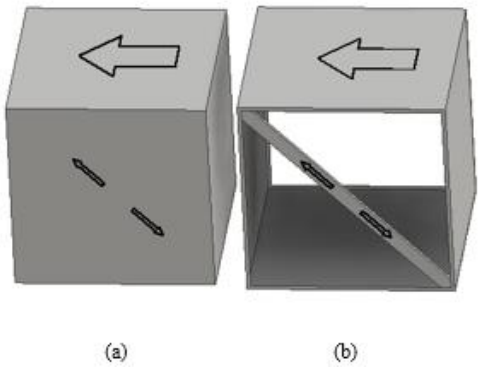

Figure 2.5: (a) Monocoque reacting to applied load, (b) spaceframe reacting to applied load

The monocoque is more favourable as it is essentially triangulated in both diagonal directions, as it is a 'complete' face and not just a single support as with the spaceframe. This means that it will still be loaded in tension when the force is applied in the other direction, Figure 2.6 (a), as opposed to being loaded in compression as in the spaceframe, Figure 2.6 (b). This negates the buckling failure mode to an extent, unless the allowable stresses are exceeded.

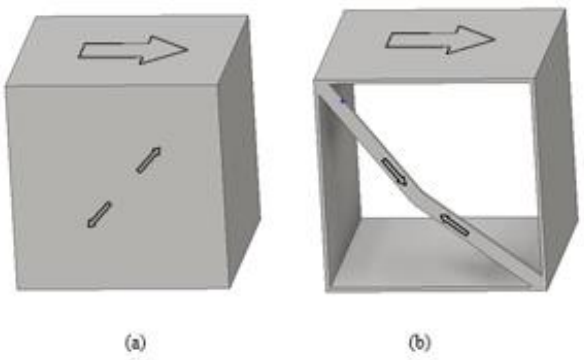

Figure 2.6: (a) Monocoque loaded in tension, (b) Spaceframe loaded in compression under same load

Both types of chassis can be made just as strong and rigid as each other, Figure 2.7; however, the same strength monocoque will be lighter, as lighter materials can be used. A spaceframe of equivalent rigidity would require diagonals from each corner to the opposite corner, Figure 2.7 (b), which results in a heavy and cumbersome structure. The monocoque is more complicated to design and manufacture, and requires, that the structure formed by panels, be 'complete' because an open end of the box will deform if loaded accordingly. Therefore, where an open end exists in a monocoque, the chassis must handle the loads through a supporting sub-structure.

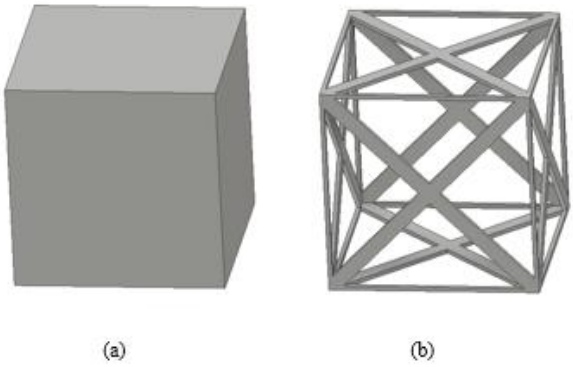

Figure 2.7: (a) Monocoque representation, (b) Equivalent spaceframe

2.1.1 Existing Monocoque Chassis

Carbon Fibre monocoque chassis are implemented in many aircrafts, spaceships and racing vehicles of today. Monocoque construction was first widely used in aircraft in the 1930s. The monocoque chassis has almost never been implemented in commercial vehicle bodies. Generally, most commercial vehicles use a method called variously unibody construction, which uses box sections, bulkheads and tubes providing most of the vehicle's strength, while the skin adds relatively little strength or stiffness. The term monocoque is frequently misused when referring to unibody cars. The unibody design blends the body panels into the frame, making them a stressed member of the chassis (Happian-Smith, 2001). By using this construction method, the frame components can be made from lighter materials, such as carbon fibre reinforced polymers (CFRP) and aluminium, without compromising the overall structural reliability of the vehicle.

The overall construction is more conventional, with larger sections of the body cast into single pieces and welded to the chassis structure. This enables the entire body to become a stressed member, alleviating high stresses from the undercarriage chassis. This typically results in a vehicle that produces less noise and vibration, and a better ride quality.

In motor racing, the safety of the driver depends on the car body, which must meet inflexible regulations. *McLaren* was the first to utilize CFRP to construct the monocoque chassis of the 1981 *McLaren MP4/1* (McLaren, 2016), and in 1992 the *McLaren F1* became the first production car constructed from a carbon-fibre monocoque chassis. This innovation paved the way for many CFRP monocoque chassis to be implemented.

The *2015 World Solar Challenge* cruiser class winners, *Solar Team Eindhoven*, implemented a CFRP monocoque chassis design in their vehicle, *Stella Lux*, Figure 2.8 (Solar Team Eindhoven, 2015). The chassis consisted of a dual-hulled shroud, similar to that of the 2015 *University of Kwa-Zulu Natal* solar car, *Hulamin*, with a tunnel underneath the chassis centre that stretches over the length of the vehicle. This reduces the total frontal area of the vehicle. The dual-hull design allows space for four passengers, two seated in the left and right hulls respectively. This design consisted of a roof, upon which the solar panels were positioned, that encapsulated the occupants, thereby resembling the cockpit of a conventional road vehicle. This makes the design favourable as it yields a lot of cabin space for the occupants, making the ride more like that of a production vehicle.

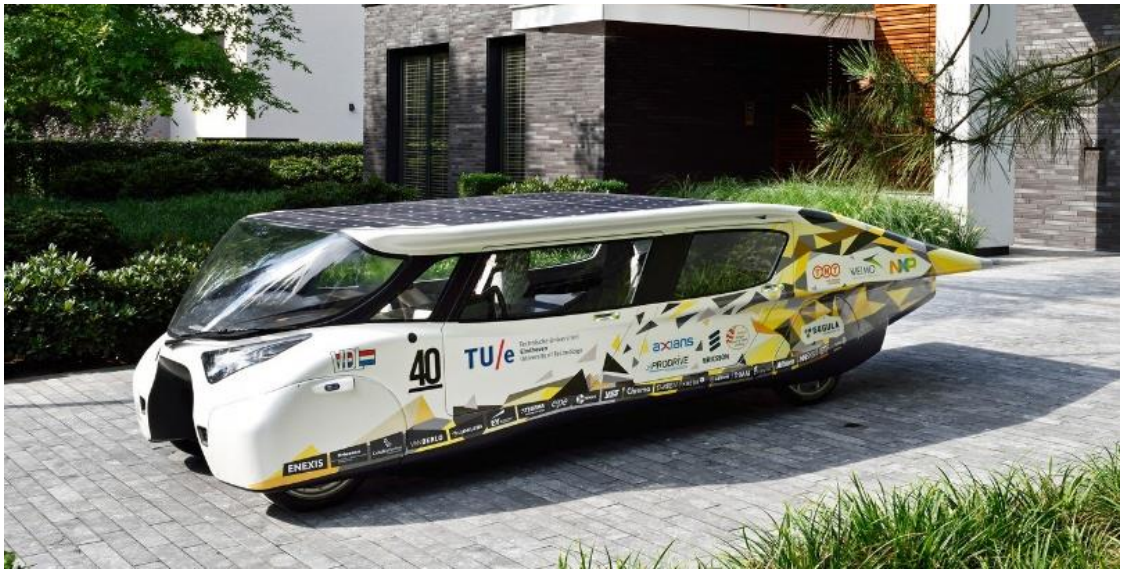

Figure 2.8: Stella Lux (Solar Team Eindhoven, 2015)

The 2014 *University of Kwa-Zulu Natal* solar vehicle, *IKlwa*, Figure 2.9 (Rugdeo, et al., 2014), and the 2015 UKZN solar vehicle, *Hulamin* (Denny, et al., 2015), were constructed from the same monocoque chassis. Although these vehicles were only single seater performance vehicles that

competed in the 2015 World Solar Challenge challenger class the design of the chassis could be implemented in a monocoque composite chassis passenger vehicle. The chassis makes use of a dual-hulled design that allows space for the driver in the right hull and space for all the electronics in the left hull. This vehicle was made with a detachable top-shell to which all the solar panels were attached. This design could be modified such that the dual hulls could be used for passenger seating area and the centre console used for mounting of the electronics. This design consisted of a canopy that covered the driver rather than a roof that encapsulated a cockpit.

Figure 2.9: UKZN, South Africa, solar vehicle IKlwa (Denny, et al., 2015)

The *University of New South Wales* entered the *2015 World Solar Challenge* cruiser class with the vehicle *Sunswift*, Figure 2.10 (World Solar Challenge, 2015). This vehicle holds the *Guinness World Record* for the fastest solar powered vehicle. The chassis of the vehicle is a carbon fibre monocoque with foam and an aramid honeycomb core. The chassis was designed to fit two occupants, including the driver. This chassis is designed similar to a conventional road vehicle whereby the chassis is not made from hulls where the passengers sit, but rather it has a cockpit where the passengers sit. The hood, roof and rear of the vehicle make provision for the solar panel mounting points.

Figure 2.10: UNSW, Australia, Sunswift solar vehicle (World Solar Challenge, 2015)

2.1.2 Characteristics of the Composite Monocoque Chassis

A monocoque is both the chassis and the body of the vehicle. This vastly reduces the complexity of the assembly of the vehicle. No joining of the panels once manufactured would be required. This saves time and resources when assembling or dissembling the vehicle for transport. The manufacturability of monocoque chassis is a relatively complex procedure, and if done without sufficient experience or expertise, may result in a laborious and expensive production.

Composite monocoques offer the highest stiffness to weight ratio, when compared to any other combination of a material and chassis type (Eurenius, et al., 2013). Torsional stiffness is important because it allows the front and rear suspension systems to act in the correct manner with respect to each other. It has a significant impact on the cornering ability of a vehicle (Happian-Smith, 2001). If a vehicle has insufficient torsional stiffness, it would simply twist when loaded accordingly, lifting one end of the vehicle, thereby losing traction (Thompson, et al., 1998). This shows that the torsional stiffness of a vehicle is of great significance when determining the handling performance of the vehicle (Eurenius, et al., 2013). Carbon fibre composites are a fibrous material that offers high strength to weight and stiffness to weight properties, with the fibres being the load-bearing component of the composite material. The weight of the chassis can be substantially reduced by selecting a composite monocoque chassis. This will improve the vehicle's ability to accelerate and decelerate, as well as increasing the efficiency of the vehicle. In a formula 1 vehicle, the carbon fibre composites amount for approximately eighty-five percent of the volume fraction of the vehicle but only account for about twenty-five percent of the weight (Savage, 2008).

Composite monocoques do not withstand loads efficiently when loaded perpendicularly to the direction of the reinforcement material fibres. Therefore; it is imperative that the chassis absorbs

the loads in the direction of the fibres such that the reinforcement material is loaded in tension. Fibre reinforced composites can be divided into two main categories. The first being short fibre reinforced composites, discontinuous fibres, and the second being continuous fibre reinforced composites. Continuous fibres exhibit superior mechanical properties than discontinuous fibres, because fibres become weak at discontinuous points present in short fibre composites. The reinforcement material is generally combined with a core material to form a sandwich structure. The purpose of the core material is to increase the thickness of the structure, with a low weight increase. Allowing the inner and outer reinforcement material of the sandwich structure to be in an approximately forty-five-degree arrangement generally offers improved torsional stiffness properties. Woven composite fibres are easier to form complex shapes, have greater resistance to damage, and reduce layup time (Barbero, 2011).

Carbon composite materials should be handled with the utmost precaution as the slightest damage to the material could result in drastic material mechanical property deterioration. Surface damage, such as cracks and scratches, are detrimental to the strength of the material, because cracks propagate very easily through carbon. Geometries must be simplified wherever possible, as a shape that is too complex will not be able to be accurately layered in a mould. Simpler shapes are also easier to remove from moulds. Warpage is reduced by ensuring that the draft angle is substantial, which is recommended to be one degree for vertical surfaces. Larger radiuses are easier to manufacture, and reduce the stress concentrations that arise due to sharp corners. A general rule of thumb is that a minimum inner corner radius of two millimetres and minimum outer corner radii of one and a half millimetres are recommended (Mazumdar, 2002).

2.2 Material Selection

The selection of an appropriate material is important in any engineering application for design optimisation. Material properties limit performance. This limit is illustrated by material charts, Figure 2.11 (Ashby, 2011) and Figure 2.12 (Ashby, 2011). Generally, it is a combination of materials properties that are of concern, such as; the need for low weight, high stiffness, high strength, and corrosion resistance. The material charts concise a large volume of information into a compact, easily understood form. They show various correlations between material properties, to assist with checking and estimating data, and are a reliable means for material selection.

As can be seen from Figure 2.11, most these materials, due to their low stiffness to weight ratio, are not suited for chassis construction. However, certain materials such as diverse types of steels, woods and composites tend to be the most suitable materials for chassis construction. In general, the point at the upper left of the diagram is the optimum point. A set of performance indices are used to determine the most suitable material choice. From the Figure 2.11, there are three performance indices for this particular chart. If a high stiffness to weight ratio is required, the

ratio E/ρ is to be maximised. If buckling is to be avoided, $E^{1/2}/\rho$ is to be maximised. If failure in bending it to be avoided, $E^{1/3}/\rho$ is to be maximised. The material choice alone does not define the effectiveness of a chassis; its geometry and shape also play a vital role in determining its effectiveness. The selected material is also dependent on the type of chassis being designed, for example, a material such as steel would be an effective material choice for a space frame chassis but not for a monocoque design. This is because steel tubes are welded together to form a spaceframe but it would be inefficient to produce a monocoque from sheet steel, as the structure would not be rigid.

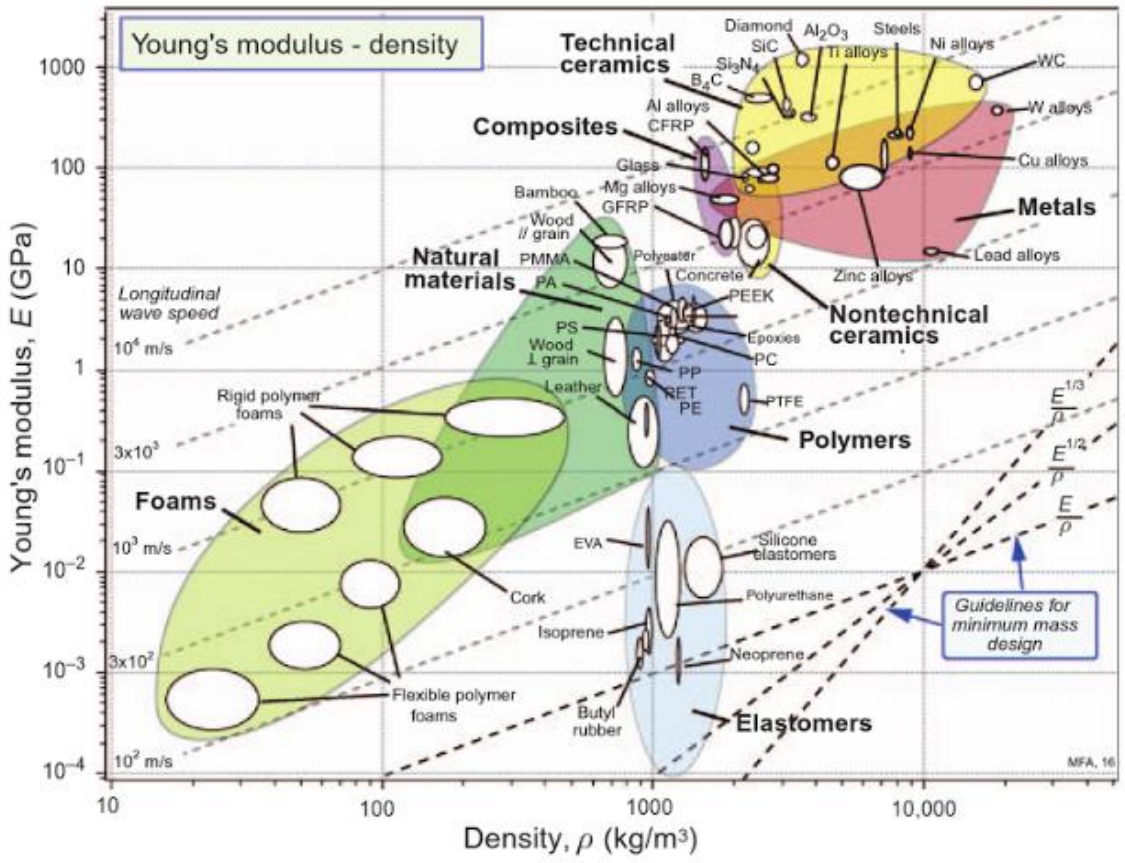

Figure 2.11: Young's modulus vs density material chart (Ashby, 2011)

The stiffness to weight ratio of a material is not the only material property to consider for chassis design. The strength to weight ratio is also of utmost importance. As with the previous material chart, the materials in the upper left region are the most suitable. Again, the optimum point is not easily determined, and it is required that performance indices be investigated. If a high strength to weight ratio is required, the ration σ_f/ρ is to be maximised. It can be seen from Figure 2.12 that engineering ceramics, alloys and composites exhibit the highest strength to weight ratios. If failure in bending is to be avoided, the ratio of $\sigma_f^{1/2}/\rho$ must be maximised. Table 2.1 (Savage, 2008) summarises material properties of various appropriate materials and compares them as well as

their performance indices from the material chart for strength to weight and stiffness to weight ratios.

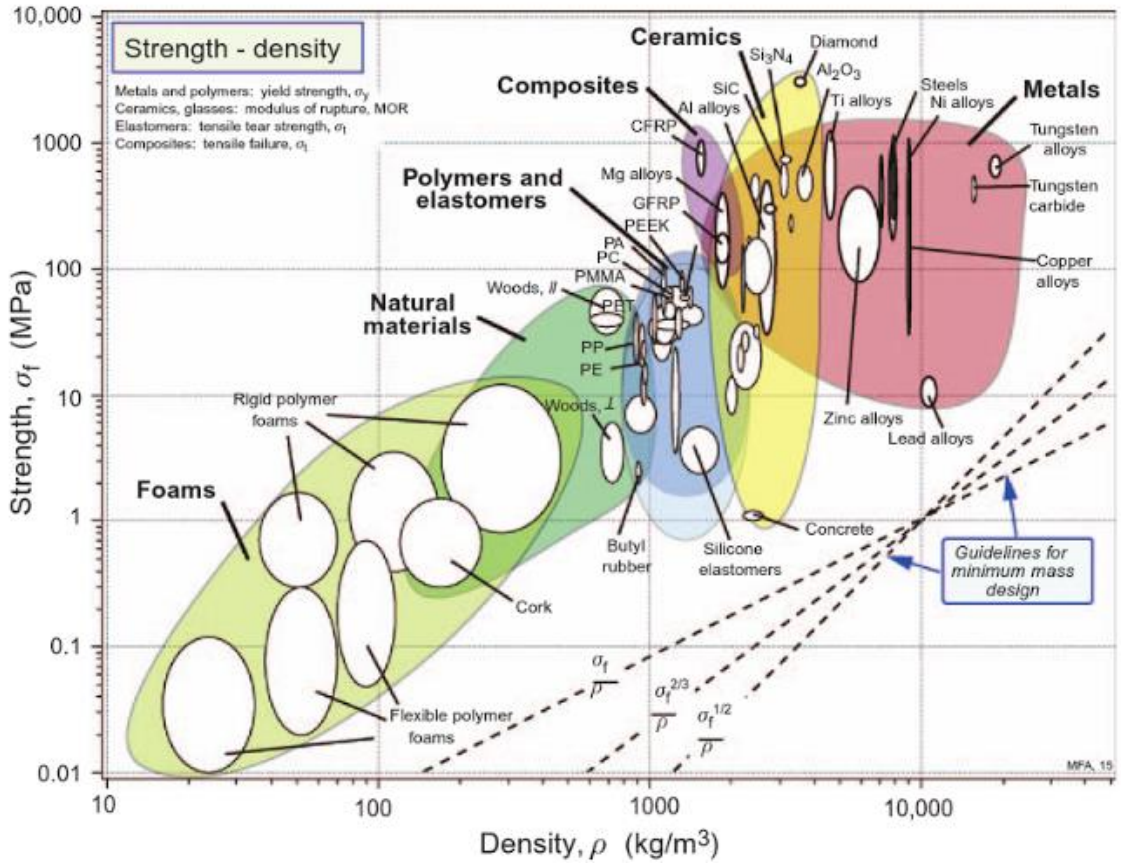

Figure 2.12: Strength vs density material chart (Ashby, 2011)

Table 2.1: Summary of relevant material properties (Savage, 2008)

Material	Density, ρ (g/cm^3)	Tensile Strength, σ_f (MPa)	Young's Modulus, E (GPa)	Strength to Weight, σ_f/ρ	Stiffness to Weight, E/ρ
Steel	7.8	1300	200	167	26
Aluminium	2.81	350	73	125	26
Fibre Glass	2.1	1100	75	524	36
Aramid Fibre	1.32	1400	45	1061	34
Intermediate Modulus Carbon Fibre	1.51	2500	151	1656	100
High Modulus Carbon Fibre	1.54	1550	212	1006	138

Table 2.1 shows that carbon fibre reinforced polymers have a higher stiffness and strength to weight ratios than that of the other materials. For this reason, CFRP will be the material that will be investigated for application in this research.

2.2.1 Composite Materials

A composite material is fashioned by the combination of two or more separate materials to form a new material with enhanced properties. The most common composites are constructed with a reinforcement material held together with a matrix material. Maximising rigidity and strength, and minimising weight are imperative to an effective chassis. Therefore, materials that exhibit high strength to weight and high stiffness to weight ratios are favourable. A composite, like CFRP, consists of carbon fibre reinforcement, fused by a polymer matrix material, like epoxy. The fibres are designed to carry the loads and the matrix material transmits the loads to the fibres. The matrix material also serves the purpose of protecting the fibres and improving the ductility of the composite structure. The fibre orientation, amount of fibres and the type of weave affect the ability of the composite material to withstand loads. The addition of a core material forms a composite sandwich structure, Figure 2.13 (Ashby, 2011), and is purposed with increasing rigidity. A sandwich structure offers similar structural advantages to an I-beam, but with the overhangs and webs extended in all directions (Mallick, 1997), increasing the cross-section's moment of inertia and section modulus. The skins of the sandwich structure act as the overhangs of an I-beam, and the core correlates to the I-beam's web. When loaded, one of the skins experience tension, and the other experiences compression, and the core is loaded in shear. The core holds the two skins in together so that the panel does not buckle, snap, or deform. The CFRP forms the face material, which surrounds a core on its upper and lower side. This combination yields a high bending strength to weight ratio, due to the core increasing the structure's polar moment of area, moment of inertia and section modulus (Ashby, 2005).

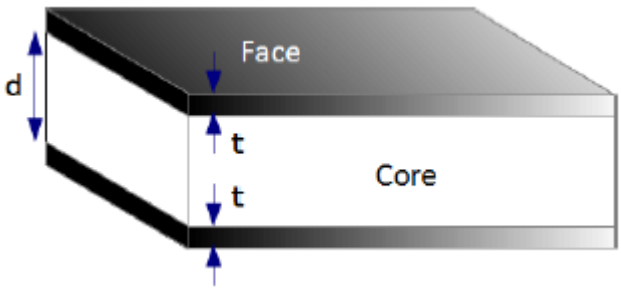

Figure 2.13: Typical sandwich structure (Ashby, 2011)

2.2.1.1 Fibre Material

The fibre or reinforcement material is responsible for giving the composite primarily its tensile strength but also some shear strength. It is important to first determine the performance index to be maximised when selecting a fibre material, as well as the various loads it is exposed to. As

previously mentioned, the performance indices from the material charts need to be maximised for the most appropriate material to be selected. Table 2.2 illustrates the performance indices for the materials in Table 2.1.

Table 2.2: Performance indices of relevant materials

Material	Stiffness to Weight (E/ρ)	Avoiding Failure in Buckling ($E^{1/2}/\rho$)	Avoiding Failure in Bending ($E^{1/3}/\rho$)
Steel	26	1.8	0.7
Aluminium	26	3	1.5
Fibre Glass	36	4.1	2
Aramid Fibre	34	5	2.7
Intermediate Modulus Carbon Fibre	100	8.1	3.5
High Modulus Carbon Fibre	138	9.5	3.9

Table 2.2 shows that carbon fibre is superior to the other materials due to its greater values obtained for the ratios of stiffness to weight, avoiding failure in buckling and in bending. The slope of the lines in Figure 2.11 and Figure 2.12 on the material chart correspond to the performance indices in Table 2.2. The ideal material is selected by shifting the line until it touches the material group that is closest to the upper left region of the chart. By this method, CFRP is the most suitable material for monocoque chassis applications.

Other materials that exhibit comparable properties to CFRP are polymeric fibre materials. This group of materials includes aramid and zylon. Aramid is typically known as Kevlar and exhibits higher toughness and lower density properties than carbon fibre. It is famously known for being used in the production of bulletproof vests. It is as strong in tension as CFRP but far weaker in compression. Zylon has high tensile strength, modulus of elasticity, and flame resistance. It does however exhibit poor resilience to UV-radiation and tends to degrade when exposed. It is generally used as a protective shell around the driver in racing vehicles, where it is covered by the vehicle's body panels (Bunsell & Renard, 2005).

2.2.1.2 Core Material

The core material of a sandwich structure is responsible for giving it strength in bending and shear, by increasing the structure's polar moment of area, moment of inertia and section modulus. Various core materials are available as well as the different possible structures of the core material. This is significant to obtain the most effective composite material. The thickness of the

core material is directly proportional to the stiffness, strength and weight, as illustrated in Table 2.3 (Hexcel Composites, 1997), of the sandwich structure. The stiffness and strength of the sandwich structure increases exponentially with only a slight increase in weight.

Table 2.3: Illustration of relationship between sandwich structure mechanical properties and core thickness (Hexcel Composites, 1997)

	Solid Fibre Material	Core Thickness (t)	Core Thickness (3t)
Diagram	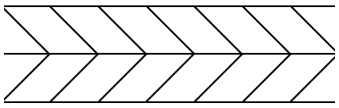	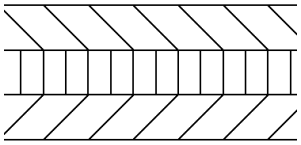	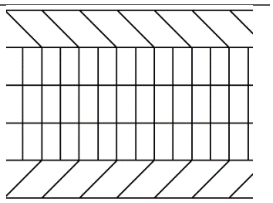
Weight	1	1.03	1.06
Flexural Strength	1	3.5	9.2
Stiffness	1	7.0	37.0

Foams are popular for core material applications. They can also be supplied in various densities and thicknesses. They can be manufactured from a variety of synthetic polymers including polyvinyl chloride (PVC), polystyrene (PS), polyurethane (PU), polymethyl methacrylamide (acrylic), polyetherimide (PEI) and styreneacrylonitrile (SAN). A foam is usually made from a combination of a solid and gas. The solid is usually made from expanding polymers, metals or ceramics, and is responsible for most of the foam's mechanical properties. The density and thickness of the foam core are the most important parameters to consider, as it is imperative that the core is as light as possible. It is also important to consider the selected foam material's behaviour under loading conditions. Generally, when loaded, the foam's cell edges deform inwards where the load is applied, Figure 2.14 (Ashby, 2005).

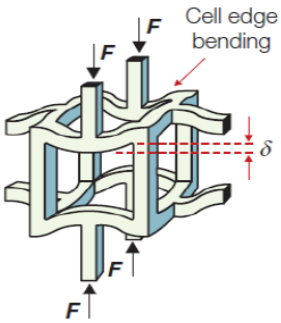

Figure 2.14: Foam cell edge bending (Ashby, 2005)

The cell edge will continue to deform until the cell edges meet the opposite edges. This is known as densification and only occurs if the material is ductile enough to not crack. From this point,

further deformation is not possible and an increase in applied stress will occur. Foams made from a polymeric material exhibit this failure mode. Shown in Figure 2.15 (Ashby, 2005), image a) illustrates that if the foam is brittle, the cell edges will snap under the load, and image b) illustrates if the foam material is made from an elastomer, it generally fails by elastic buckling.

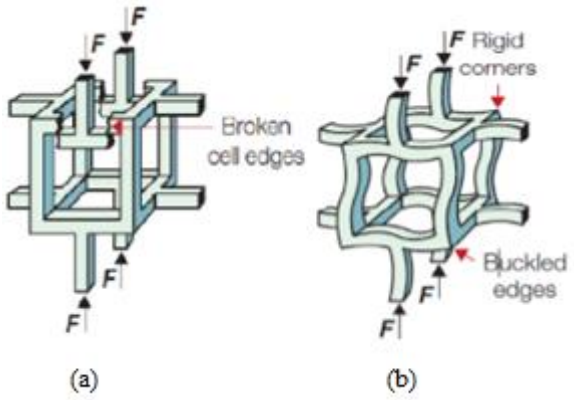

Figure 2.15: (a) Snapping of foam cell edge, (b) Foam cell elastic buckling (Ashby, 2005)

Another way of constructing the core is using a honeycomb structure, Figure 2.16 (Bitzer, 1997), which can comprise of several materials. It consists of symmetrical pattern, usually hexagonal, to which the face material is bonded. A honeycomb structure provides relatively high compression and shear combined with low density. They can be formed into both flat and compound curved structures without excessive force or heating. Honeycomb core materials include materials such as aluminium, thermoplastics, CFRP and woods. The cells of the honeycomb structure can also be filled with foam to increase the bond area and improving the stability of the cell walls, as well as increase thermal and acoustic insulation properties. The properties of the honeycomb depend on the size of the cells, and the thickness and strength of the web material (Thomsen, et al., 2005).

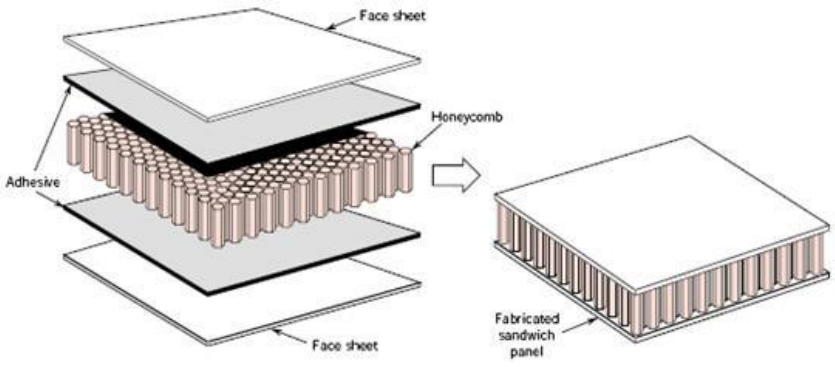

Figure 2.16: Typical honeycomb sandwich structure (Bitzer, 1997)

There exists a vast number of materials that can be used for honeycomb core applications. Some of the most popular include carbon, aluminium, Kevlar, fibreglass and wood. The selected material is dependent on the types of loads that the structure will experience and the environment that the structure will be operating in. The shape and size of the honeycomb cells are also

important to consider. Generally, the larger the cell, the cheaper it is. However, larger cells may result in a dimpled outer surface of the sandwich structure due to their smaller bonding area. A hexagonal shape, Figure 2.17 (Hexcel, 2015) image a), is the preferred cell but rectangular shapes, Figure 2.17 image b), have also been used.

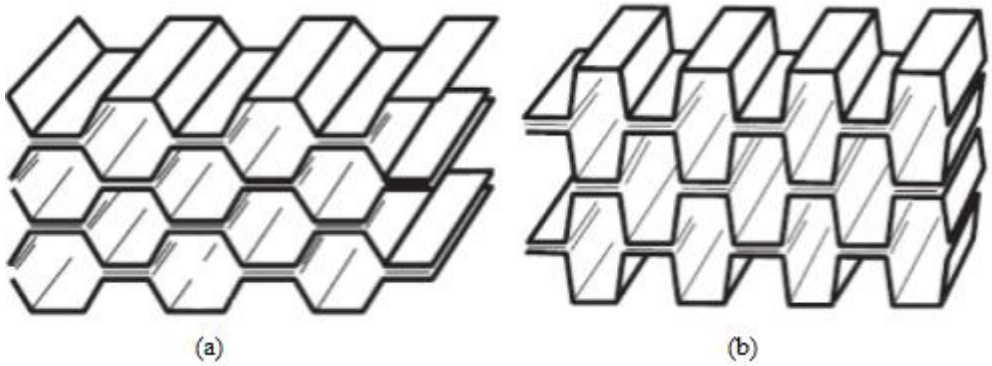

Figure 2.17: (a) Hexagonal cell core, (b) Rectangular cell core (Hexcel, 2015)

2.2.1.3 Matrix Material

The matrix material is the component that surrounds and holds the fibres in place. It provides the composite's compressive strength and added shear strength, stopping the fibres from shifting in relation to each other. Thermosetting, such as epoxy, and thermoplastic, such as polycarbonate, polymers are the most popular materials for matrix material applications. Thermosetting polymers cross-link during the curing process and become a glossy, brittle solid. They are the matrix material of choice among the racecar industry. Thermoplastic polymers become crystalline or amorphous at room temperature, which provides strength and shape. The most common matrix material used in industry is polyacrylonitrile (Wanberg, 2009). Other popular materials include rayon and pitch. It is important when designing a composite chassis that an equally suitable matrix and fibre material be selected. This ensures that neither compromise another's performance. For example, if one were to select a strong fibre material and a sub-standard matrix material, the composite would be limited to the capacity of the latter.

Not only are the properties of the matrix material dependent on the choice material, but the treatment temperature and applied tension during processing as well. The treatment processes affect all the ductility, toughness, strength and modulus of the matrix material. As with any material, a composite is limited to how much load it can withstand. Generally, the loads can be simplified to either be tensile or compressive loads. In tension, it is possible to either have fibre cracking or matrix cracking, depending on which is the limiting material. In compression, it is common for the fibre to kink. This further reinforces the notion that both a suitable fibre and matrix material be selected such that they fail simultaneously, as to not have a limiting component.

2.2.2 Composite Sandwich Structure

Composite sandwich structures have emerged as a most promising type of material combination for many applications where weight reduction is key. This structure comprises of a core, matrix, and upper and lower faces. It yields improved fatigue performance, superior energy absorption, corrosion resistance, and weight reduction, when compared to each individual material used to construct the sandwich. The face material gives the structure the bulk of its tensile strength, the core material increases the bending and shear strength, and the matrix material bonds the structure together such that each component works in unison (Thomsen, et al., 2005). To determine the optimal parameters of the structure, the various failure modes for sandwich structure must be investigated. In Figure 2.18 (Allwood, 2009), faceplate fracture, image (a), occurs when the face yields under an exerted pressure from a load. This depends on the yield strength of the face material. Core shear failure, image (b), occurs when the core shears due to the applied stress and hinges in the face damaging the core. Local indentation, image (c), is different from faceplate fracture as it depends on the area of impact. It occurs at concentrated loads, such as fittings, corners, or joints, and is avoided by applying the load over a sufficient area. Delamination, image (d), is failure in a laminated material, which leads to separation of the face and core. It can be caused by the adhesive fracturing or by the debonding of the adhesive.

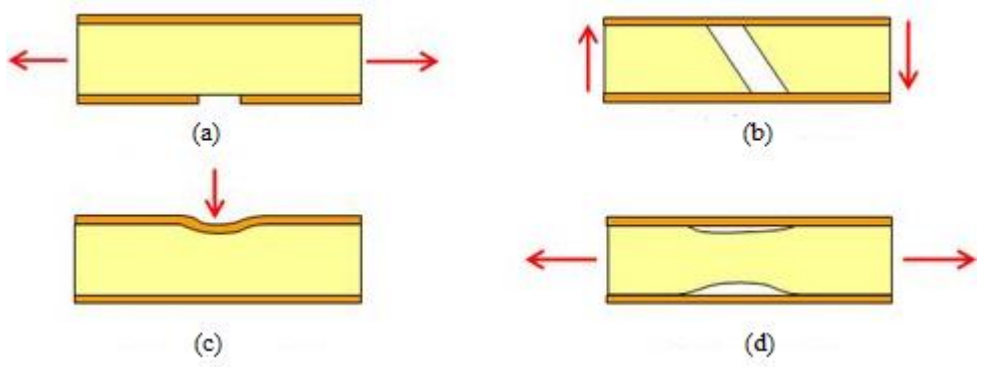

Figure 2.18: Typical sandwich structure failure modes including (a) faceplate fracture, (b) core shear, (c) local indentation, and (d) delamination (Allwood, 2009)

2.2.2.1 Fibre Orientation

The orientation of these fibres is important in determining the composite's physical properties, such as their volume fraction, orientation to the applied stress and their construction. Since the theoretical parameters of a fibre material is known, it is possible to predict the behaviour of the composite, however, manufacturing methods, such as weaving, cause fluctuations of fibres which unknowingly alters the physical properties of the material. Fibres either are woven into a weave or are made to be unidirectional, where all the fibres in a layer are laid in the same direction. Unidirectional orientation results in a better translation of fibre properties as they are not bent, as with a weave, and contain less matrix material than a weave, increasing its fibre volume fraction. The fibre volume fraction is the percentage of fibre volume in the entire volume of a fibre-

reinforced composite material (Messiry & Deeb, 2016). It is designed to be maximised in a composite material, but also designed to have a precisely defined number of fibres in the correct location and orientation, with minimum polymer matrix material to ensure that the composite is as strong as possible (Mallick, 1997). The disadvantage with unidirectional fibres is that the mechanical properties of the unidirectional structure are only valid when the load is applied in the direction of the fibres. If the load is not applied in this direction, the composite's properties become like that of a stiff polymer matrix. Woven structures require less manufacturing time, are more robust and can easily be formed into complex geometries. They also exhibit mechanical properties in multiple directions, depending on the type of weave. All fibre structures contain a tow, which is an untwisted bundle of continuous filament of carbon fibre that is designated by the number of fibres they contain (Wanberg, 2009).

With the weave structure, it is possible to use different variations of a weave to obtain different mechanical properties. Since the composite weave is like a two-dimensional co-ordinate system, there are two degrees of freedom when selecting the type of weave. The lateral direction is called the weft and the longitudinal is called the warp. The most common types of weave are the plain, twill and satin weaves. In a plain weave, the weft strand goes over one warp strand and then under the next, forming a symmetrical structure. The twill is similar, but the weft goes over the warp strand and then under at a certain number of strands until it goes over again. This certain number is usually two or four, creating 2x2 and 4x4 twill. Satin weaves do not follow an obvious pattern and have minimal interlacing. This could mean that at first the weft passes under a number of warp strands but then only goes over one or two. This results in the satin weaves performing differently in each direction (Wanberg, 2009). A plain weave is considered the most stable weave regarding strand slippage and distortion. However; the high level of fibre crimp results in relatively low mechanical properties compared with the other weave styles. The long fibre sections in a satin weave result in better load absorption and mechanical properties, due to low fibre crimp, but reduced stability and increased chance of fibre distortion. A 2x2 or 4x4 twill offers a compromise between the factors that control the choice of weave. In industry, the most common weave is the 2x2 twill. Table 2.4 summarises the relevant properties of each weave.

Table 2.4: Summary of common weave properties

Weave Type	Weave Stability	Drapability	Low Crimp	Formability of Curvature
Plain	Excellent	Good	Poor	Poor
Twill	Good	Good	Good	Good
Satin	Poor	Poor	Excellent	Excellent

In Figure 2.19 image (a) shows an example of a plain weave (Fibremax Composites, 2014), image (b) shows an example of a 2x2 twill weave, and Figure image (c) shows an example of a 4H satin weave.

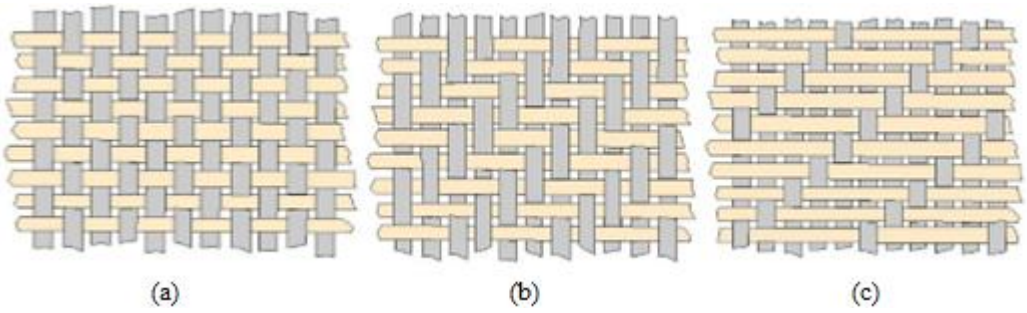

Figure 2.19: (a) Plain weave, (b) 2x2 twill weave, (c) 4H satin weave (Fibremax Composites, 2014)

2.2.2.2 Core Properties

The material properties of the core are important to determine the most suitable core for the application. There are various parameters that need to be specified when selecting a core, namely being: the type of material, the cell configuration (for honeycomb only), the cell size (for honeycomb only), the density, and the foil gauge (for aluminium honeycomb only). A core must be designed to satisfy the required failure modes. In Figure 2.20 (Hexweb, 2000), image (a) shows it must be strong enough to avoid skin compression failure, image (b) shows it must be stiff enough to avoid excessive deflection, image (c) shows it must be thick enough to avoid panel buckling, and image (d) illustrates the effects of shear crimping.

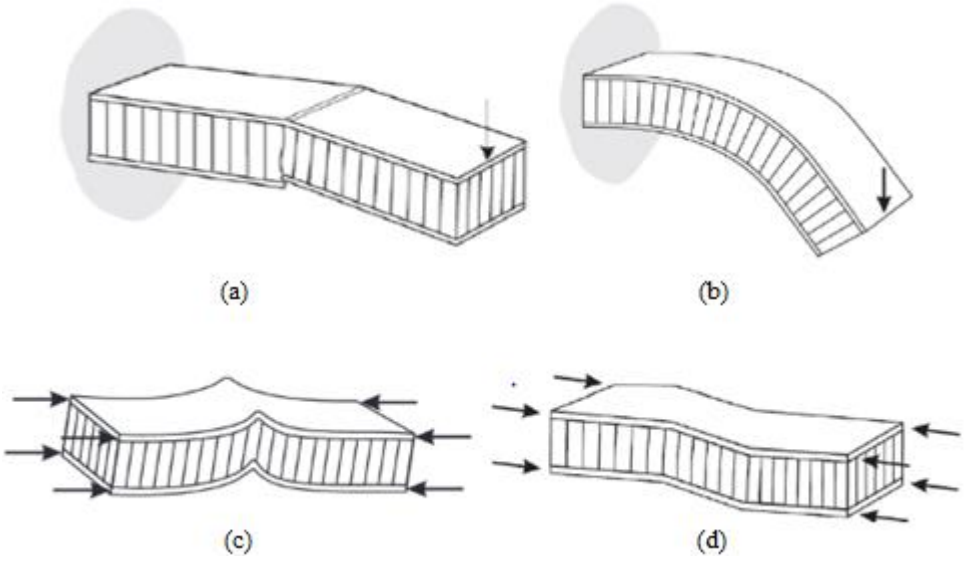

Figure 2.20: (a) Skin compression failure, (b) Excessive deflection, (c) Panel buckling, (d) Shear crimping (Hexweb, 2000)

Honeycomb cores offer superior stiffness properties than foam cores (Bitzer, 1997). It is also important to consider the design attributes required when selecting a honeycomb core. Some of these attributes are as follows: the cost vs. performance, strength to weight ratio, reaction to

moisture, ultraviolet light exposure, environmental exposure, flammability, and machinability of the core. The varied materials used in the manufacture of honeycombs have specific advantages over one another. Table 2.5 summarises the properties of common core materials.

Table 2.5: Summary of common core properties

	Aluminium	**Aramid Fibre**	**Kevlar**	**Carbon**	**Polyurethane**
Stiffness	Very High	High	High	Average	Average
Weight	Low	Low	Low	High	Average
Energy Absorption	Very High	High	High	High	Average
Cost	Average	Very High	Very High	Very High	Low
Formability	Average	Average	Average	Very High	Very High
Insulative Properties	High	Average	High	Low	Low

Polyurethane foam is the most common core material in use today. It is easily manufactured, has low density, formable, and cost effective. Although not as strong as its honeycomb counter-parts, this foam negates the effect of face dimpling, common with honeycombs, and has a larger bond area, decreasing the risk of delamination. The most common honeycomb core materials being implemented in vehicle design are aluminium and aramid fibre (Nomex honeycomb). Aluminium honeycombs exhibit maximum stiffness and one of the highest strength to weight ratios. It is corrosion, fire, and fungus resistant, and will not absorb moisture. It is easily machined and formable. Nomex honeycomb is considered the standard choice for lightweight non-metallic composite manufacture. It exhibits a high strength to weight ratio and, when coated with heat resistant phenolic resin, offers exceptional resiliency, low density, low cost, and high formability. Kevlar honeycomb is the latest addition to the honeycomb industry. It is manufactured from para-aramid fibre paper that is impregnated with a heat resistant phenolic resin and displays a high strength to weight ratio, excellent thermal and moisture stability, high toughness, low weight, and improved shear strength and shear modulus of competitive honeycomb materials. It is claimed that Kevlar honeycomb exhibits up to forty percent higher properties than comparable density Nomex honeycomb and being up to four times stiffer (Lee, 1993). Availability is also important to consider. Nomex commercial grade and aerospace grade honeycombs are readily available in sheets, blocks or cut to size pieces in both rectangular and hexagonal cell configurations. They are also available in a variety of cell sizes, ranging from 1/8 to 1/4 inch. The same goes for the Kevlar honeycomb. It must also be noted that if the strongest core material, Kevlar, is selected for the application, its properties may result in the optimal cell size to be so big and the cell wall

thickness to be so thin, that suppliers do not manufacture it. In this case, it would be better to select a Nomex or aluminium core of a smaller cell size that is readily available.

An aluminium honeycomb core is the most appropriate choice to be implemented in a monocoque chassis. This is due to its high stiffness and strength to weight ratios, corrosion resistance, availability, machinability, and energy absorption parameters. However, an aluminium honeycomb core can only be implemented in areas of low curvature, meaning that a combination of foam and aluminium honeycomb cores would need to be used for a complex structure. Another drawback with selecting an aluminium honeycomb is that the sandwich structure becomes susceptible to galvanic corrosion. The carbon fibres in CFRPs are electrically conductive and electrochemically noble. When coupled with a metal, galvanic corrosion arises, and is worsened when CFRP components are coupled with relatively small metallic components (such as bolts and nuts). The CFRP acts as the cathode and the metal acts as the anode. This situation can be mitigated by the anodization of the metal and the formation of a thick, protective aluminium oxide layer on the surface. Another solution is to insulate the CFRP from the aluminium core by using an insulating material, such as a layer of fibre-glass, between the two. Epoxy resins can also be used to seal the CFRP to negate environmental corrosion.

2.3 Design Parameters

Chassis design requires that design parameters be investigated when conducting a chassis creation. There are multiple design parameters to consider when designing a vehicle, but, for the purposes of this dissertation, only the most significant design parameters will be investigated. This is because the purpose of this research is to generate a finite element analysis technique to model the performance of a composite monocoque chassis, and not to model the other vehicle components that will have a minor effect on the chassis performance.

2.3.1 Torsional Stiffness

The torsional stiffness of a vehicle chassis is defined as the ratio between a roll torque applied to the wheel hubs of the front axle and the consequent rotation, when the rear axle hubs are fixed to the reference system (Genta & Morello, 2009). The torsional stiffness is largely responsible for the handling of the vehicle. The suspension of a vehicle ensures that the wheels stay in contact with the ground, but this cannot be accomplished with a chassis of insufficient torsional stiffness (Velie, 2016). The required torsional stiffness, detailed in section 3.6, varies depending on the application of the chassis. This is because the chassis will simply twist, lifting one corner of the vehicle and thereby raising the suspension. A chassis with a high torsional stiffness, such as that of a *Formula One* which 20000 Nm/deg and higher (Abrams, 2008), will be able to corner sharper and faster, without losing traction. This makes the vehicle more controllable. If the chassis is not

sufficiently stiff, understeer will occur, and in extreme cases, the vehicle will sway across the driving surface.

2.3.2 Chassis Weight

The weight of the chassis is imperative in achieving an effective chassis design. The aim is to minimise the weight of the chassis without compromising its structural integrity. This improves the vehicle's acceleration, as the weight is inversely proportional to acceleration, handling, as a lower weight results in less weight transfer when cornering, and efficiency, as less weight means that the motor needs to exert less force to accelerate the vehicle. The magnitude of the forces experienced due to load transfer of a vehicle when cornering, braking, and accelerating are directly proportional to the weight of the chassis. A heavier vehicle will be subjected to higher load transfer forces than a lighter vehicle, due to its inertia. When cornering, a heavier vehicle will tend to have a greater resistance to remain on its intended path, making cornering more difficult, with an increased risk of the vehicle rolling. In the event of a crash, a heavier vehicle will have higher kinetic energy, at the same speed, than a lighter vehicle. This means that more energy will be transferred, increasing the damage suffered by the vehicle and its occupants. This improves the safety of the vehicle.

2.3.3 Aerodynamic Drag

The aerodynamic properties, such as skin friction etc., of a vehicle are among the most crucial factors to consider when designing a vehicle to be as efficient as possible. Designing the geometry of the chassis to improve its aerodynamic properties as much as possible is key. Aerodynamics is denoted as the study of how air flows over and around objects. At high speed, the flow of air over a vehicle becomes more pronounced as the flow becomes more turbulent. In addition, drag force is proportional to velocity squared. This affects, among others, the fuel consumption of the vehicle as the vehicle needs to overcome more aerodynamic drag (Thiede, 2000). It must however be noted that for the purposes of this research that complex aerodynamic properties are not of primary concern and only general aerodynamics will be considered.

At any speed, aerodynamic drag will always be present, unless operating in a vacuum and a vehicle will always expend some energy in overcoming it. There are three sources of aerodynamic drag, namely:

- Skin friction, created by air moving over the body surface of the vehicle. This depends on the surface area of the vehicle and the roughness/smoothness of the surface. Smoother surfaces result in less energy lost to skin friction.
- Frontal pressure, created by a vehicle displacing the air out of its intended path. This depends on the frontal area of the vehicle and the shape of the front of the vehicle.

- Rear vacuum, created by the ‘hole’ left in the region of air as the vehicle passes through it. The displaced air attempts to move back to its original position by following the contour of the vehicle. This creates a continuous vacuum that sucks the vehicle in the opposite direction of travel.

The drag co-efficient is a dimensionless value that gives a numeric value to drag produced by a vehicle. The goal is to minimise this value as much as possible. It is a good indicator to how energy efficient a vehicle is. Typically, vehicles with a low drag co-efficient have the following characteristics (Sovran, 1978):

- Small frontal area, this reduces the volume or air that is displaced by the front of the vehicle as in moves forward.
- Minimal ground clearance, to minimise volume of air flowing underneath the vehicle.
- Sloped bodywork, to allow the airflow to remain attached to the vehicle, streamlining the vehicle.
- Greatly sloped windshield, to avoid pressure build ups in the front of the vehicle.
- Closed wheel covers, to reduce the airflow turbulence in the wheel arches.
- Gradually blended bodywork, to minimise junction drag. Bodywork, which converges quickly, produces drag by forcing the airflow into a turbulent state.
- Keep protrusions away from bodywork, protrusions from the vehicle’s body disrupt the airflow over the surface, generating high-pressure zones and increasing the drag experienced by the vehicle.
- Raking the chassis, the chassis is capable of being slightly lower to the ground in the front than in the rear, to reduce the air able to pass underneath the vehicle and generating an expanding space where a vacuum effect can form underneath the rear, decreasing the pressure underneath the vehicle.

Another important aerodynamic characteristic to consider is the Whitcomb area rule. This states that any change in area of a flow will create pressure changes at that area. This increases aerodynamic drag (Wallace, 1998). This rule is important to consider when designing a tunnel, which travels underneath the centre of the vehicle, to reduce frontal area. If the area of the tunnel is not kept constant, aerodynamic drag reductions created by this will be negated, or even aggravated, by the pressure changes that arise.

2.3.4 Manufacturing Techniques

Manufacturing limitations of the available workshop, as well as the budget restrictions must be considered in any engineering development. It is also important that a manufacturer be selected with the correct equipment and sufficient expertise to manufacture the design effectively. Many imperfections can arise from substandard manufacturing, which could be detrimental to the

effectiveness of the design and render the design unsuccessful. This manufacturing techniques chapter will focus on the concerns for manufacture and design geometries with the purpose of simplifying the process.

2.3.4.1 Mould Manufacture

A mould is defined as a hollow container, with a particular shape, into which materials in a pliable or liquid state are poured. These substances are allowed to set such that they take the shape of the mould. Moulded parts emerge perfectly shaped and require little post-fabrication work. When constructing a mould, it is important to consider numerous factors to ensure that the design is manufacturable. These include how the mould should be made, what it should be coated with, what material it should be made from, should it be portable, and mould weight. There are three types of mould that available for selection, namely the female, male, and compression moulds. A female mould or cavity mould is milled from a solid material within which the laminate material is laid and allowed to take the shape of. It is more expensive to construct but manufacturing time is significantly reduced, and the surface finish is excellent, therefore requiring very little post-fabrication work. This mould needs to be robust to withstand the high stresses it may experience whilst undergoing processes, such as an autoclave process. An autoclave is a pressure chamber that may need to be used to conduct a manufacturing process that requires higher temperature and pressure than atmospheric. The male mould or positive mould is the cheapest moulding process available. It is essentially a master-tool that mimics the final shape of the part being manufactured, but the part is fabricated over the mould's outer surface. The construction time of this moulding process is quick, but the component requires a lot of finishing work as it yields a rough outer surface. Compression moulds are made using a combination of both a male and female mould and is used for producing precision products. The moulds are compressed together to force any excess material out, usually the resin of a composite structure. This produces a smooth surface on each side of the part. This process is considered the costliest of the moulding processes, due to the cost of essentially producing two moulds (Barbero, 2011).

2.3.4.2 Composite Shell Layup

Composites manufacturing consists of four basic steps. The first being the impregnation step whereby the matrix and reinforcement materials are mixed to form the laminate. The matrix material is painted onto the reinforcement material sheets. This could result in an uneven spread of the resin. Alternatively, the more popular method is to purchase pre-impregnated sheets (prepreg) from a supplier. Carbon/epoxy is lighter and stronger than other prepreg materials. This method yields a higher volume fraction of carbon fibre within the laminate. The second step is the layup step whereby the laminate is moulded to form the anticipated geometry. This is the step where the laminate is used in a mould by placing the laminate sheets in the required orientation and number of layers. A release agent must first be applied to the mould so that the laminate does

not stick to the mould after setting. The direction of the fibres of the laminate sheets, number of layers, and placement of plies are all done according to the plybook. This is generated in the finite element analysis stage of the design process. This third step is to strengthen the area where the sheets and piles make connections with each other. This is known as the consolidation step and is done by overlapping, usually between two and ten millimetres, the laminate sheets and forcing them together via rollers or a vacuum process. This alleviates the stress concentrations that arise from the discontinuation of the fibres. The final step is to allow the laminate to set and take the shape of the mould. The time required depends on the matrix material used and under what environmental conditions the composite is allowed to set. Any holes that may need to be cut into the structure should be done after this process to prevent any deformations after the bagging process (Barbero, 2011).

Pre-impregnated carbon fibre sheets are generally used in the aerospace industry. It is an expensive process that is laborious, but results in high stiffness to weight and strength to weight ratios due to a high fibre volume fraction, approximately sixty-five percent (Mazumdar, 2002). This process requires advanced machinery and manufacturing techniques. The prepreg is cut, slightly larger than required to allow for overlapping, into the required shapes to be laid in the mould as per the plybook. Rollers, scrapers, and vacuum processes are used to remove and air bubbles. The debulking process is where the mould, with all the laminate sheets laid, is placed in a vacuum to squeeze all the air out between the prepreg laminates to ensure that the composite structure follows the exact mould contour. This process can be done for each layer of the composite structure but is only necessary for the first. A cheaper alternative is to use a heat gun to heat the prepreg and a scraper to force the prepreg along the contour of the mould. This method is far more labour intensive and time consuming. The next stage is the bagging process where pressure is applied to the laminate once laid-up to improve its consolidation. A release film is placed on top of the laminate structure to allow excess resin and air to diffuse through it. A bleeder is applied to absorb the excess resin. On top of this, another film is placed that only allows air to diffuse through it. A transparent plastic film is then placed over the entire wet layup and onto the mould and is made airtight. The air under the bag is extracted by a vacuum pump. If an autoclave process is to be applied, the same arrangements as mentioned previously are completed but once the vacuum bag is set up, the entire assembly is placed into the autoclave. The various connections are made and the cure cycle is entered. After curing and cooling, the component is removed from the mould.

An alternate method to the prepreg is the cheaper infusion process, Figure 2.21 (J Composites, 2012). This process can be accomplished at almost any workshop, as advanced machinery is not required. The process yields a fibre volume fraction of approximately fifty-five percent, which is only ten percent lower than that of prepreg (Mazumdar, 2002). This process is done by placing

the dry carbon fibres in a mould and infusing it with a liquid resin, under heat and vacuum to distribute the resin throughout all the fibres. The first few steps of the infusion process are the same as with the prepreg process. The difference in manufacturing comes when the dry fibres, in fibre cloth form, are placed in the mould instead of the prepreg sheets. The cloth is cut slightly larger than the mould to ensure that the fibres cover the entire mould. The cloth can be held in place via tape or epoxy spray. The next phase is the bagging process, which is used to achieve a steady vacuum during the consolidation and solidification phases. A peel ply is placed over the fibre cloth to stop fibres sticking to the bagging material. Then an infusion mesh, or breather material, is placed over that to help the resin flow more easily. To assist in distributing the resin in the mould, an infusion spiral is placed along the entire side of the inlet. A silicone collector is then placed and taped on top of the infusion spiral for the resin inlet. Additional layers of infusion mesh are placed by the outlet to ensure the resin is evenly spread. The vacuum collector is secured to the outlet. The vacuum bag is then placed over the assembly. Sealing tape is used to ensure that the bag is sealed around the edges. Holes are cut into the vacuum bag for the vacuum and resin tubes to be installed. These tubes are secured into the bag with tape to make a seal. The entire assembly is then placed into a vacuum to ensure that the bag is airtight. The resin is then mixed and degassed to remove any air bubbles that may be present. This can be done by placing the resin in a vacuum for a few minutes. The inlet tube is placed into the bucket of resin and the outlet is connected to the resin trap. The resin trap is connected to a pump via tubes. The inlet is clamped and the pump used to remove any air in the bag. The clamp is removed and the resin is allowed to flow through the fibre cloth. Once cured, the bagging material and peel ply are removed and the part removed from the mould (Wanberg, 2010).

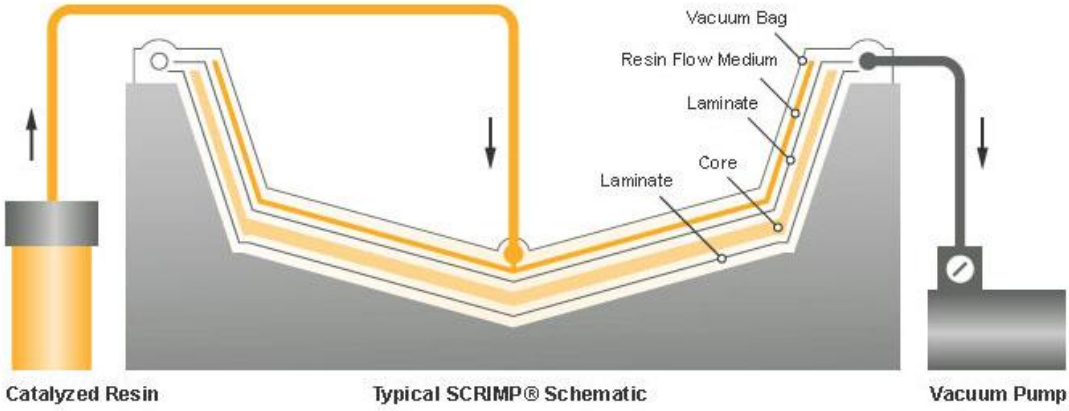

Figure 2.21: The infusion process (J Composites, 2012)

2.3.4.3 Fitting the Core to the Moulded Shell

The selected core material and thickness would be determined from analytical methods and as per the plybook instructions. It is important to consider the thickness and position of the core material before bonding it to the moulded composite structure. The core material must also be designed to

follow the inner and outer contours of the monocoque. A honeycomb structure is difficult to bend around double curvature and often needs to be reshaped to follow the mould contour. This can be done by hand or machined as per a template. A problem that arises from doing this is human error when sizing the core to fit the mould. That means that inaccuracies are going to be present, especially if done by someone of insufficient expertise. It is also important to note that to obtain as light a chassis as possible, to only use core material where necessary. The areas of low stress will be exposed in the FEA and, if possible, no core must be present at areas where the stresses are low enough. A combination of several cores can be used to maximize the performance of the complete monocoque. Different core materials can also be used at the various positions of the structure as some cores provide higher strength, while some are easier to bend around complex shapes.

The next phase is the bonding process of the sandwich structure. This entails bonding the two skins to either side of the core material to achieve maximum load transfer inside the laminate. The bonding is done by coating the entire outer skin, the structure in the mould, which will have foam bonded to it with epoxy or the chosen adhesive. The core will then be bonded and the next layer of laminate material is ready to be completed as per the same steps as previously mentioned. It is important to note that the inside skin of the sandwich structure be designed in the CAD-program for ease of manufacture.

2.3.4.4 Joining Monocoque Sections

A join or split in a monocoque arises when the chassis is manufactured from more than one part. This means that more than one mould was created to manufacture the chassis. If this is not the case it would mean that a single mould would need to be manufactured, which results in an enormous would mould being made. Therefore, the various parts of the chassis need to be joined together. This can either be done by constructing many moulds, doing the layup in each mould separately, and then joining the parts using an adhesive, or the moulds themselves could be joined to form a single mould and one single-shell layup, which requires no joining afterwards.

Some of the advantages of opting for using a separate layup are that if a mistake is made whilst manufacturing one of the chassis parts, not all the parts need to be remanufactured. Another is its simplicity as one has a total overview of the monocoque parts during layup and core fitting. This also means that many people can be working on the various moulds, which means that the manufacturing process will be faster. A disadvantage with this method is that more than one autoclave processes will be required, if being used already. Another is that it results in a line of adhesion on the outside, which may hinder the surface finish and the aerodynamics. Another is that each individual mould may not directly line up with the others, making the part not being able to fit together with the others accurately.

Some of the advantages of using a single-shell layup are that joining of multiple sections is not required, which would reduce the finishing time, however the moulds do need to be joined or machined from a single billet. Only two autoclave processes, one for the outer skin and one for the inner, would be required. There will be no adhesive used to combine the separate parts and therefore the design will weigh less. A disadvantage is that only a limited number of people, usually one, can work inside the mould at once. Another is that it is difficult to lay the laminates within a single mould due to space limitations and that the design is limited in that it would need to be removable as a single piece from the mould.

2.4 Design Simulation and Modelling Techniques

Chassis design requires that the effects of different loading cases during vehicle operation be acknowledged. The load cases can be divided into global and local cases, where the global load cases are concerned with the loads affecting the entire vehicle body, whereas the local load cases are concerned with certain high-stress points, such as mounting locations and boltholes.

2.4.1 Finite Element Analysis

A vehicle's chassis is subjected to various loads whilst in operation, the bulk of which originate from the suspension. The suspension of a vehicle loads the chassis in cornering, braking, and general bump, with the cornering and general bump being the most severe. These loads need to be simulated to determine if the chassis will be able to withstand the operating conditions of the vehicle. A finite element analysis is conducted to accurately simulate this. The attachment points of the chassis, for the front and rear suspension, are required to be analysed to ensure that the chassis is structurally comprehensive. For the purposes of this research, impact loads are not to be simulated, as they are not commonly occurring loads that the vehicle will be subjected to whilst in operation. Only the structural integrity of the chassis under normal operating loads needs to be verified. Thermal loads are also not considered since the vehicle is a solar car and will not generate sufficient heat, such as from an internal combustion engine, to compromise the chassis material.

Regarding modelling the composite material structure of the vehicle, there are two possible approaches. The first approach involves modelling the material core with homogenised solid elements and the skins with shell elements, connected by a contact formulation ('shell-solid-shell' approach). This method simulates skin/core debonding, yields a better representation of core shear deformations and core indentation. However, this is a rather expensive approach. The second approach is to model the whole sandwich structure within a multi-layered shell element ('layered shell' approach). With this method, a particular quantity of combination points are defined through the thickness of the shell element in a user-defined integration rule, representing the core and skin laminate layers (Liu, et al., 2013).

2.4.2 Global Loading Conditions

There are four main global loading scenarios, namely torsional loading, vertical bending, lateral bending, and horizontal lozenging. Torsional loads attempt to twist one end of the chassis in relation to the other. This severely decreases a vehicle's handling, ride comfort and stability. In order to design against this, the torsional stiffness parameter of the chassis must be maximised, without compromising the mass of the vehicle. The suspension of a vehicle ensures that the wheels stay in contact with the ground, but this cannot be accomplished with a chassis of insufficient torsional stiffness. This is because the chassis will simply twist, lifting one corner of the vehicle and thereby raising the suspension, Figure 2.22. Therefore, the wheel will no longer be in contact with the ground. Different situations can cause various torsional loads to arise. The most common case is when a wheel hits a bump while the other three remain at the original ride position. This applies a torque to the chassis, due to the upward movement of the wheel that hits the bump. The resistance to torsional deformation is expressed in Nm/deg.

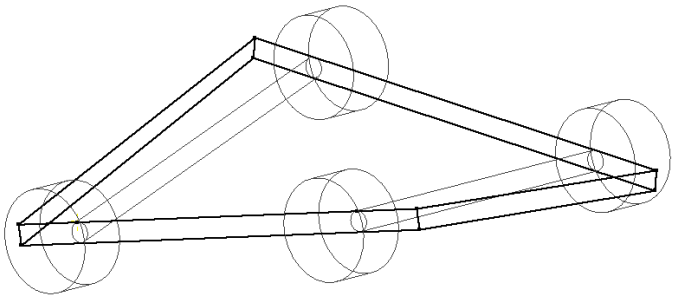

Figure 2.22: Effect of torsional load on a chassis

Vertical bending means that the chassis either squats or dives, due to the longitudinal load transfer under acceleration or deceleration. The weight of the vehicle is transferred to the rear of the vehicle during acceleration, causing the middle of the chassis to bend downward, Figure 2.23. The opposite happens under braking. This vertical deflection does not affect the wheel loads, and generally, a chassis with sufficient torsional stiffness has sufficient bending stiffness (Milliken & Milliken, 1994).

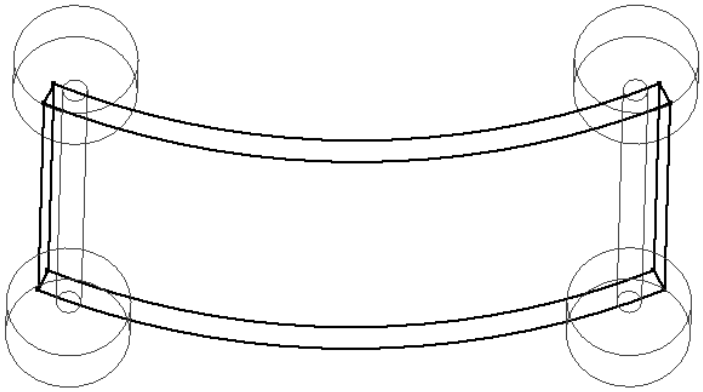

Figure 2.23: Squatting effect due to acceleration

When cornering, centrifugal forces cause lateral bending, Figure 2.24, and roll of the chassis, which tend to throw the vehicle off its projected path. Chassis roll decreases tyre traction, due to the wheels cambering. The weight, height, roll centre, and the resistance from the suspension of the vehicle are some important factors to consider that influence lateral bending and chassis roll (Goerge & Riley, 2002). When cornering, a vehicle's tyres keep the vehicle on its intended path. This induces a torque load that transfers some of the load from the inner tyre face to the outer, which is then transferred to the chassis. This results in lateral chassis bending and vehicle roll. Chassis roll should be limited because it largely affects the stability of the vehicle, however, it does not affect stability as severely as torsional stiffness.

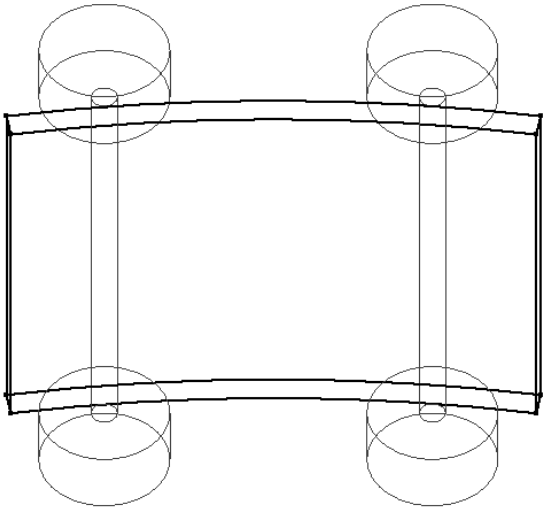

Figure 2.24: Effects of lateral bending on a chassis

Horizontal lozenging, Figure 2.25, occurs when better traction is present on one side of a vehicle. This means that the sides of the vehicle experience unequal horizontal force, causing the chassis to deform in a parallelogram-like fashion. This would occur for example if one side's set of wheels were to lock up under braking and the other were to continue rolling. This scenario is considered

less of a concern than torsional stiffness, vertical bending and lateral bending parameters of chassis design because it is more dependent on the braking system of the vehicle than the chassis (Broad & Gilbert, 2009).

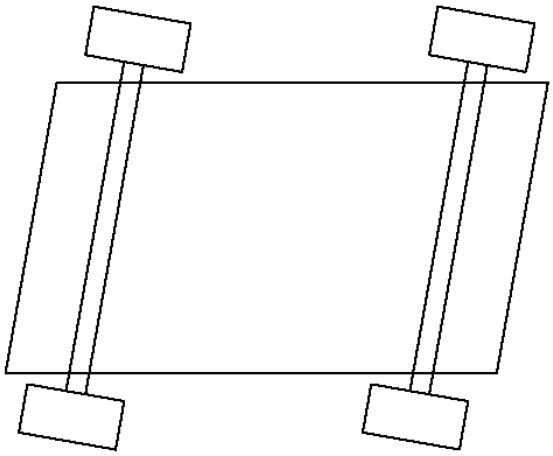

Figure 2.25: Effects of horizontal lozenging

Determining the torsion stiffness of a chassis based only on its geometry can be difficult, due to the complex geometries present in a vehicle. However, by expanding on the principles of solid mechanics and making some simplifications a method can be developed to give an approximate value for the chassis. If the applied torque (T) is related to the angle of twist of a chassis (φ) through equation 2.1:

$$T = \frac{JG\varphi}{L} \tag{2.1}$$

Where J is the polar moment of inertia, G is the material shear modulus of elasticity and L is the characteristic length. Due to the various complex cross sections present in a chassis, the chassis is to be considered as a sequence of different cross-sections secured together. With this assumption and the superposition method, it is possible to analytically determine the overall torsional stiffness for the vehicle's structure by superimposing the individual stiffness values of the components (Crocombe, et al., 2010). As previously mentioned, due to the complex geometries present in a vehicle chassis and the uncertainty of how these geometries will react to torsional loading, it is difficult to analytically determine its torsion stiffness. Therefore, the geometry is simplified by assuming that the cross sections remain undistorted in their own plane. This is a good initial approximation; however, it does yield some inaccuracies in the value obtained (Hibbeler, 2008).

To accurately simulate how the chassis will fair under operating conditions, a finite element analysis is required. Once the CAD design is drawn, it is to be modelled in simulation software. For the finite element analysis of a chassis, the most important design parameter is the torsional

rigidity of the chassis, i.e.: its ability to resist twisting. This is done by fixing the rear suspension mounting locations and applying equal and opposite loads to the front suspension mounting locations (Law, et al., 1998). The torsional stiffness, K_T, of the vehicle is given by equation 2.2:

$$K_T = \frac{T}{\varphi} = \frac{FB}{\varphi_p + \varphi_d} \tag{2.2}$$

where:

$$\varphi_d = tan^{-1}\left(\frac{v_d}{B/_2}\right) \tag{2.3}$$

$$\varphi_p = tan^{-1}\left(\frac{v_p}{B/_2}\right) \tag{2.4}$$

The applied force (*F*) to the front suspension mounting locations induces the torque (*T*) due to the track width of the vehicle (*B*). The angular deflections (φ_d and φ_p) for the driver and passenger sides respectively are determined by the vertical deflections of the passenger (v_p) and driver (v_d) sides of the vehicle, as well as the track width, shown in equations 2.3 and 2.4. Due to the small differences in the vehicle's geometry and the possibility of it having an uneven weight distribution, the angular deflections are not necessarily equal.

2.4.3 Local Loading Conditions

Local load cases are important as they ensure that the attachment points for all the vehicle's components, such as the suspension and power source, are sufficiently strong and rigid enough to support the components under operating conditions. Stress concentrations are generally present at these areas and it is vital that suitable areas are selected for mounting points of the vehicle's components. It is imperative that these mounting locations are sufficiently rigid and have adequate strength to withstand the concentrated loads present. A 'hardpoint' analysis is required to be conducted at these points. This involves analysing the principal stresses at the mounting locations, ensuring that the maximum principal stress does not exceed the ultimate tensile strength of the laminate material. The direction of the maximum principal stress indicates the orientation of the laminate material fibres. This ensures that the failure mode of fibre fracture does not occur.

There are a few methods that are used in the manufacture of 'hardpoints'. The first is the 'pan-down' method, typically used for bolted connections to a composite structure. A 'pan-down' removes the core material at the 'hard point' location and connects the inner and outer skins (Alexander, 1999). This method is done by firstly laying the outer skin, with added layers at the 'hard point' area, and core in the mould as per the plybook. The number of added layers (plies) is determined analytically or by the FEA results. Then it is required to 'pan-down', inside of the

chassis, by cutting a hole in the core material where the ‘hard point’ needs to be and bevel or taper the edges of the hole such that fibres will lay easily over it. It is important that all sharp edges are eliminated, and a nice smooth taper is achieved. The skins are ramped down such that they form a connection with each other. The inside skin is then simply laid as would have normally been done, however, again extra layers are added to build up the area. A ‘pan-down’ is done as opposed to simply inserting a ‘hard point’ to replace the core because removing the core from the bolted connection site alters the mechanical properties of the sandwich structure at that location. Without this, the risk of ripping the skin sheets off the core is high.

The most common technique of fabricating a ‘hard point’ in a composite structure is to drill out a small amount of core material between the inner and outer skins. This method is typically applied for foam core sandwich structures. It is imperative that no reinforcement material is removed from the inner and outer skins. A method to do this is to place a piece of wire, with a ninety-degree bend, in a drill to create a small hole in the inner skin, which is then used to break up the foam core at the desired location. A large enough radius must be made by the bent wire to ensure that the reinforced area is large enough to accommodate the size of the hole to be drilled. The fragmented core material may then be removed using a vacuum. This void is then filled by injecting a mixture of resin and milled fibre through the drilled hole. Once the area has completely cured, a hole may be drilled through the skins and reinforced area to allow a bolt to pass through (Alexander, 1999).

Chapter 3. Chassis Design

The chassis is the central structure of a vehicle, which must support all the components, such as the drive system and the suspension, and withstand the subjected loads, including the mass of each component and the forces exerted during acceleration, braking, and cornering. A well-designed chassis is important to warrant safety, handling, and ride comfort of a vehicle (Mat, et al., 2012). A solar passenger vehicle is a type of vehicle, which is designed to operate solely on the energy harnessed from the sun. This is done using a solar array, which converts the solar energy to electrical energy. This is stored in batteries, which power electric motors to drive the wheels. With the aim of competing in the *Bridgestone World Solar Challenge*, it is imperative that a vehicle that is efficient as possible be designed. Regarding chassis design, this means that the weight must be minimised. As previously mentioned in section 1.2, the chassis will adhere to the *2017 Bridgestone World Solar Challenge* rules and regulations.

3.1 Composite Monocoque Design Methodology

The research developed in this dissertation aims to design a composite monocoque chassis and, in doing so, develop a procedure for future chassis designs. An iterative finite element analysis approach was used to develop and optimise the composite monocoque chassis. Figure 3.1 illustrates the developed design mehtodology process for developing a composite monocoque chassis.

Customer requirements define criteria that the chassis design developers are required to meet. Customer requirements include stipulating the design specifications that the chassis must adhere to. This research adopted customer requirements, detailed in section 1.2, from the *2017 Bridgestone World Solar Challenge*.

Conceptual designs are developed from the knowledge gained by reviewing existing chassis designs and types, and adhering to the customer requirements. Various advantageous chassis design techniques, such as reducing frontal area and providing sufficient area for an appropriate solar array, were adopted from existing solar vehicle chassis designs and applied to the conceptual designs. Once concepts were generated, they were compared with one another and the most suitable design was selected for the preliminary model geometry.

Existing solar vehicle knowledge was used to develop the monocoque geometry, including geometry features such as aerodynamic geometries detailed in section 2.3.3. Material data knowledge gained by reviewing literature concerned with monocoque chassis material selection, detailed in section 2.2, was also used in developing the preliminary design. An initial layup was developed from existing solar vehicle knowledge. Manufacturing processes and limitations were also considered in developing the preliminary model geometry.

Target parameters, including torsional stiffness, strength and weight, were developed from investigating chassis loading conditions and constraints, detailed in section 3.5. The loading conditions were used to develop the finite element analysis model. The torsional loading case developed a torsional stiffness model used in determining the chassis torsional stiffness. Composite chassis failure criteria, discussed in section 3.6, were used to determine a benchmark torsional stiffness value for a lightweight race vehicle chassis.

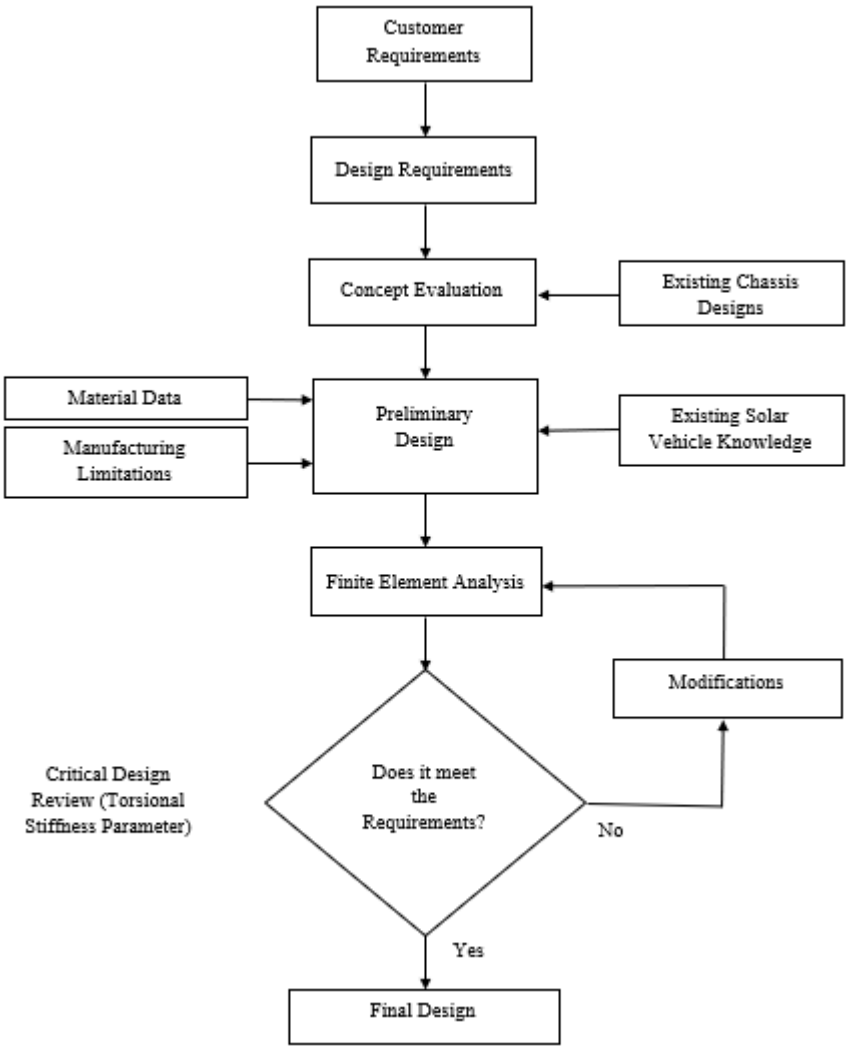

Figure 3.1: Composite monocoque design methodology

The finite element analysis of the composite monocoque chassis begins with the geometry preparation, discussed in section 3.7, of the model. The mesh generation phase, section 3.8, defines and models the composite laminate layers and applies them to the geometry developed in the pre-processing phase. A mech quality analysis, section 3.9, compares several parameters that influence the quality of the mesh and dictates the validity of the mesh. The finite element analysis follows an iterative design process where the torsional stiffness parameter analysed. Geometry and layup modifications are applied to the model until a suitable torsional stiffness value is attained. The purpose of the modifications is to alter the geometry and layup at strategic regions

of the chassis with the intention of increasing the moment of area, and thereby the torsional stiffness, about the rotational axis of the torsional loads. A suitable torsional stiffness indicates that the chassis failure criteria are satisfied and the model can be implemented in the final design phase.

3.2 Conceptual Designs

All the considered conceptual designs for the composite chassis will be discussed in this section. As previously mentioned, due to a composite monocoque chassis being best suited for the application, it was the selected chassis type for all the conceptual designs. Generating conceptual designs aid with determining the final shape of the chassis. This is advantageous because it is important to have an idea of the chassis geometry before optimising it through finite element analysis simulation. Each conceptual design was developed considering the design specifications and requirements of the project. The advantages and disadvantages of each conceptual design were compared and the most suitable design was selected for application in the final design.

3.2.1 Minibus Conceptual Design

The minibus conceptual design, Figure 3.2, is a four-wheeled, dual-hulled monocoque chassis with a tunnel under the chassis centre to reduce the frontal area of the vehicle. This improves the aerodynamic properties of the vehicle, increasing efficiency. The large, box-shaped design, which contributes to its name, means that the vehicle can accommodate four passengers, including the driver, and the four doors make the vehicle more accessible for occupants. The large shape also means that there is plenty of cabin and storage space for the battery pack and various devices. The large roof makes provision for the maximum six square meters of solar panel array. Detachable front and rear shroud covers improve the accessibility of the wheels and suspension systems. The windows all around the vehicle improves the driver's vision around the vehicle. The advantages with this design is that it can carry up to four passengers, has provision for the maximum battery capacity and solar panels which increases the vehicle's driving range for a single charge, and that it is more practical as a passenger vehicle than a smaller vehicle with less cabin space. The disadvantages are that the vehicle is relatively large, increasing weight, and therefore slower and less efficient, and less aesthetically pleasing than a more conventional solar vehicle-looking design. This design would also be expensive to manufacture, as it would require more material than a smaller vehicle to construct the chassis. Manufacturability would also be an issue as the complex geometry of the design would be difficult to layup in, and remove from, a mould.

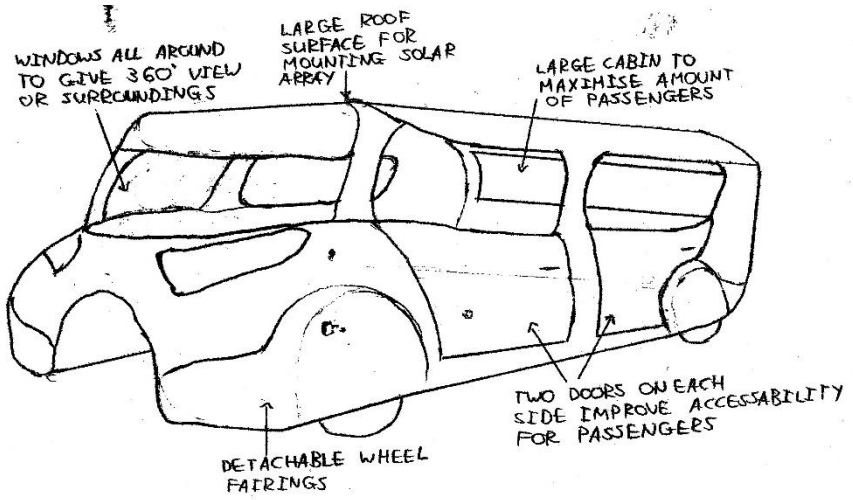

Figure 3.2: Minibus conceptual design sketch

3.2.2 Sports Vehicle Conceptual Design

The sports vehicle conceptual design, Figure 3.3, consists of a four-wheeled vehicle with a monocoque chassis that resembles a sports vehicle. The design is intended to mimic that of a coupe', a closed two-door vehicle body style with a permanently attached roof. Although there are only two doors in this concept, if a large enough cabin is designed, provision for more than two seats may be possible. This design has a tunnel under the centre of the chassis, along the length of the vehicle, to reduce the frontal area of the vehicle, similar to that of four occupant conceptual design. The gradual curves and geometry changes of the hood, roof and shroud of the vehicle make it aerodynamic and more aesthetically pleasing. The hood and roof will be the area intended for the solar panels to be fitted. The chassis has detachable wheel arch covers that improve the aerodynamic properties of the vehicle and allow for improved accessibility of the wheels and suspension systems. The side of the vehicle has an inward curve that also reduces the frontal area of the chassis. The provision for only two occupants results in a more compact design when compared to the four-occupant concept, reducing weight. This does mean that the vehicle should be faster and more energy efficient. The advantages of this design are that it is a compact vehicle that is fast, efficient and aesthetically pleasing. The design is lightweight and has seating space for at least two passengers, including the driver. The smaller design means that less material is required to construct the chassis than with the larger design of conceptual design one. The smaller size of this design also means that a more compact suspension system could be implemented, as the vehicle will weigh less and have less occupants, which would allow for smaller shrouds and a larger cove beneath the vehicle, reducing its frontal area. The disadvantages are that there is less cabin space in the vehicle and less space for solar panels. This means that it will be difficult to accommodate the allowable battery pack and six square meters of solar panels, however, if the roof is made as large as possible and a rear windscreen is sacrificed, more solar panels could be fitted to the chassis. It will be challenging to manufacture this design as it will be

difficult to remove such a geometry from a mould without destroying the mould. Therefore, a reusable single mould would be impossible to implement. A split moulding technique may be a solution to this.

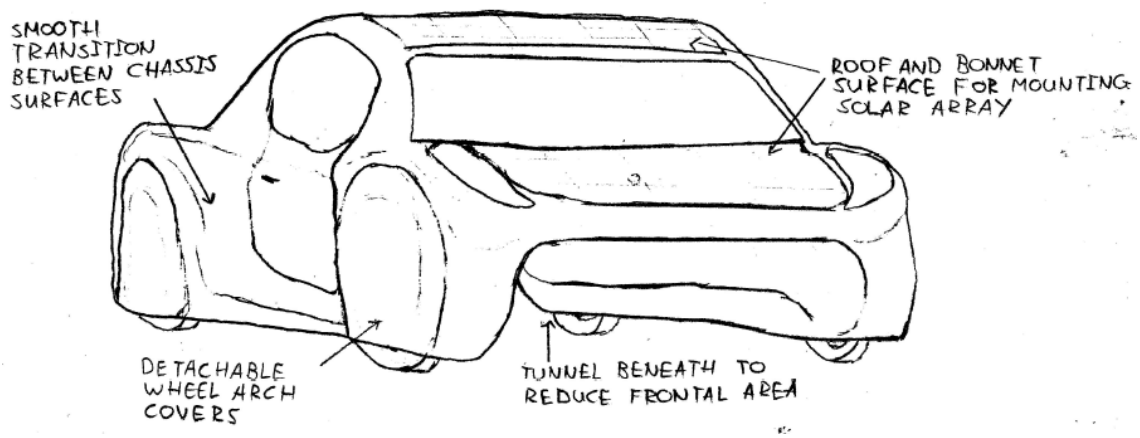

Figure 3.3: Sports vehicle conceptual design sketch

3.2.3 Catamaran-like Solar Vehicle Conceptual Design

The conventional solar vehicle conceptual design, Figure 3.4, is a dual shroud catamaran-like design that benefits from the concept of symmetry. This allows for equal weight distribution since each shroud will seat a single passenger. This design is similar to that of the *2015 UKZN Solar Vehicle, Hulamin*, with the difference being that the right-hand shroud will have provision for a passenger rather than mounting points for the various electronics. A middle compartment could be designed for the storage of the electronic components. Each shroud would have a canopy that encapsulates each passenger, which reduces the frontal area of the vehicle. The height of the canopies will be designed to the size of the passengers' head height. A thin top shell could be utilized to mount the solar array. This also reduces the surface friction as well as frontal area. The advantages of this design are that it utilizes the concept of symmetry, improving the weight distribution and ease of manufacture of the monocoque. The long shrouds will provide a smooth airflow over the vehicle. The dual shrouds and canopies greatly reduce the frontal area and thus improves the aerodynamics of the vehicle. However, the canopies do not have a gradual slope, to maximise the area for solar panels, which reduces the aerodynamic properties of the design. *UKZN* has a great deal of experience with a solar vehicle of this shape because this design is similar to that of the *2015 UKZN Solar Vehicle, Hulamin*. Therefore, there is experience and knowledge concerning the manufacture optimal design for this geometry. The bottom shell of this design is the only part that is required to be laid-up in a mould, which makes it relatively easy to layup in, and remove from, a mould. Therefore, the cost to manufacture this vehicle should be relatively low when compared to the other conceptual designs. The disadvantages of the design are that second canopy decreases the available area to mount the solar panels. The fact that the main body and top shell are not a single member will reduce the torsional stiffness properties of

the design. The design does not resemble that of a conventional road vehicle and is therefore not very aesthetically pleasing.

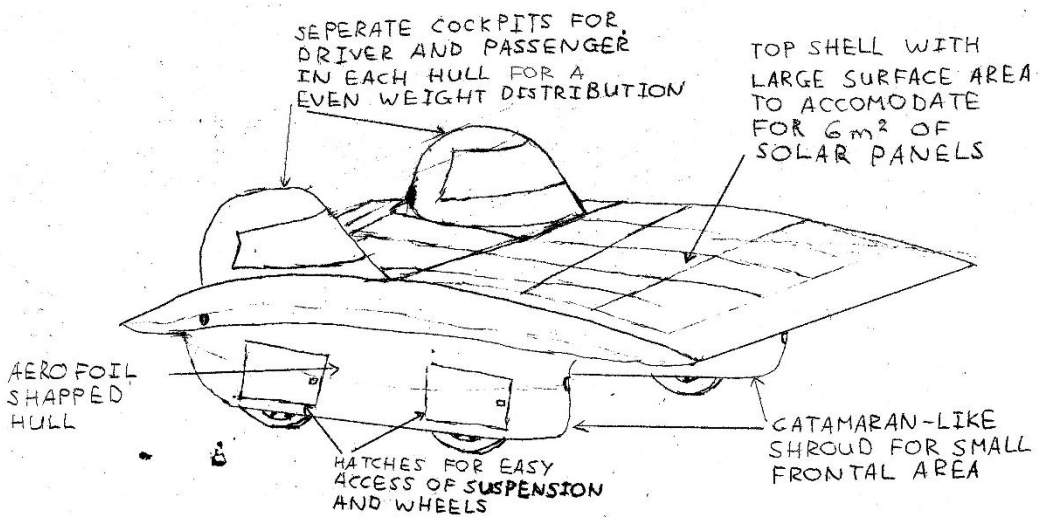

Figure 3.4: Conventional solar vehicle conceptual design sketch

3.3 Conceptual Design Selection

In this section, the conceptual designs were compared to one another regarding the categories of: mass, manufacturability, practicality, cost, aesthetics, and frontal area. Each of these categories will be given a score out of 5 for each concept and the significance of the category weighted accordingly. The score of each category will be multiplied by the weighting for that category. The mass of the vehicle is a key performance indicator regarding chassis design, therefore this category will be weighted by 5, with the lowest mass scoring the highest. The manufacturability will be weighted by 2, with the easiest to manufacturing scoring highest, since modern advances in manufacturing techniques have resulted in many complex manufacturing processes, enabling the manufacture of intricate geometries. Since this is a passenger vehicle, practicality is a very significant category to consider. Therefore, it shall be weighted by 7, with the more practical vehicles scoring higher. The cost of producing the design is weighted by 1, with the cheapest scoring highest, as a budget has not been specified. The aesthetic properties will be weighted by 5, with the most aesthetically pleasing scoring highest, because this parameter depicts how appealing the vehicle is. The aerodynamic characteristics, including frontal area, contribute greatly to the vehicle's efficiency and it will be weighted by 3, because the optimisation of the aerodynamic properties is beyond the scope of this research, with smaller frontal area and more aerodynamic geometry scoring higher. The sum of each conceptual design's points was compared and the concept which scored the highest was selected as the most suitable final design. Table 3.1 illustrates the selection matrix of the conceptual designs.

Table 3.1: Conceptual design selection matrix

Category	Weighting	Minibus Concept	Sports Vehicle Concept	Conventional Solar Car Concept
Mass	5	1	3	5
Manufacturability	2	2	3	5
Practicality	7	5	4	2
Cost	1	2	3	4
Aesthetics	5	3	5	1
Aerodynamic Characteristics	3	3	5	4
Total		**70**	**92**	**70**

Key: 1 Very Poor, 2 Poor, 3 Medium, 4 Good, 5 Excellent

The minibus concept is the heaviest of the three concepts, due to its enormous size, and therefore is scores a 1 in this category. It is also a challenging geometry to manufacture and would require complex moulding techniques to manufacture. It scores 2 for manufacturability. This concept scores 5 for practicality as it can accommodate the most occupants of the concepts as well as having the greatest surface area for mounting solar panels. It scores a 2 for cost because it will require the most material to manufacture, due to it being the largest shape. This is not an aesthetically pleasing design; however, its shape resembles that of a minibus. Therefore, it scores a 3 for aesthetics. This concept scores a 3 for aerodynamic characteristics because it will most likely have the largest frontal area of the conceptual designs, and therefore be the least aerodynamic. However, it still maintains a respectable score as the cove beneath its centre decreases its frontal area.

The sports vehicle conceptual design would most likely weigh less than the minibus concept, due to its geometry being more compact, but more than the conventional solar car concept, due to its larger cabin space and body. Therefore, it scores a 3 in this category. Once again, this geometry is challenging to manufacture. It will require similar complex manufacturing methods to those used to manufacture concept one. However, its smaller size may make it more manageable to manufacture than the minibus concept, and therefore it scores a 3 for manufacturability. This concept scores 4 for practicality because it can only accommodate two occupants and has less surface area to mount solar panels than the minibus concept. It scores a 3 for cost because its complex geometry will require a great deal of material to manufacture. It will require less material than the minibus concept to manufacture as it is a more compact design. This concept scores a 5 for aesthetics. Its sports car resemblance makes it visually appealing and aesthetically pleasing.

This concept has a smaller frontal area than the minibus concept but a larger than the conventional solar car concept, therefore it scores a 5 in this category.

The conventional solar car concept scores a 5 for weight, as it is the lightest of the three concepts. This is due to its extremely compact catamaran-like design. Although challenging to manufacture, being separated into a top and bottom shell improve the manufacturability of this design. The bottom shell would be easy to remove from a single reusable mould. It scores a 5 in this category. This is the least practical of the concepts due to its limited cabin space of each canopy for the two allowable occupants. This means that occupants will experience great discomfort when seated for prolonged periods. In addition, the design makes it difficult to get in and out of the vehicle, with the lack of doors and requiring access via the canopy. The large surface area for mounting solar panels does however improve its practicality. Therefore, it scores a 2 for practicality. It scores a 4 for cost because although it requires less material to manufacture than the other two concepts, its catamaran-like shape decreases the torsional stiffness of the chassis, meaning that a lot of reinforcement will be needed to improve this performance parameter. This increases the manufacturing time and amount of material needed. It scores a 1 for aesthetics as its shape does not resemble that of any commercial vehicle and is not visually appealing. This concept has the smallest frontal area of the three designs, however, its dual canopies are not of a gradual enough slope to avoid flow separation, greatly decreasing the aerodynamic properties. It scores a 4 for aerodynamic characteristics.

3.4 Preliminary Design

The preliminary design was selected to be based off sports vehicle concept. The vehicle was designed as a full monocoque chassis that can accommodate two occupants. Figure 3.5 illustrates the preliminary model geometry. The vehicle is symmetrical on the left and right-hand sides. The geometry of the vehicle is designed such that smooth contours exist over the outer shell of the vehicle, to improve its aerodynamic and aesthetic properties. The roof and hood of the vehicle only curve in one direction, to ensure that solar panels can be mounted efficiently. The cove that runs underneath the vehicle, to reduce its frontal area, has a constant area and gradual shape changes for aerodynamic purposes. It must be noted that these aerodynamic geometries were created from a simple understanding of solar vehicle aerodynamics and the optimisation of these are beyond the scope of this research, however, the geometry changes that these aerodynamic attributes cause affect the finite element analysis of the vehicle and must be considered in the simulation.

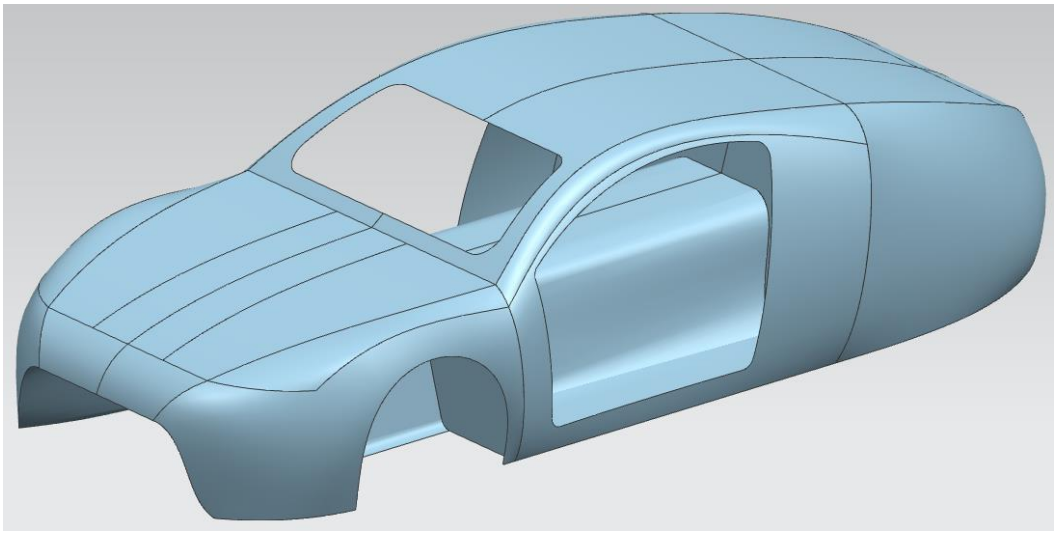

Figure 3.5: Preliminary model geometry

The front shroud, Figure 3.6, has been designed to accommodate a double wishbone suspension system and mechanical steering system. Although this dissertation does not entail the design of these systems, they must be considered so that the chassis can be designed to accommodate them at a later stage. A double wishbone requires the largest shroud space, due to its geometry, and is the suspension system of choice, for the front suspension, for many solar vehicle teams, including *Solar Team Nuon*. This can be attributed to its lightweight design and excellent handling properties. Mechanical steering is a system where all the steering components are mechanically connected by gears and conrods, which results in virtually zero play in the system, improving handling. This is the system used by all vehicle manufacturers in modern vehicles. The support plate, illustrated in Figure 3.6, insolates the cabin occupants from the suspension components. It also serves as a structure to increase the stiffness of the vehicle and forms part of the inner structure. The shroud is open to allow for ease of access of the suspension components and ensure that the wheel can turn as much as possible without encountering the shroud.

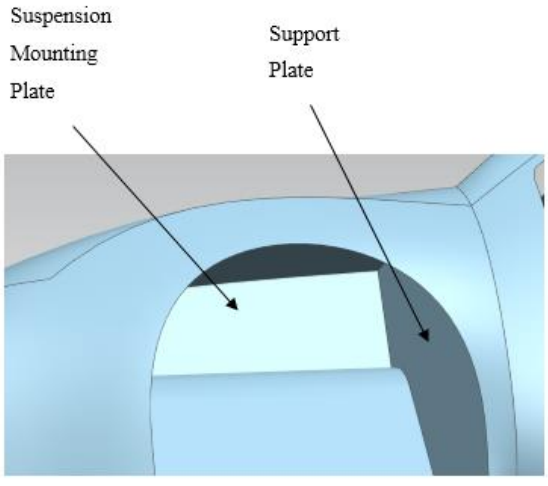

Figure 3.6: Front shroud illustrating suspension mount and support plate

The hulls of the vehicle, Figure 3.7, are shaped to that of an aerofoil, where the front shroud tapers off to a point at the rear, improving aerodynamic properties. There are slots at the bottom of the rear shroud to allow for the rear wheels to contact the road. The front shroud is open to make space for the front wheels to turn for steering. Another support plate, Figure 3.8, is used to stiffen the structure and insolate the vehicle occupants from the rear suspension system. This plate also acts as the mounting plate for the rear suspension system. A trailing arm system was selected to be accommodated for as this suspension is the system of choice for many solar vehicle teams, such as *Solar Team Nuon*. This suspension type is relatively simple, lightweight and stable, as long as the rear wheels do not steer.

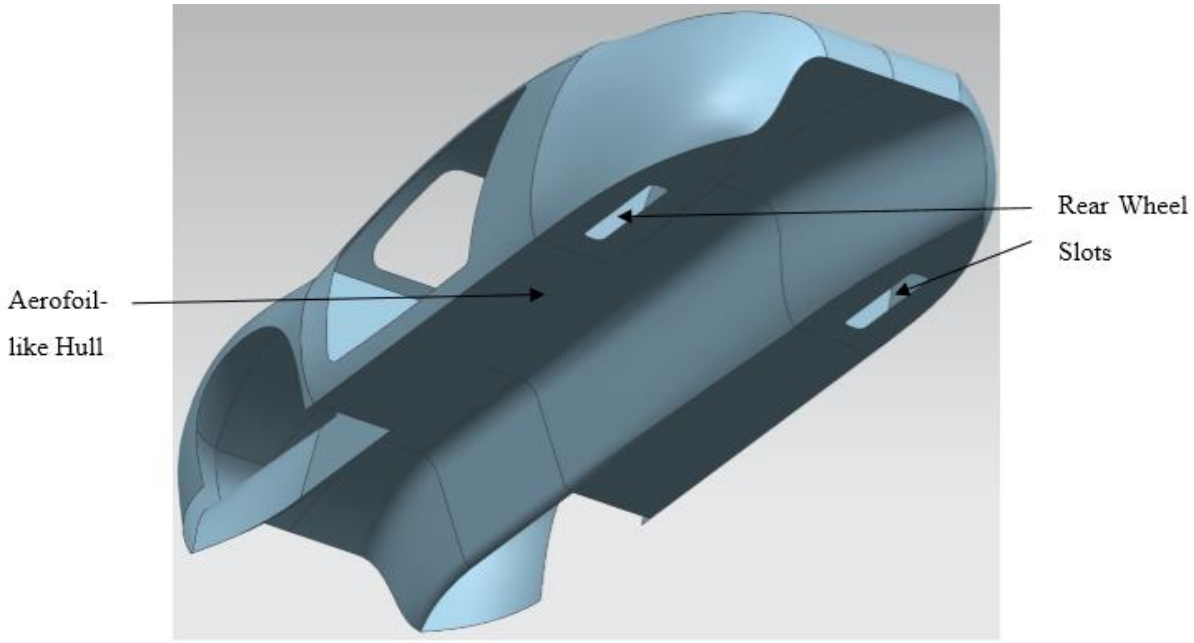

Figure 3.7: Underneath and rear geometry

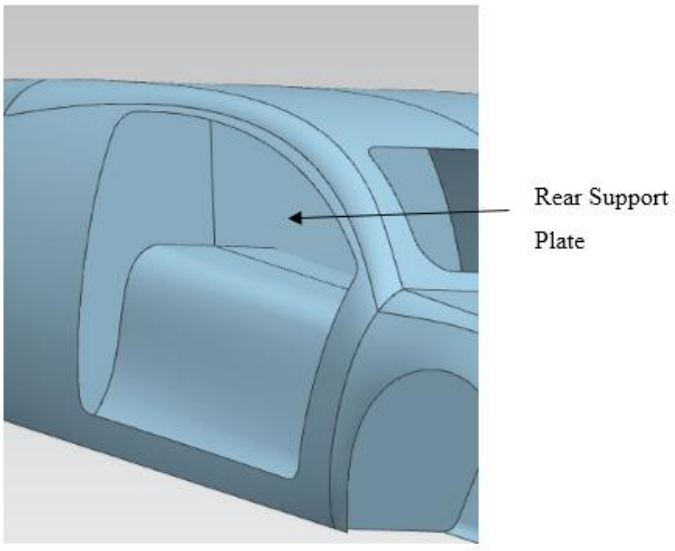

Figure 3.8: Rear support plate

3.5 Loading Conditions and Constraints

Solar vehicle bodies are unique in their design from composites. The chassis is designed in such a way that the body itself experiences very little stress, to minimise weight, as the mounting points and inner structure absorb most of the loads from the suspension. Regarding chassis design, the torsional stiffness is the most important attribute to be satisfied, which requires equal and opposite loads be experienced by the front suspension mounts, whilst the rear suspension mounts are fixed constraints. This simulates the twisting of the vehicle when hitting a bump or pothole, and highly influences the handling of the vehicle. Secondly, comes the strength characteristics, which determines if the chassis will fail under the loading conditions. As previously mentioned, the most severe load case is the bump case, which simulates one the vehicle's wheels hitting a bump of a pothole at high speed. This is the same case used for the torsional stiffness model. This transmits a vertical force through the suspension system to the chassis mounting points. It is difficult to determine the precise magnitude of this load but, a conservative estimate is three times the weight at that wheel, 3g (Carrol, 2003). Next, is estimating the weight of the vehicle. The entire body, including the solar array, battery box, mechanical systems, and electronics, should weigh approximately 90 kg. This is assuming 40 kg for the chassis, 35 kg for the battery box, 10 kg for the mechanical systems, and 5 kg for the electronics. This weight excludes that of the motors and suspension systems as these components are unsprung masses, which do not contribute the weight experienced by the chassis. The weight of the occupants must be included in this as they are considered as sprung mass. As per the *Bridgestone World Solar Challenge* rules and regulations, the mass of each occupant must be at least 80 kg, yielding a total unsprung mass of approximately 250kg for a vehicle with two occupants. Assuming that the vehicle weight is evenly distributed, each wheel should experience a weight of 62.5 kg (625 N). With the bump case exerting a force of approximately 3g, the force from the suspension will be 187.5 kg (1875 N) at each wheel. To accommodate for any miscellaneous component weights this weight can be increased by ten percent, yielding a force of approximately 200 kg (2000 N). Although much greater than the actual weight at each wheel, this force is a conservative approximate to ensure that failure in both yield and fatigue are avoided.

3.6 Failure Criteria

Failure occurs when a structural element cannot perform its intended function. Failure can range from fracture to excessive deflection, with the latter being the easier to detect and correct. The topic of failure criteria of composite materials has been investigated by many researchers for decades. There exist several different approaches to determining the failure of composite materials, each with their own pros and cons. There is no criterion that is universally recognised as being the standard for general loading conditions.

Composite failure criteria can be divided into two main groups, failure criteria not associated with failure modes and failure criteria associated with failure modes (Camanho, 2002). Failure criteria not associated with failure modes use analytical expressions to describe the failure surface as a function of the material's strength, which are based on fitting an expression to a curve attained through experimental methods. Proposed by Tsai and Wu (Tsai & Wu, 1971), the *Tensor Polynomial Criterion* is the general polynomial failure criterion for composite materials, and is expressed by equation 3.1:

$$F_i \cdot \sigma_i + F_{ij} \cdot \sigma_i \cdot \sigma_j + F_{ijk} \cdot \sigma_i \cdot \sigma_j \cdot \sigma_k \leq 1 \tag{3.1}$$

where, for a three-dimensional case, $i, j, k = 1, 2, 3, 4, 5, 6$.

The lamina strengths in the principal directions are given by the parameters F. The stresses in the principal direction are given by σ. Generally, the third order parameter can be neglected. This is because numerous constants are required and laminate properties perpendicular to the reinforcement material direction can be neglected (Tsai & Wu, 1971). This yields equation 3.2:

$$F_i \cdot \sigma_i + F_{ij} \cdot \sigma_i \cdot \sigma_j \leq 1 \tag{3.2}$$

Furthermore, since the material failure is not influenced by the change of direction of shear stresses, all first order shear stresses are negligible, ie: $F_4 = F_5 = F_6 = 0$. For orthotropic materials with three planes of symmetry with the coordinate directions corresponding to the i, j, and k directions, assuming $F_{ij} = F_{ji}$ and no coupling between the normal and shear stress terms, yields equation 3.3:

$$\begin{aligned} &F_1 \cdot \sigma_1 + F_2 \cdot \sigma_2 + F_3 \cdot \sigma_3 + 2F_{12} \cdot \sigma_1 \cdot \sigma_2 + \ 2F_{13} \cdot \sigma_1 \cdot \sigma_3 + 2F_{23} \cdot \sigma_2 \cdot \sigma_3 + \ldots \\ &F_{11} \cdot \sigma_1^2 + F_{22} \cdot \sigma_2^2 + F_{33} \cdot \sigma_3^2 + F_{44} \cdot \sigma_4^2 + F_{55} \cdot \sigma_5^2 + F_{66} \cdot \sigma_6^2 \leq 1 \end{aligned} \tag{3.3}$$

This quadratic formula forms the basis from which other quadratic criteria have been proposed, namely by: Chen (1971), Azzi-Tsai and Tasia (1965), Hoffman (1967), and Gibson (2015). They differ in the method that they determine the tensor stress, varying them to obtain an appropriate fit of the failure surface to the experimental results. It must be noted that these failure criteria do not consider the failure modes, such as fibre fracture, matrix cracking, and delamination.

Damage to composite materials can occur due to various failure modes. These include, amongst others:

- Fibre fracture – snapping of fibres due to high stresses and may occur below the material's ultimate tensile strength.

- Matrix Cracking – high external loading causes the matrix polymer to form cracks. These can be as large as the fibre diameter or more.
- Delamination – the separation of the laminate layers. This is dependent on the bonding material used.
- Fibre debonding – the separation of the fibre and matrix material. Can occur if inadequate resin is applied to the fibre material.

Incorporating these failure modes into the design is difficult and it is simpler to use empirical, lamina composite failure criteria, that is like the failure criteria used in the design of isotropic materials. Governing equations of the lamina failure criteria are modified, with parameters, to fit experimental data, and are then used to describe scenarios for which no experimental data is available.

The torsional stiffness of a chassis is the most important parameter to optimise. However, there comes a point when a chassis is 'stiff enough', where any further increase in the chassis torsional stiffness will not yield any noticeable improvement in the vehicle's performance. In order to determine this, existing chassis were investigated. Table 3.2 summarises the torsional stiffness of various production vehicles (Youwheel, 2016).

Table 3.2: Summary of various vehicle torsional stiffness (Youwheel, 2016)

Vehicle Make	Model	Years of Production	Torsional Stiffness (Nm/deg)
Volkswagen	Golf V GTI	2005 - 2008	25000
McLaren	F1	1995	13500
Mazda	RX-8	2004 - 2011	30000
Chevrolet	Corvette C7	2014 - Present	14500
Ferrari	355	1995	10000
Ford	Mustang Convertible	2003	4800
Lamborghini	Countach	1974 - 1990	2600
Koenigsegg	Agera R	2011 - Present	65000

Table 3.2 shows that modern vehicles have a higher torsional stiffness value than older vehicles. This is because driving safety has become a greater concern in modern years, meaning that vehicles are required to handle better to avoid accidents. It is also due to modern advances in technology and manufacturing that make it possible to create a vehicle chassis with a much greater torsional stiffness value. This is evident as the McLaren F1, which was once the world's fastest production vehicle, capable of attaining speeds of 400 km/h, has a torsional stiffness of 13500 Nm/deg, which is lower than that of a modern VW Golf GTI, which is not capable of

achieving such high speeds, but has a torsional stiffness of 25000 Nm/deg. In addition, older vehicles were manufactured using a separate chassis and body, as opposed to the modern vehicle unibody design, which does not take advantage of the vehicle being a 'one-piece' structure, and therefore has a lower torsional stiffness. It can also be seen that modern high-performance vehicles, such as the Koenigsegg Agera R, have immense torsional stiffness parameters to ensure that the vehicle retains good handling at high speed. It must be noted that these vehicles have such high torsional stiffness parameters because they weigh in excess of 900 kg, and a high torsional stiffness value is needed to ensure that such a heavy mass, travelling at high speed, can be driven safely and effectively.

For lightweight vehicles, such as solar vehicles weighing approximately 250 kg, a lower torsional stiffness value. These small race vehicles generally have torsional stiffness values of roughly 4000 Nm/deg, as opposed to that of a formula one car, which is 20000 Nm/deg and higher (Abrams, 2008). Small race vehicles, such as solar vehicles, do not operate at the high speeds of a formula one vehicle and therefore are not required to be as rigid. Formula one vehicles are required to accelerate, corner, and brake as fast and hard as possible in order to be competitive. The speeds that they reach are more than 300 km/h and it is required that they take sharp corners as fast as possible, which puts immense stress on the chassis, which must deform as little as possible to maintain handling performance. A solar vehicle competes in endurance racing, in which efficiency is key. The vehicle may only travel at highway speeds, between 100 km/h and 120 km/h, and will not encounter any sharp corners that are to be taken at high speed. Only gradual highway curves and bends will need to be prepared for. This means that a solar vehicle does not require an exceptionally high torsional stiffness value, however, in order to stop the vehicle from swaying across the road, or losing control when hitting an irregularity on the road, a high torsional stiffness is needed. A solar vehicle can be considered a small race vehicle, for which a torsional stiffness ranging from 1000 to 4000 Nm/deg is sufficient (Jiang, et al., 2012). A torsional stiffness of 4000 Nm/deg was decided upon as threshold to yield a high-performance chassis.

3.7 Geometry Preparation (Pre-processing)

The geometry preparation phase is where the model of the part to be simulated is generated. This is the first phase of the FEA to analyse the chassis where the geometry model is developed, the pre-processing of the FEA. It is important that when developing a model that the geometry be simplified. This reduces the solution run time of the model and allows for a speedy design iteration. A more complex model can be developed after the base structural analysis. To simplify the geometry, one must avoid sharp edges and high curvature where possible, at areas that are not crucial to the simulation. It is also important to clean up the model where possible by ensuring that geometry edges line up and duplicate features are not present. This can prevent surfaces from merging when sewing or stitching. The studio spline tool is effective in the generation of the wire

frame of the vehicle. This tool allows the user to plot points that form a three-dimensional cure. Each point can be positioned by the user in all three directions to obtain the desired shape. The studio surface tool is used to create a surface within a wireframe boundary. Once all the surfaces are created, the sew tool is used to merge the surfaces together to create a single piece structure. If the surfaces do not sew together, they can be merged using the stitch edge command in the FEM file. This tool enables the user to manually stitch surfaces such that they merge and become one. This creates a monocoque and ensures that all material layups match up with one another.

3.8 Mesh Generation

The laminate composite will be managed by the zone-based process, in the *Siemens NX* Laminate Composites simulation software, which allows the for laminate physical properties to be created and assigned to mesh collectors. Mesh collectors are used to assign specific material layups to meshes. For this four-different laminate physical properties are required. The procedure for conducting a zone-based process is as follows:

1. Create and generate mesh using shell elements.
2. Set the material orientation.
3. Create the laminate physical properties on the mesh collector. Creating plies and determining a layup.
4. Validate the laminate (mesh quality check).

Since a monocoque chassis is essentially a skin, the composite surface structure will be modelled as 2-D shell (CQUAD4) elements to accurately simulate the material behaviour. The split quads command was used, which splits the elements that become too small when approaching high curvature areas and skew as a result. The 2-D laminate elements assume that each ply is in a state of plane stress, plies are perfectly bonded, the transverse displacement and in-plane rotations are continuous, and shear deformation through the thickness of the laminate is constant. Relatively small element sizes, an average of 10 mm, were used to compensate for varying changes in curvature. This was decided to be sufficient because the geometry is relatively large in comparison to this, with a length and width of approximately 4500 mm and 1800 mm respectively, which ensures that the elements will accurately represent the areas of high curvature exhibited by the geometry. The laminate coordinate system is consistent across the mesh. This is the coordinate system that the ply orientation angle will make reference to. The stacking recipe operates on the ply list in the ply layup group to create the selected laminate. A regular stacking recipe builds the ply as per the ply list. It is important that the 2-D element normals be consistently orientated in the direction of the anticipated layup. Since the material is orthotropic and the analysis conducted is 2-D, the Young's moduli, E_1 and E_2, and the Poisson's ratio, NU_{12}, are required along with one of the optional properties, being mass density, shear moduli, strength or strain limits, to name a

few. It must be noted that if tensile, compressive and shear limits are not defined, the ply metrics will not be calculated. When creating a fibre material the fibre type, fibre material, matrix material, and fibre and matrix volume fractions must be specified. Since a woven material type is being used it is required that, in addition to these properties, both warp and weft materials, the ratio of weft to warp fibres, and the weft fibre angle must be specified. The warp fibre direction corresponds to the laminate orientation coordinate system.

3.9 Mesh Quality

The mesh has a noteworthy influence on the solver convergence and solution of every finite element analysis model. It is important to ensure that a quality analysis is conducted on the mesh to improve the quality of the simulation results. This ensures that false confidence in simulation results is not yielded. The relative size and shape between connected elements also have a significant effect on the simulation results. There are several parameters that influence the quality of a mesh, namely being:

- Aspect Ratio – the aspect ratio is the ratio between the shortest and longest side of a 2-D quadrilateral element, with a value closer to one being ideal, and is considered the most important mesh quality parameter to satisfy. For triangulated elements, it is the ratio between the radius of a circle that fits within the triangle boundary and a triangle that encapsulates the triangle, Figure 3.9, in the form of $2R_i/R_o$. Equilateral triangles possess an aspect ratio of 1. This ratio has a substantial effect on the analysis results and if the value is very small, it may be difficult to obtain justifiable results.

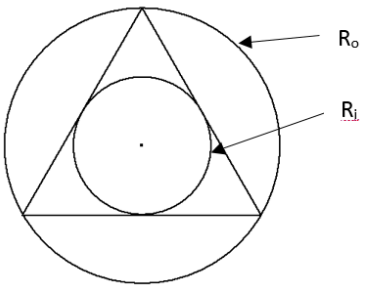

Figure 3.9: Aspect ratio diagram illustrating an equilateral triangle element with a circle radius R_i fitting within the element and the element fitting within a circle radius R_o

- Skew Angle – the skew angle (skewness) is how much the shape deviates from being perpendicular. It is calculated by subtracting the angle, θ, created between the centrelines drawn from each side of the element from 90 degrees, Figure 3.10. The skewness ranges from 0 – 90 degrees, with 0 degrees being ideal.

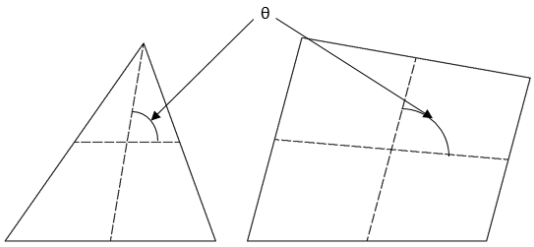

Figure 3.10: The angle *θ* illustrating the deviation of the element from the perpendicular used to determine the skew angle

- Warpage – the warpage assesses how distorted out of plane the element shape is. For 2-D elements, with all nodes lying within the same plane, yielding a warpage value of zero. As the shape distorts out of plane, this value increases. For a 3-D element, the warpage is evaluated for each rectangular face, and the smallest value is chosen as the warpage value. If the warpage value is very large it will negatively affect the analysis result.

Siemen's NX Nastran offers an integrated element quality analysis tool that accounts for the above-mentioned mesh quality checks on each element. The user can control the threshold parameters, such as the aspect ratio, to suit the accuracy required. Once run, the elements which do not satisfy the mesh quality threshold parameters are exposed, illustrated by the elements highlighted as red in Figure 3.11, and the user is required to assess the defective elements and correct them.

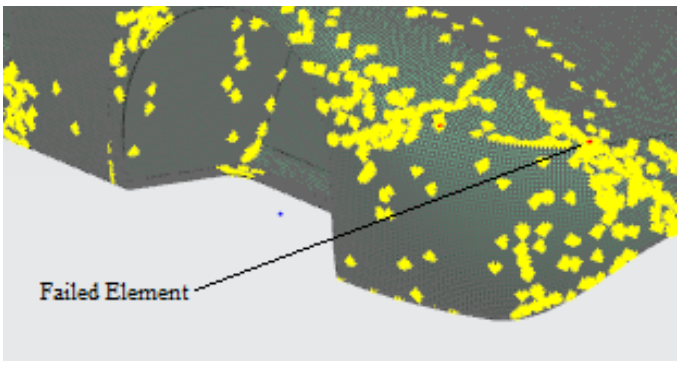

Figure 3.11: *Siemens NX* failed element mesh quality check

The elements highlighted in yellow, Figure 3.11, are not perfect elements, meaning that they do not have a perfect aspect ratio and/or are moderately deformed, however, they are not sufficiently deformed to affect the results of the simulation. The failed elements, in red, are few in number and are not sufficiently significant to affect the simulation results. In addition, the failed elements are located at non-critical areas and therefore do not affect the results.

Chapter 4. Design Simulation

A monocoque chassis is inherently difficult to accurately analyse by analytical methods. It would involve a combination of highly complex mathematical models and assumed simplifications in order to be possible. A computational approach, which is fundamentally based off analytical methods, is a more feasible method in analysing a monocoque chassis. Computational simulations are often used to obtain an approximate idea of how the design will react to operating loads before building a physical model, and yields a means of determining the most suitable materials and geometry design for the application. A finite element analysis can simulate the loads the chassis is subjected to in a shorter period than if analysed by numerical methods. Despite the advantages of finite element analysis, there exists disadvantages. A simulation is only a representation of the real performance, and does not necessarily reveal the influence of the loads by problem variables, such as material properties and geometry topographies, and user input data errors can result in false simulation results.

4.1 Finite Element Analysis Results

The results of the finite element analysis can be divided into the torsional stiffness and hardpoints results. Before these results can be analysed, an optimised model geometry and layup must be generated to ensure that the lightest possible chassis is designed. This is achieved through an iterative process, whereby simulations of a preliminary model are analysed and refined based on the FEA results. To determine the optimal model and layup for the design, a simple static structural analysis of the torsional stiffness loading condition was conducted. The torsional stiffness model was selected because it is the most important parameter to optimise regarding chassis design.

The preliminary model to be simulated, Figure 4.1, was based off the model shown in Figure 3.5, the preliminary model geometry. The geometry was also divided into sections to apply the relevant layups, Figure 4.2. Alterations were made to the geometry to include the suspension mount representations, Figure 4.3, to enable loads and constraints to be implemented. There are two rear suspension mounts, one on each side, to accommodate a trailing arm system, excluding the shock absorber mounts. The front suspension has eight mounting points, four on each side, to accommodate a double wishbone suspension, excluding the shock absorber mounts. The mounts at the front are smaller because there are more of them to distribute the force through the panel, whereas the forces must be distributed at a single mounting area at the rear.

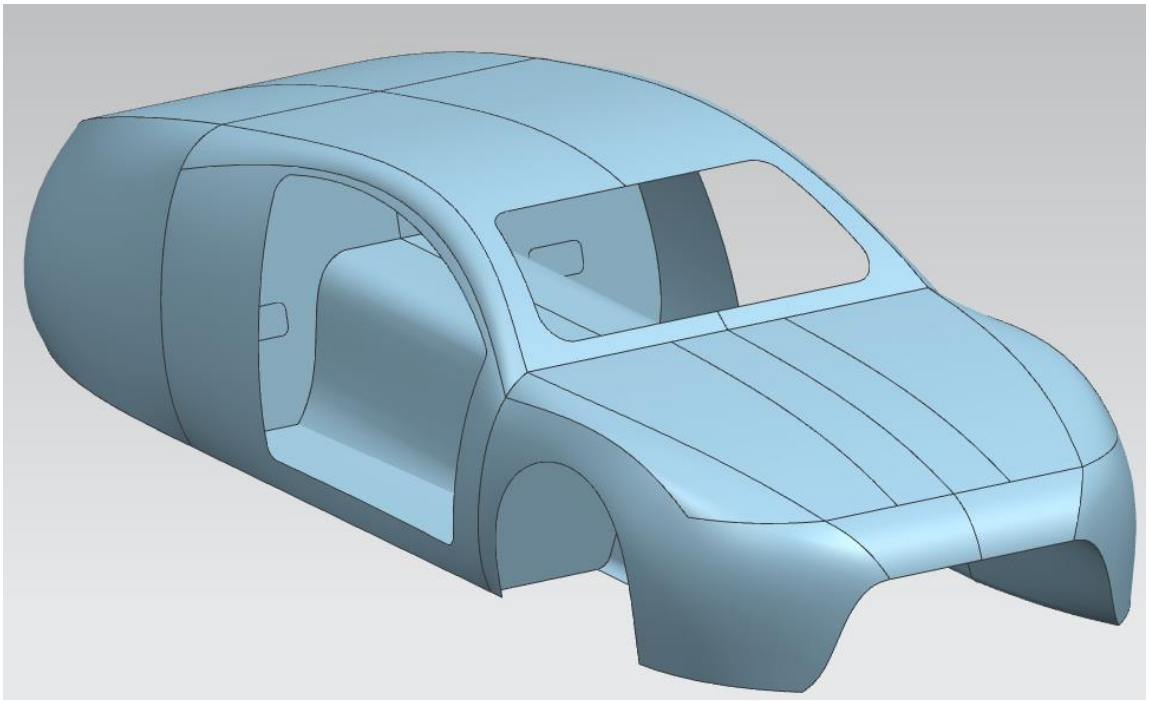

Figure 4.1: Altered preliminary design with suspension mount representations

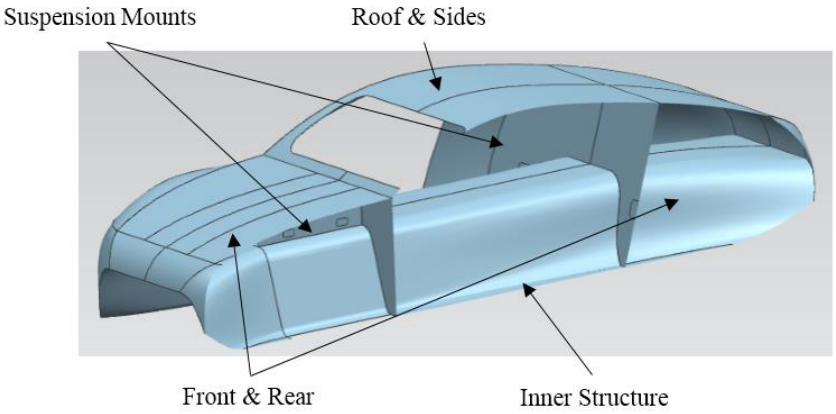

Figure 4.2: Geometry division of model for layups

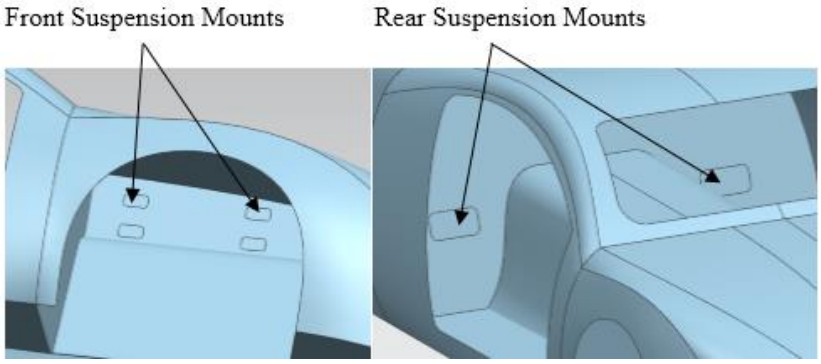

Figure 4.3: Proposed suspension mounts

The details of the mesh are given in section 3.8. In summary, a 10 mm element size, because this met the criteria of compensating for varying changes in curvature of the relatively large geometry

while commencing in adequate computational time, CQUAD4, two-dimensional shell laminate element mesh was used to simulate the material. For these iterative simulations, the *AMT* 2x2 twill weave carbon fibre skin material and cell M60 foam core were used as the materials to simulate the sandwich structure (AMT Composites, 2017). The properties of these materials are summarised in Table 4.3. These materials were selected because the twill weave offers a good compromise between the favourable properties of the plain and satin weave, while the M60 foam core has a low density and has high formability. Once the most suitable geometry is determined from this initial finite element analysis, various core and fibre material combinations can be investigated to determine the most suitable layup. For the simulations, the geometry was divided into sections to apply the appropriate mesh 2-D collector at each section. To determine an initial layup, the 2014 UKZN solar car, *IKlwa*, was decided to be a good starting point. A 2x2 twill CFRP weave fibre material and *Airex* foam core were used in the production of the vehicle. The layups for the relevant sections are shown in Table 4.1 (Rugdeo, et al., 2014).

Table 4.1: 2014 UKZN solar car *IKlwa* material layup (Rugdeo, et al., 2014)

Chassis Section	Layup
Suspension Mounts	$0^o/90^o$; $0^o/90^o$; $\pm45^o$; 10 mm foam core; $\pm45^o$; $0^o/90^o$; $0^o/90^o$
Seat	$0^o/90^o$; $0^o/90^o$; $\pm45^o$; 10 mm foam core; $\pm45^o$; $0^o/90^o$; $0^o/90^o$
Bottom Shell	$0^o/90^o$; 3 mm foam core; $0^o/90^o$
Centre Box Section	$\pm45^o$; $\pm45^o$; 3 mm foam core; $0^o/90^o$; $0^o/90^o$
Longerons	$0^o/90^o$; 10 mm foam core; $0^o/90^o$

The layups above were investigated and the initial layup of the chassis was determined from this, with the exception that a twill weave fibre material and cell M60 foam core material being used. An aluminium honeycomb core will also be investigated as an appropriate core material for the chassis. Since a twill weave is used, only fibre orientations of 0° and 45° are used, as a 0° orientation is the same as a 90° orientation, the same being for a 45° and -45° orientation. Each 2-D collector chassis section layup is shown in Table 4.2.

Table 4.2: Initial chassis layup

Chassis Section	Layup
Roof and Sides	$0^o/90^o$; $\pm45^o$; 10 mm foam core; $\pm45^o$; $0^o/90^o$
Suspension Mounts	$0^o/90^o$; $\pm45^o$; $0^o/90^o$; 10 mm foam core; $0^o/90^o$; $\pm45^o$; $0^o/90^o$
Inner Structure	$0^o/90^o$; $\pm45^o$; 5 mm foam core; $\pm45^o$; $0^o/90^o$
Front and Rear Panels	$\pm45^o$; 3 mm foam core; $0^o/90^o$

The 1-D collectors represent the front suspension, Figure 4.4. The RBE2 elements are rigid connections, of negligible mass, that represent the front suspension arms, and transfer the load experienced from the wheel to the chassis, without influencing the result. This representation is used to generate a means of the force creating a moment about the centre of the vehicle, causing it to twist, to determine the vehicle's torsional stiffness. The rear suspension is constrained to be fixed, as previously mentioned, and equal and opposite forces are placed on the front suspension arms, as illustrated in Figure 4.4.

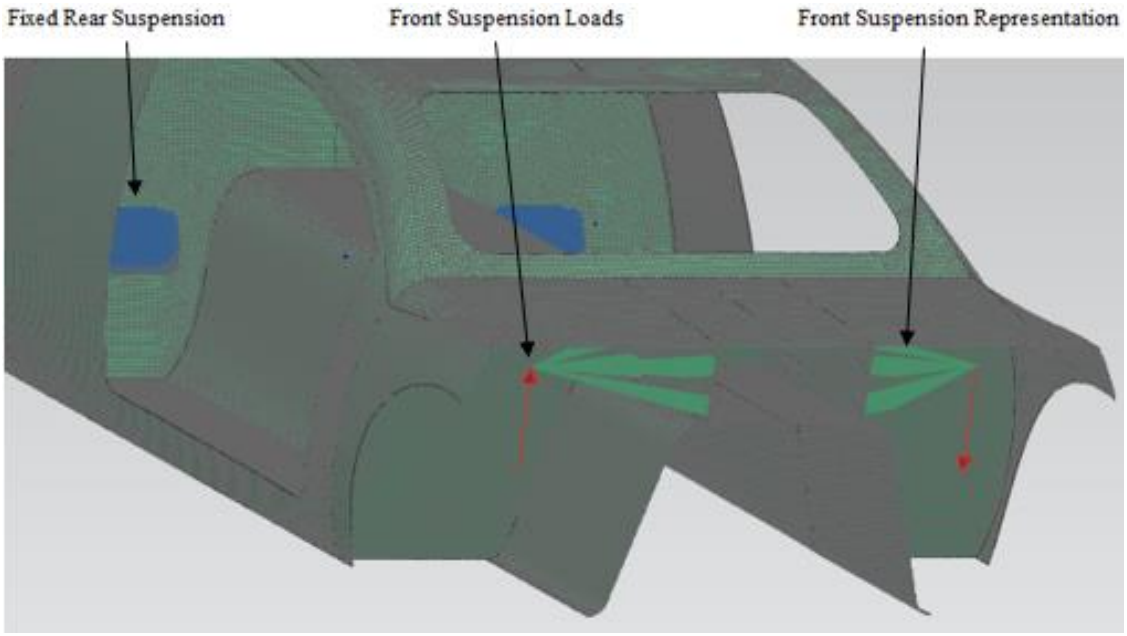

Figure 4.4: Representation of front suspension, constraints and loads

Once the respective meshes were generated, the materials were assigned to their respective layers. The properties of the three materials used as specified by *AMT Composites*, Table 4.3, are as follows:

Table 4.3: Simulation material properties as specified by *AMT Composites*

Material	AMT 2x2 Twill Weave	M60 Cell Foam Core	PCF Aluminium Core
Young's Modulus (E1)	47000 MPa	44 MPa	6.9 MPa
Young's Modulus (E2)	47000 MPa	44MPa	6.9 MPa
Young's Modulus (E3)	N/A	N/A	1241.6 MPa
Density	1600 kg/m^3	65kg/m^3	4919 kg/m^3
Poisson's Ratio (NU)	0.05	0.3	0.1
Poisson's Ratio (NU13)	N/A	N/A	0.1
Poisson's Ratio (NU23)	N/A	N/A	0.1
Shear Modulus (G)	5100 MPa	20 MPa	186.2 MPa
Shear Modulus (G13)	N/A	N/A	469 MPa
Shear Modulus (G23)	N/A	N/A	413.9 MPa
Tsai-Wu Interaction Coefficient (F12)	$-3.7567x10^{-6}$ mm^4/N^2	-1.122334 mm^4/N^2	$-1.051x10^{-6}$ mm^4/N^2
Tension Strength (ST)	464.4 MPa	0.81 MPa	0.7 MPa
Tension Strength (ST2)	464.4 MPa	0.81 MPa	0.7 MPa
Tension Strength (ST3)	N/A	N/A	0.7 MPa
Compression Strength (SC)	286.6 MPa	0.55 MPa	0.7 MPa
Compression Strength (SC2)	286.6 MPa	0.55 MPa	0.7 MPa
Compression Strength (SC3)	N/A	N/A	0.7 MPa
Shear Strength (SS)	53.4 MPa	0.68 MPa	1.4 MPa

4.1.1 Finite Element Analysis of Preliminary Model

The design methodology of a composite monocoque chassis, figure 3.1, specifies that a finite element analysis is conducted on the preliminary model. The preliminary model is then subjected to loading conditions and constraints specified by the torsional loading case. A two thousand newton load, details of which are given in section 3.5, was applied at each of the front suspension arms, in opposite directions. A linear static simulation was developed as it accurately simulates the torsional stiffness model. The simulation was run and the results interpreted. Figure 4.5 shows the maximum deflection result, which is used to determine the torsional stiffness of the vehicle, of 7.16 mm occurs at the outer front shroud faring under the loading conditions. It also shows that the deflection of the chassis decreases toward the rear of the chassis, where the rear suspension mounts are constrained to be fixed.

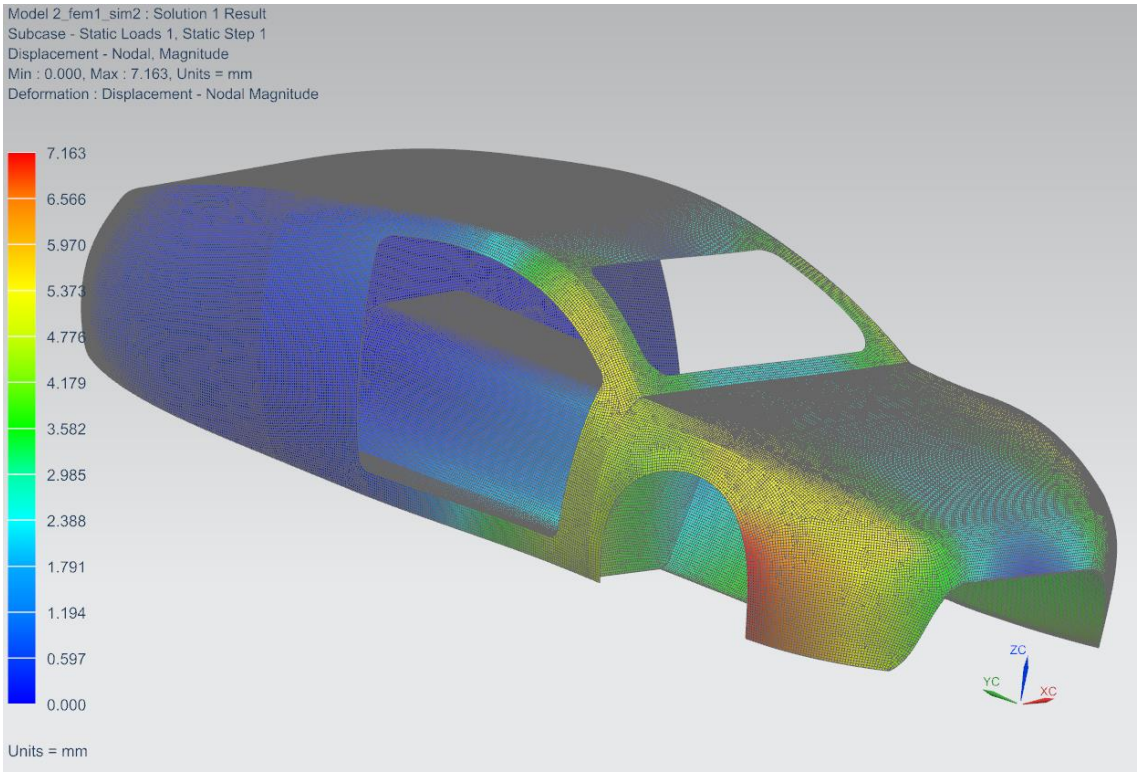

Figure 4.5: Linear static deflection result of the preliminary model

The torsional stiffness value is calculated using equation 2.2, in tandem with equations 2.3 and 2.4, detailed in section 2.4.2, sample calculations of which are detailed in Appendix A. To do this the deflection of the suspension mount ends are required. Figure 4.6 shows the deflection of the front suspension ends of approximately 5.37 mm, and when substituted into equation 2.3 and equation 2.4, which is then substituted into equation 2.2, along with a force of 2000 N and a track width of 1.3 m, yields a torsional stiffness of 2745 Nm/deg. It must be noted that this vehicle is perfectly symmetrical about the YC plane, in Figure 4.5, which means that the values yielded from equation 2.3 and equation 2.4 are the same. This torsional stiffness value below the required

parameter of 4000 Nm/deg, specified in section 3.6. In order to increase the torsional stiffness of the chassis, the geometry and the layups must be altered until a suitable torsional stiffness value is obtained under the same loading conditions.

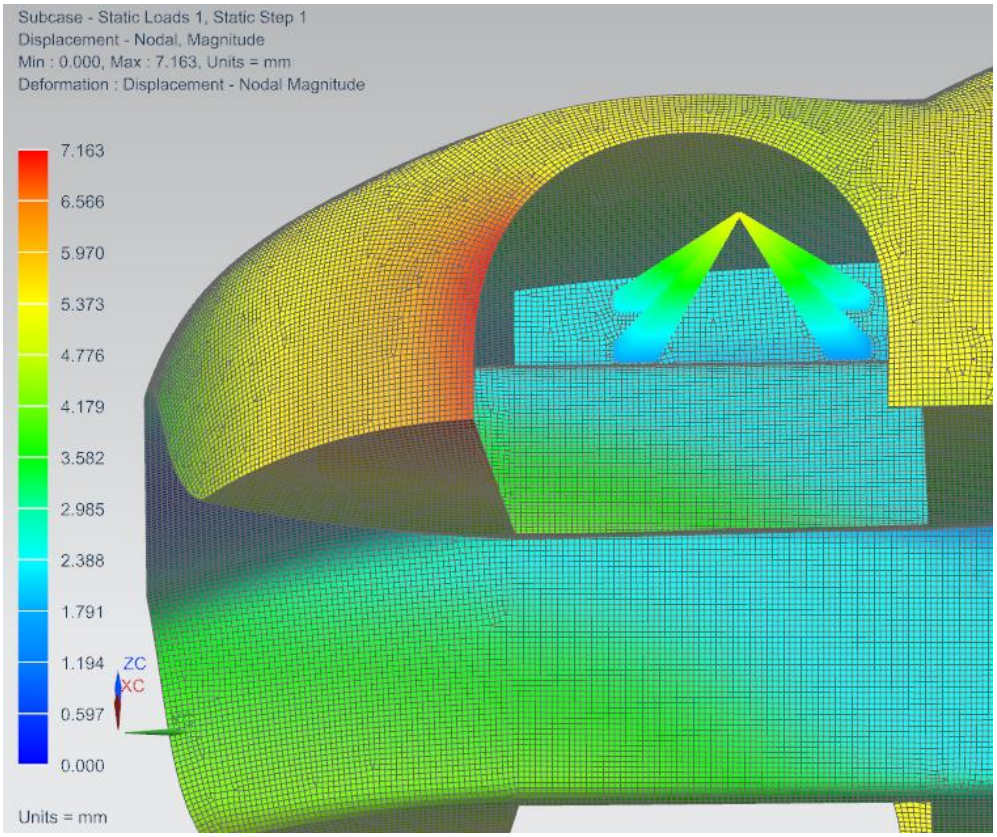

Figure 4.6: Close-up of linear static deflection result of preliminary model front suspension

To determine a geometry of minimum weight, the finite element analysis Von Mises ply stress result must be analysed. The ply stress is very low throughout most the chassis, Figure 4.7, with most of the stress being below 20 MPa. Some areas of the chassis, such as the sides of the windscreen, experience higher stresses of approximately 40 MPa, which is still well below the ultimate strength of the fibre material. The maximum ply stress of 120.55 MPa occurs at just one element at the front suspension mount, Figure 4.8, with most the panel only experiencing between 20 MPa and 40 MPa. This indicates the layup and geometry handle the stress well and can withstand the applied loads. The estimated mass of the chassis is calculated by summing the solid property individual masses from each layup section. The preliminary model yielded a mass of 43.41 kg.

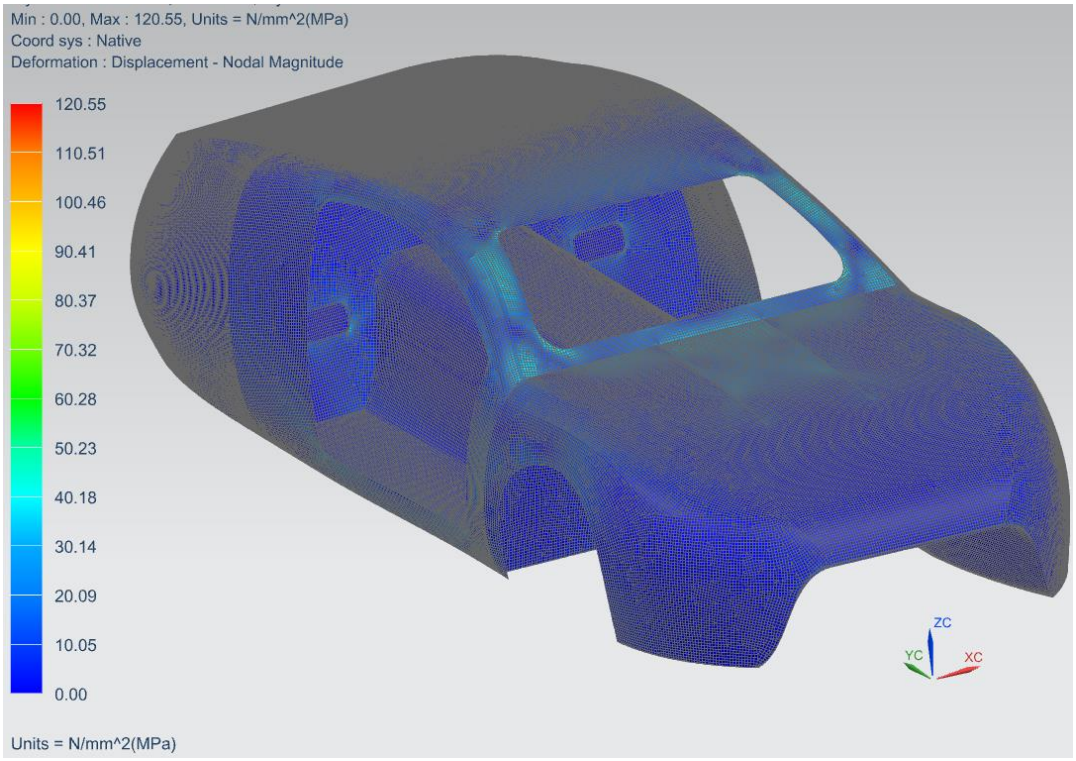

Figure 4.7: Linear static Von Mises ply stress result of the preliminary model

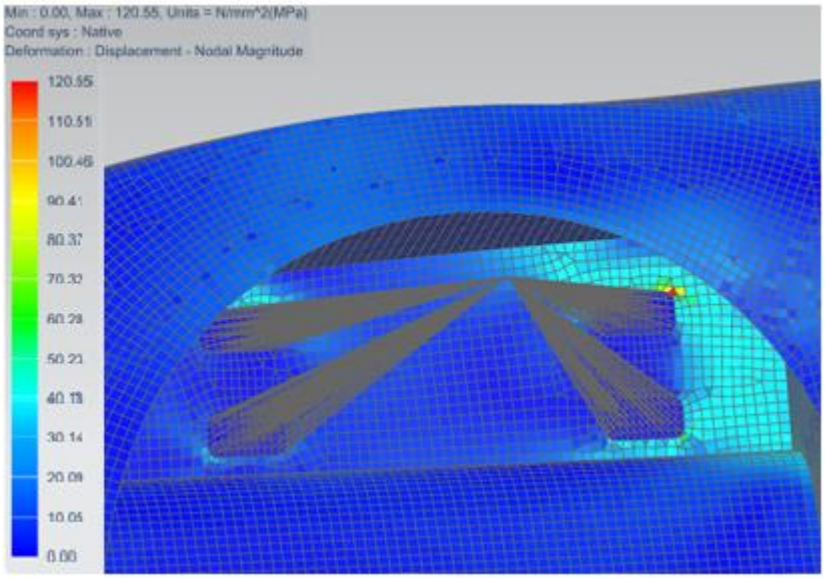

Figure 4.8: Maximum stressed element at top right chassis suspension mount of the preliminary model

The low applied stresses indicate that the geometry and layup can be altered to reduce the number of layers of the layups, as well as core thicknesses, and material can be removed from strategic areas to reduce the mass of the chassis. The rear of the chassis was shown to experience the least stress and deflection. In addition, the rear of the chassis is situated beyond the rear suspension mounting points, meaning that any alteration to the layup or geometry in that region will have little effect on the torsional stiffness of the chassis. It was decided to remove a section from the

rear support plate to reduce the weight of the chassis, and to remove sections from the rear sides, Figure 4.9, for weight reduction and rear suspension accessibility.

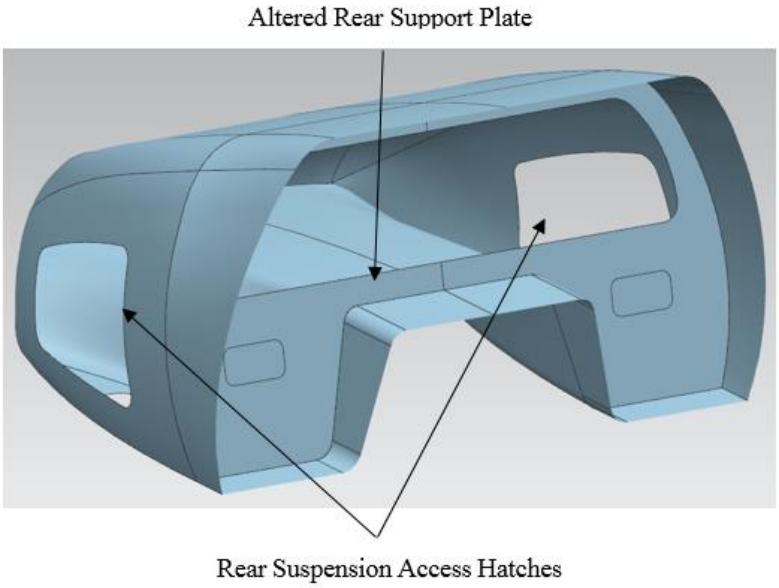

Figure 4.9: Altered rear geometry with modified rear support plate and rear suspension access hatches

4.1.2 Inner Structure Core Thickness Increase and Altered Rear Geometry Modification

The finite element analysis of the preliminary model resulted in an inadequate torsional stiffness value. Figure 3.1 dictates that the chassis model be modified, and the simulation revaluated through an iterative finite element analysis process. To address the low torsional stiffness parameter, the layups were altered by increasing the core material thickness. The core thickness of the inner structure was increased from 5 mm to 10 mm and not the amount of fibre material layers, as increasing the core material thickness yields a greater increase in the structure's moment of area than adding layers of fibre material, see Table 2.3. The chassis inner structure is largely responsible for the ability of the chassis to resist twisting and increasing its core thickness will increase the chassis torsional stiffness value. The altered layups are shown in Table 4.4:

Table 4.4: Altered Layups

Chassis Section	Layup
Roof and Sides	$0^o/90^o$; $\pm45^o$; 10 mm foam core; $\pm45^o$; $0^o/90^o$
Suspension Mounts	$0^o/90^o$; $\pm45^o$; $0^o/90^o$; 10 mm foam core; $0^o/90^o$; $\pm45^o$; $0^o/90^o$
Inner Structure	$0^o/90^o$; $\pm45^o$; 10 mm foam core; $\pm45^o$; $0^o/90^o$
Front and Rear	$\pm45^o$; 3 mm foam core; $0^o/90^o$

To accurately compare the results, the same loading conditions and constraints were applied to the altered model as in the preliminary model. Figure 4.10 shows a maximum deflection located at the front wheel arch of 8.05 mm, 0.88 mm more than exhibited in the preliminary model, Figure 4.5, at the front wheel faring. This deflection however has no consequence on the torsional stiffness of the chassis. The deflection that governs the torsional stiffness is that of the front suspension ends, Figure 4.11, which shows a deflection of approximately 5.37 mm at the front suspension ends. Substituted into the relevant equations, yields a torsional stiffness of 2745 Nm/deg. This is the same value that was attained from the preliminary model results.

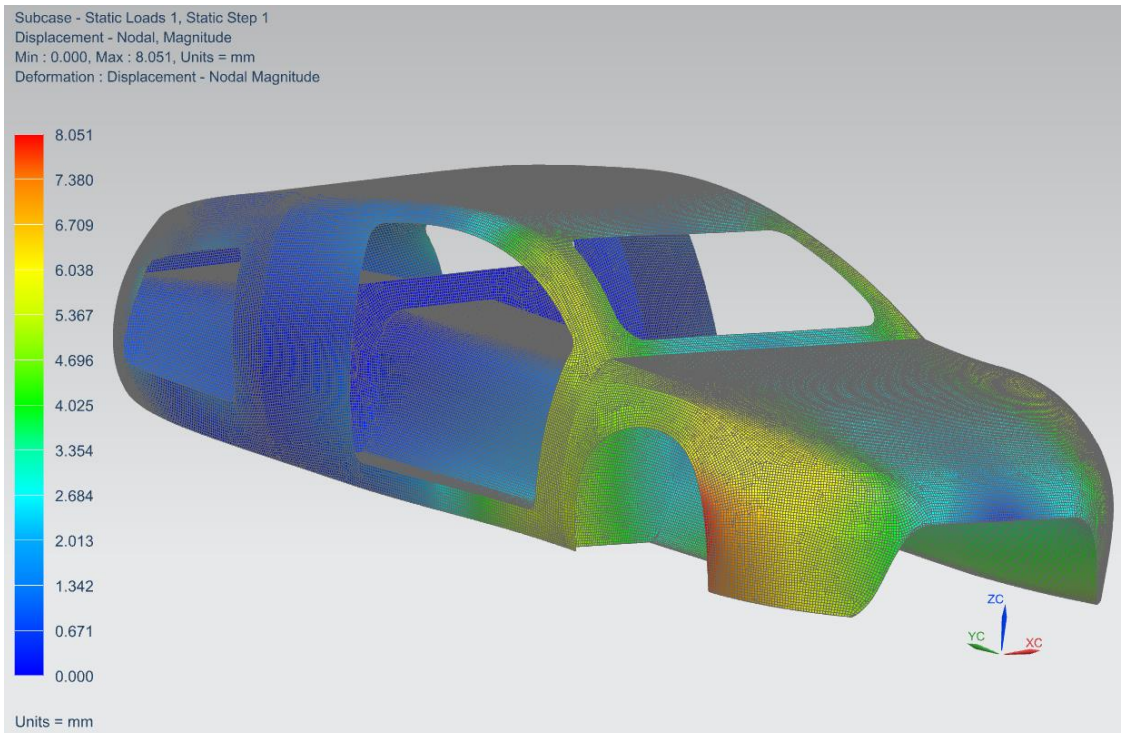

Figure 4.10: Linear static deflection result of the chassis with 10 mm inner structure core thickness and altered rear support plate and rear suspension access

The unchanged torsional stiffness, when compared to the torsional stiffness result in section 4.1.1, indicates that the modifications made did not significantly affect the chassis torsional stiffness. The addition of the rear suspension access hatches decreased the chassis moment of area about the torsional axis of the applied load, YC axis in Figure 4.10, decreasing the ability of the chassis to resist twisting. The increased inner structure core thickness increased the torsional stiffness value, particularly by restricting the deflection of the front suspension mounts, by the same magnitude that the rear geometry modifications decreased the torsional stiffness. This resulted in the chassis torsional stiffness remaining 2745 Nm/deg.

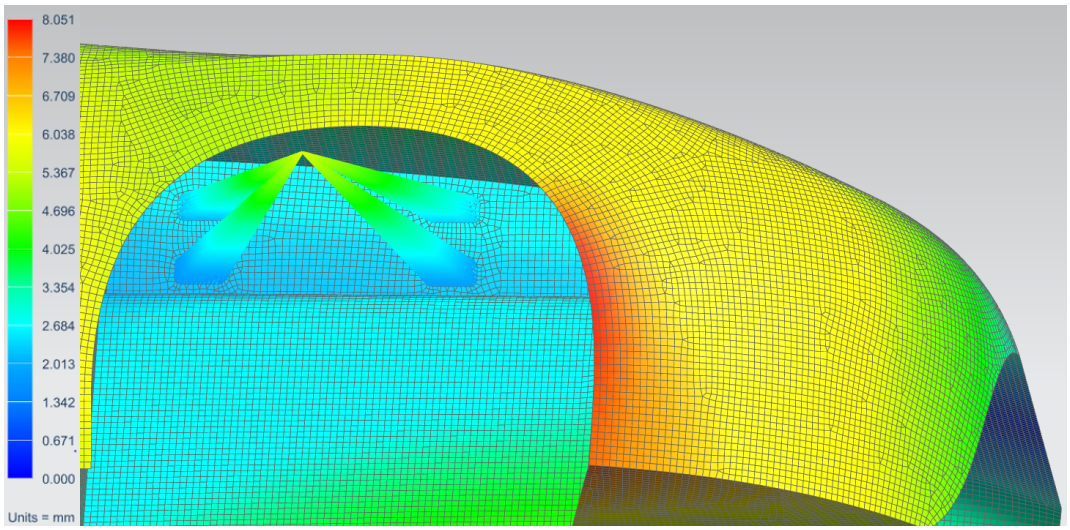

Figure 4.11: Close-up of linear static deflection result of the chassis with 10 mm inner structure core thickness and altered rear support plate and rear suspension access

Figure 4.12 indicates a maximum Von Mises ply stress, located at the same suspension mount in the preliminary model, of 145.54 MPa, 20.73 % more than the maximum ply stress experienced by the preliminary model, Figure 4.7. To ensure that the stress does not exceed the material strength, the direction of the stress is required. The maximum principal stress determines the direction of the maximum ply stress and is discussed in section 4.2. It is interesting to note that the alterations to the chassis did not result in a significant increase in the torsional stiffness, however the Von Mises ply stress experienced by the structure increased significantly. This indicates that the stress is susceptible to removing material within the structure, and if too much material is removed, the stress may exceed the yield strength of the material. The mass of the chassis increased to 43.87 kg, a 1 % increase when compared to the mass of the preliminary model in section 4.1.1, which is too high when considering that there was no increase in the torsional stiffness value. This increase in mass is attributed to the increase in the inner structure core thickness.

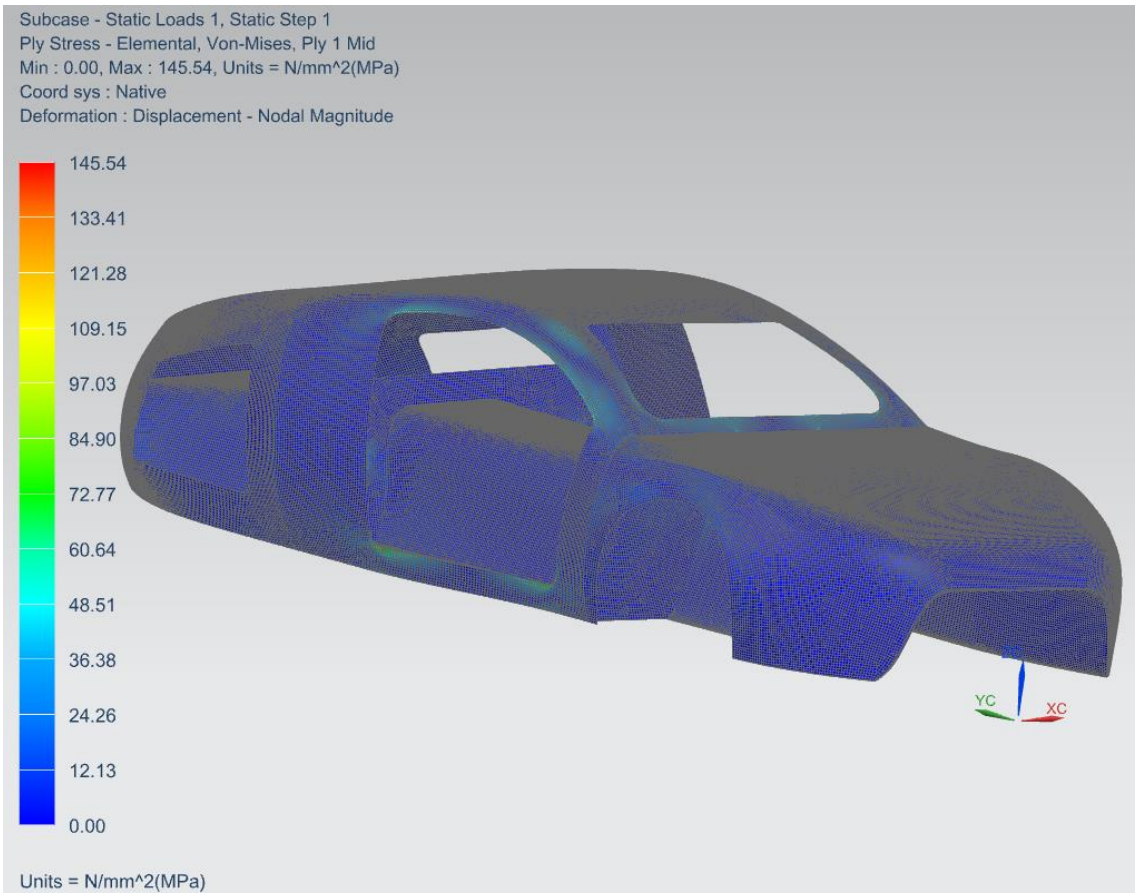

Figure 4.12: Linear Static Von Mises ply stress of altered chassis with rear support plate and rear suspension access

4.1.3 Door Recess Effect on Torsional Stiffness

The increase in the inner structure core thickness resulted in the mass of the structure increasing significantly. The torsional stiffness increase resulting from the increased inner structure core thickness does not warrant this increase in mass. A design modification that increases the chassis torsional stiffness whilst not significantly increasing the mass of the chassis was to be determined. The geometry modification made to the chassis rear geometry significantly affected the torsional stiffness by decreasing the structures moment of area. Increasing the structure's moment of area about the torsional axis will increase the chassis torsional stiffness value. The door recesses, windscreen recess and front wheel arches are essentially holes in the chassis that decrease its moment of area, and thereby the ability of the chassis to resist twisting. Only the door recesses were considered because they are the only non-standardised component to increase the torsional stiffness as opposed to the front and rear wheel arches and windscreen. In addition, they are situated in the middle of the chassis where majority of the torsional stiffness is created and are orientated parallel to the rotational axis of the torsional loading condition, yielding the largest increase in the moment of area. The door recesses were enclosed to yield the maximum increase in torsional stiffness. Although this is an unrealistic representation of the model, it is an effective means of determining the effect that the recesses have on the torsional stiffness. For this

simulation, the layups, shown in Table 4.4, and loading conditions and constraints as per the previous model in section 4.1.2 were used. Figure 4.13 shows the deflection result of the linear static simulation of the chassis with enclosed doors.

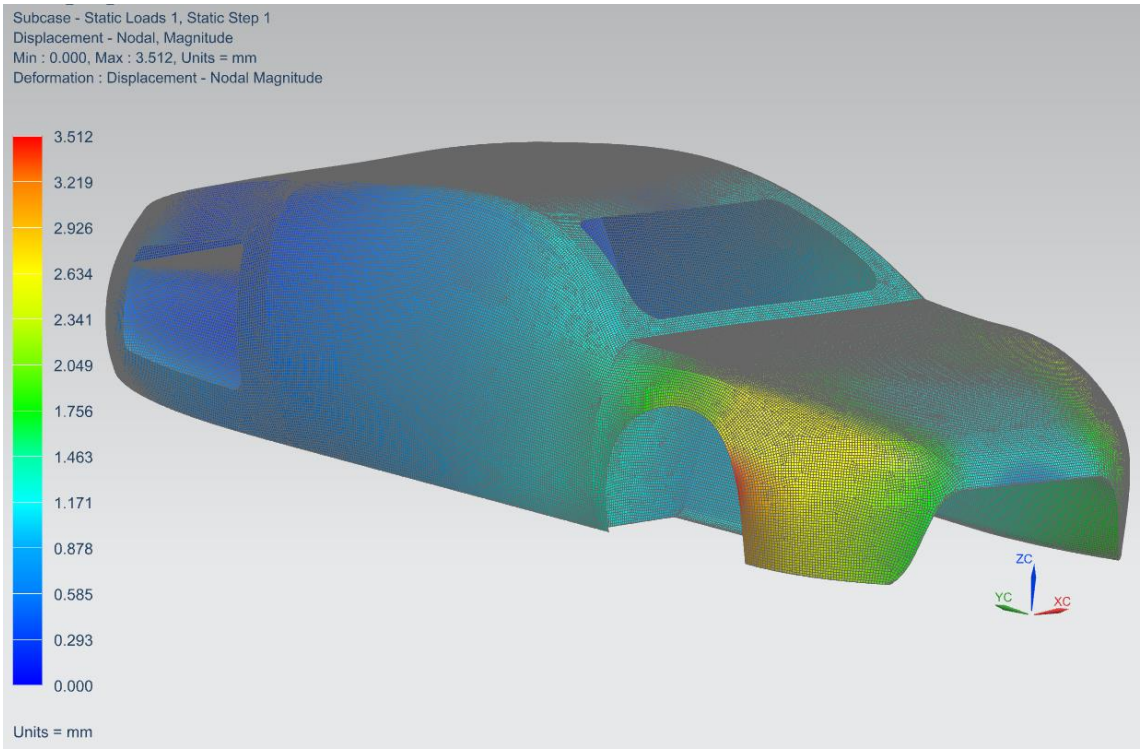

Figure 4.13: Linear static deflection result of the chassis modelled with enclosed door recesses

Figure 4.13 shows a maximum deflection of 3.51 mm, which is 4.54 mm less deflection than exhibited by the previous model. This shows a 56.4 % reduction in the maximum deflection of the chassis. To determine the effect that the enclosed doors have on the torsional stiffness, the deflection of the front suspension mount ends must be analysed. Figure 4.14 shows a deflection of 2.50 mm, 2.87 mm less than the previous model. When substituted into the relevant equations, yields a torsional stiffness value of 5899 Nm/deg, an increase of 114.7 %. This proves that the holes created in the chassis for the doors have a significant effect on the torsional stiffness of the chassis.

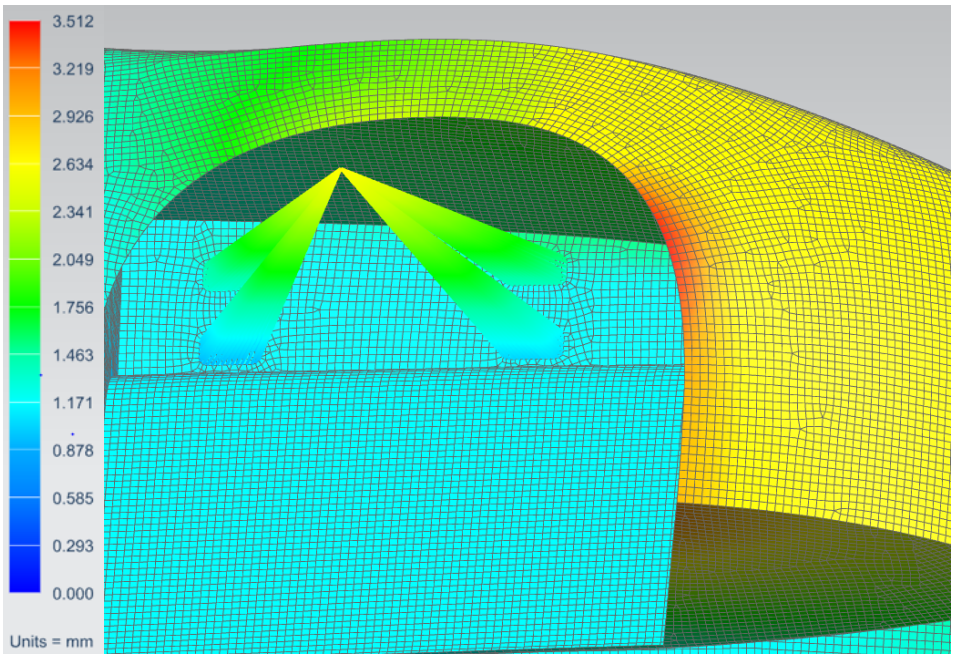

Figure 4.14: Close-up of linear static deflection result of the chassis modelled with enclosed door recesses

To remain consistent, the maximum stress in the chassis was also analysed, Figure 4.15 shows the maximum Von Mises ply stress result of the chassis modelled with enclosed door recesses. A maximum stress of 136.71 MPa was experienced by the chassis. The maximum stress in the structure had decreased by 8.83 MPa than in the previous model, however, it must be noted that although the enclosed doors resulted in a significant increase in the torsional stiffness value of the chassis, the maximum stress only decreased by 6.1 %. This shows that the holes in the chassis for the doors do not significantly account for the stresses experienced by the chassis, but do however affect the torsional stiffness greatly. The enclosed doors increased the mass of the vehicle to 44.84 kg, an increase of 1.43 kg and 0.97 kg when compared to the masses of the chassis models in section 4.1.1 and 4.1.2 respectively. It must be noted that this mass increase was due to the door recesses being enclosed. Both models in sections 4.1.1 and 4.1.2 did not consider the mass of the doors. Therefore the mass of the chassis must only be analysed once door recesses are present in order to obtain an accurate comparison.

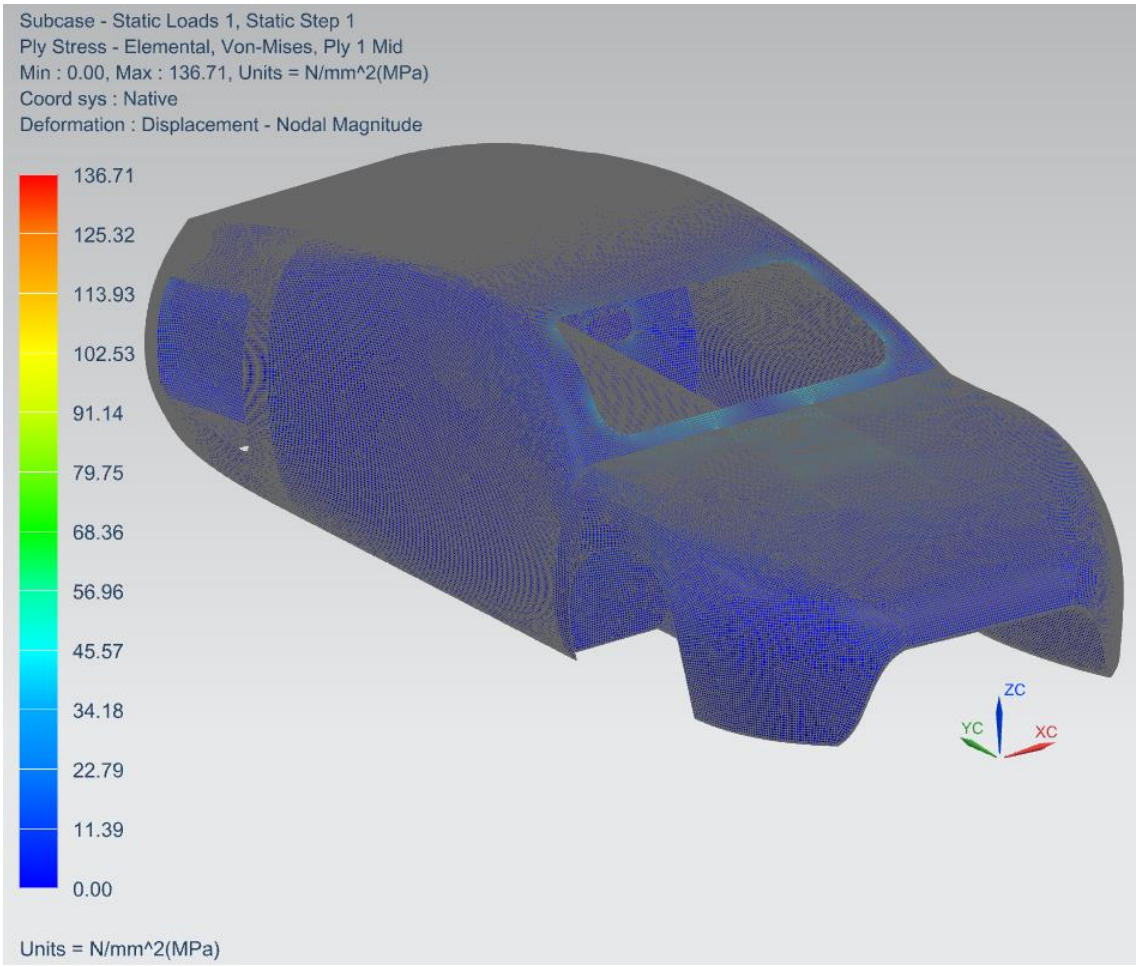

Figure 4.15: Linear Static Von Mises ply stress result of chassis modelled with enclosed door recesses

4.1.4 Door Recess Geometry Modification

The finite element analysis of the chassis with enclosed doors proved that the door recesses had a significant effect on the ability of the chassis to resist twisting. Therefore, to address the issue of achieving the required torsional stiffness parameter, it was decided to reduce the size of the door recesses on the chassis. This gives more surface area on the sides of the chassis, increasing the structure's resistance to deflection. The reduced size of the door recess geometry meant that the height of the structure could be reduced, decreasing the frontal area of the chassis and improving aerodynamic properties. Figure 4.16 illustrates altered model to be simulated with smaller door openings. The model retains the altered rear support plate and rear access holes, as evident in the previous models from sections 4.1.2 and 4.1.3. The reduced door recess size resulted in the height of the chassis decreasing, giving the chassis a slenderer geometry. This reduction in size of the geometry also decreases the mass of the structure.

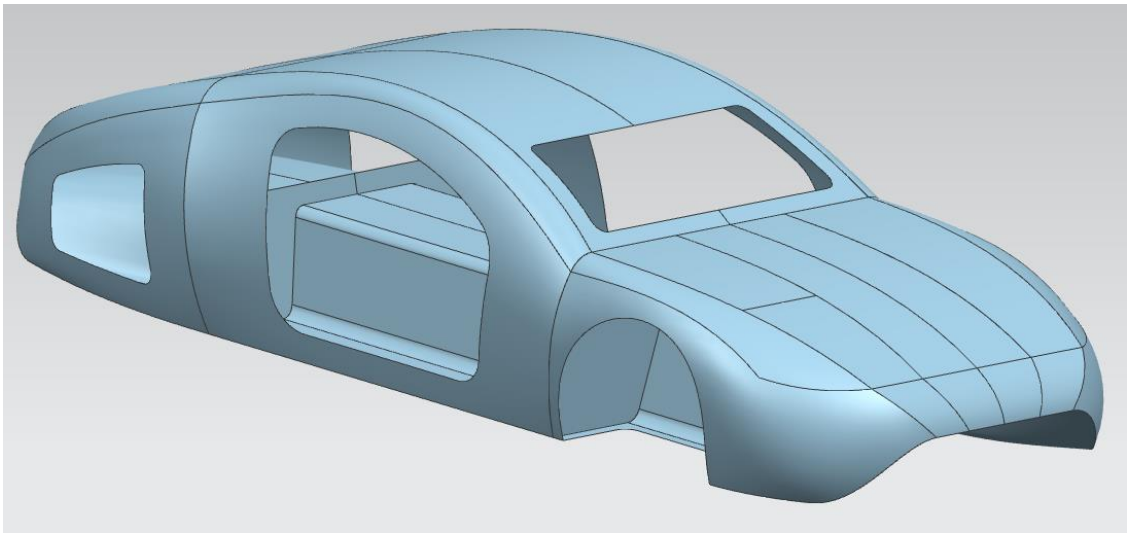

Figure 4.16: Altered model with Compact door recesses

The layups and loading conditions for the finite element analysis remained the same as used in section 4.1.2. This was decided to yield a comparison between the compact door recesses model results to the results in section 4.1.2. Firstly, the maximum deflection of the structure, Figure 4.17, was analysed. Figure 4.17 shows a maximum deflection located at the front wheel arch of 6.24 mm, 1.81 mm less deflection than shown in Figure 4.10. This is a 22.52 % reduction in the maximum deflection of the structure. The location of the maximum deflection is consistent with the maximum deflection in section 4.1.2.

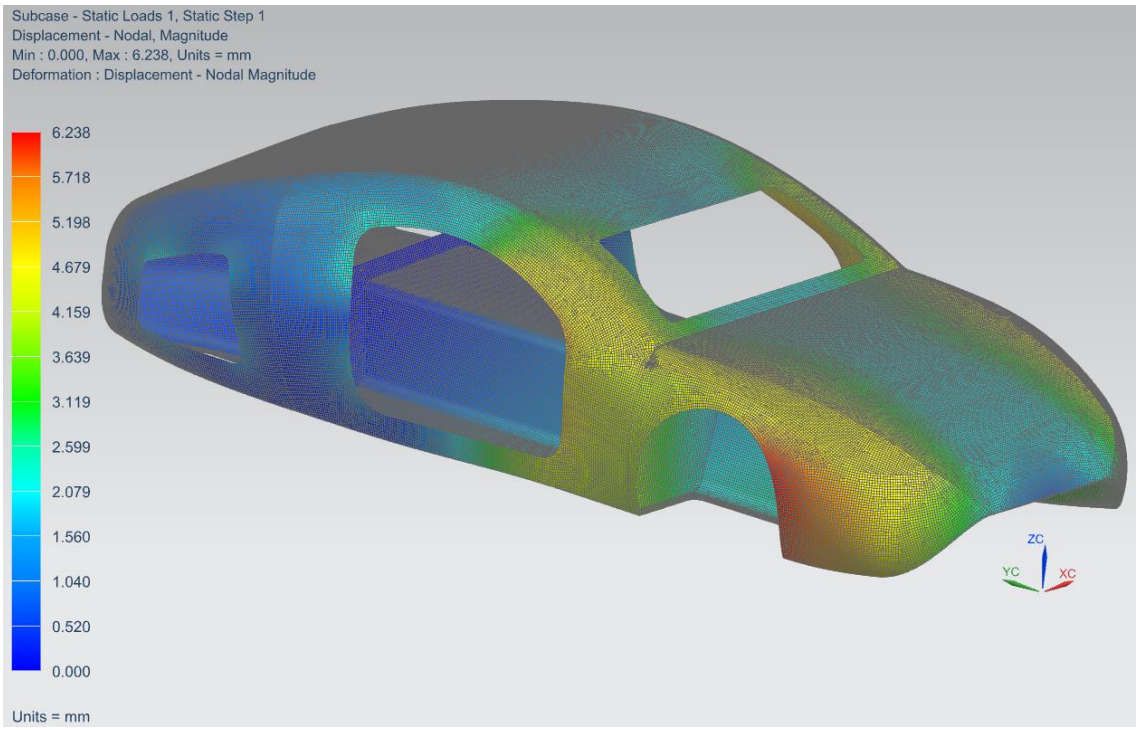

Figure 4.17: Linear static deflection result of chassis with compact door recesses

To determine the torsional stiffness, the deflection of the front suspension mount ends needed to be examined. Figure 4.18 shows a deflection of approximately 4.16 mm, 1.21 mm less than the deflection shown in Figure 4.11. When substituted into the relevant equations, the deflection yields a torsional stiffness of 3546 Nm/deg, a 29.04 % increase in the torsional stiffness. This value is only 454 Nm/deg below the required value of 4000 Nm/deg. The minor geometry modification of compacting the door recesses resulted in a substantial increase in the chassis torsional stiffness.

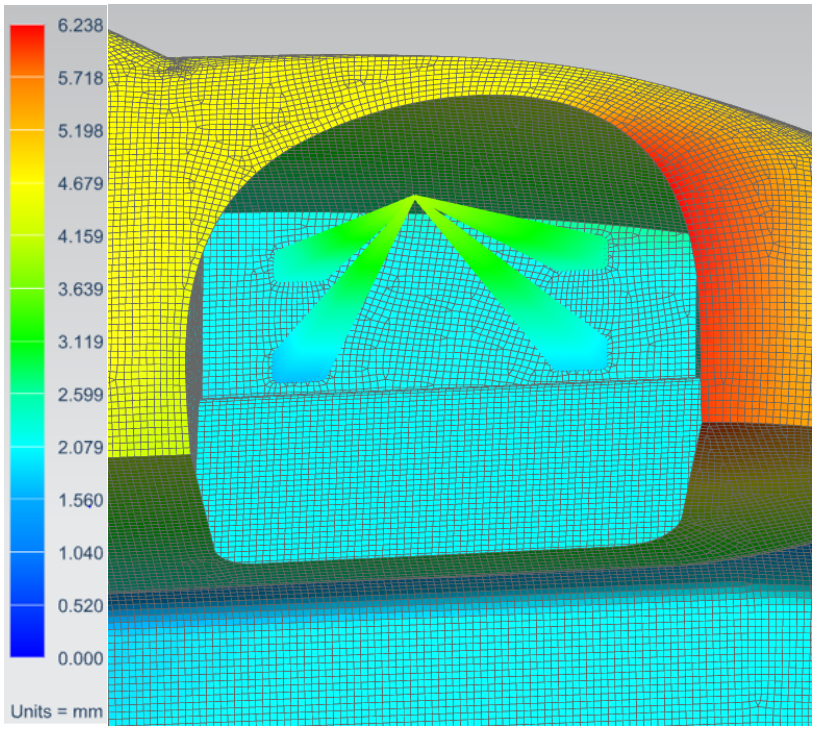

Figure 4.18: Close-up linear static deflection result of front suspension mount of chassis with compact door openings

Figure 4.19 shows a maximum Von Mises ply stress of 102.89 MPa, a decrease in the maximum stress of 42.65 MPa than exhibited by the model in Figure 4.12. The maximum Von Mises ply stress decreased by 29.3 % from a minor geometry alteration, as with the improvement to the torsional stiffness parameter. The mass of the model was reduced to 42.45 kg by compacting the model geometry, a decrease of 1.42 kg when compared to the mass of the model in section 4.1.2.

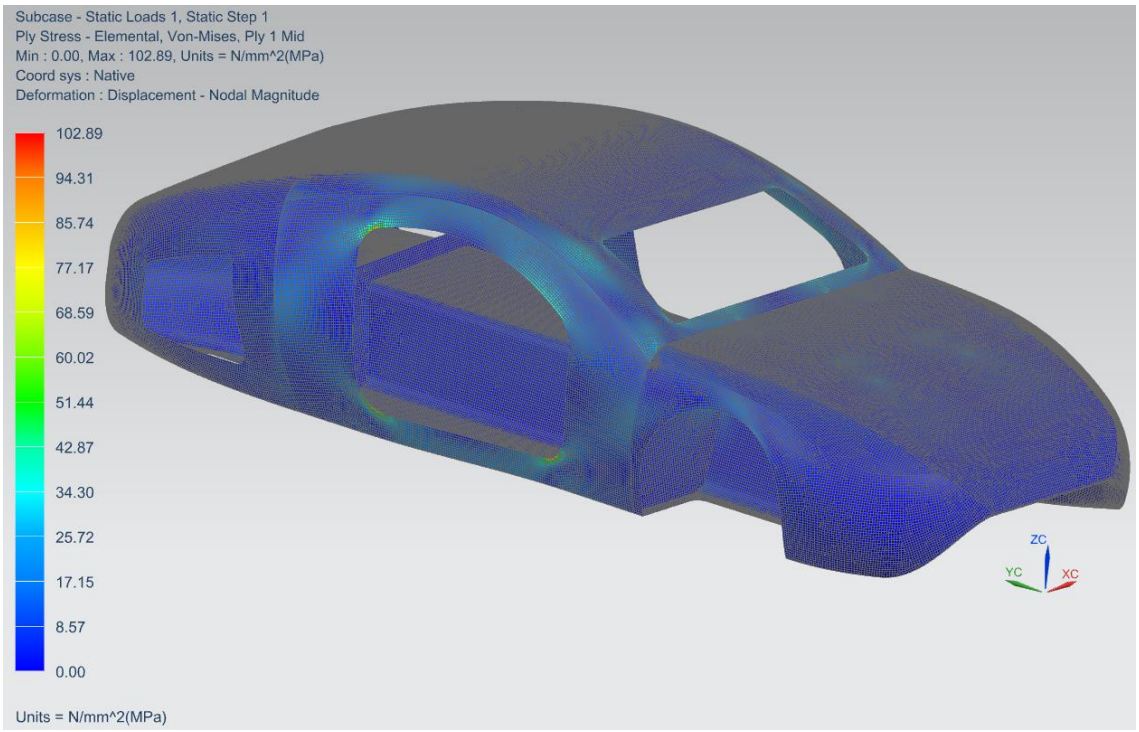

Figure 4.19: Linear static Von Mises ply stress result of chassis with compact door openings

4.1.5 Honeycomb Core Layup Modification

A honeycomb core exhibits superior stiffness properties when compared to a foam. Therefore, it would be a better suited core material for a monocoque chassis where torsional stiffness is of utmost importance. As previously mentioned in section 2.2.2.2, an aluminium honeycomb cannot be implemented at areas of high curvature, as it does not bend well in more than one direction, and therefore a combination of a foam and honeycomb core was used. A linear static analysis was conducted to determine the effect that a composite honeycomb and foam core would have on the torsional stiffness parameter of the chassis. The material selected to be implemented was a hexagonal aluminium core with a cell size of 4.4 mm manufactured by *AMT Composites*, see Table 4.3. Table 4.5 illustrates the different sections of the chassis where a foam core and honeycomb core were used:

Table 4.5: Composite foam and aluminium honeycomb core chassis layup

Chassis Section	Layup
Roof and Sides	$0^o/90^o$; $\pm45^o$; 5 mm honeycomb core; $\pm45^o$; $0^o/90^o$
Suspension mounts	$0^o/90^o$; $\pm45^o$; $0^o/90^o$; 10 mm foam core; $0^o/90^o$; $\pm45^o$; $0^o/90^o$
Inner Structure	$0^o/90^o$; $\pm45^o$; 5 mm honeycomb core; $\pm45^o$; $0^o/90^o$
Front and Rear	$\pm45^o$; 3 mm foam core; $0^o/90^o$
Hood	$0^o/90^o$; 3 mm honeycomb core; $\pm45^o$

Since the model in section 4.1.4 exhibited such a high torsional stiffness by reducing the size of the door recesses, it was decided to select this model as the final design geometry. The model with a composite honeycomb and foam core was subjected to the same loading conditions and constraints as the previous models. Figure 4.20 shows the deflection result of the linear static simulation of the chassis with a composite honeycomb and foam core.

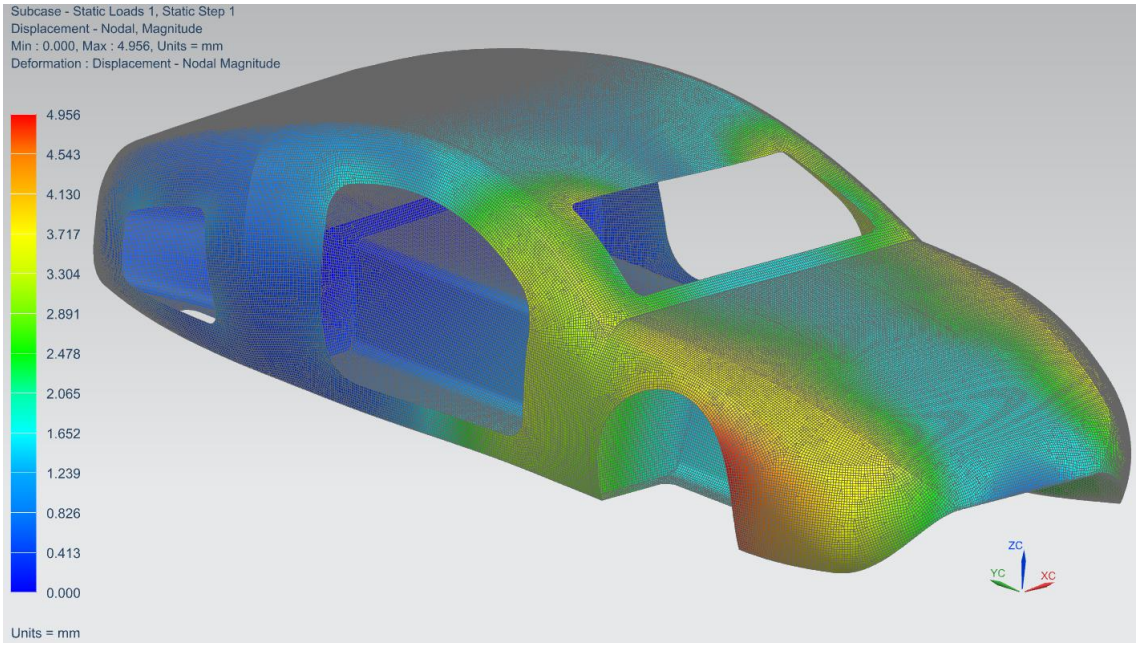

Figure 4.20: Linear Static deflection FEA result of chassis with composite honeycomb and foam core

Figure 4.20 illustrates a maximum deflection of 4.96 mm, 1.28 mm less than experienced by the previous model shown in Figure 4.17. This can be converted into a 20.6 % reduction in the maximum deflection of the chassis under the same loading conditions. With regard to the torsional stiffness parameter, Figure 4.21 illustrates a deflection of the front suspension ends of 3.60 mm, a 0.56 mm reduction in deflection when compared to the model in Figure 4.18, and when substituted into the relevant equations, yields a torsional stiffness of 4097 Nm/deg. This is a 15.5 % increase in the torsional stiffness parameter when compared to the model simulated in section 4.1.4, and exceeds the required torsional stiffness value of 4000 Nm/deg. This increase in the torsional stiffness is attributed to the superior stiffness properties of an aluminium honeycomb core when compared to that of a polyurethane foam core.

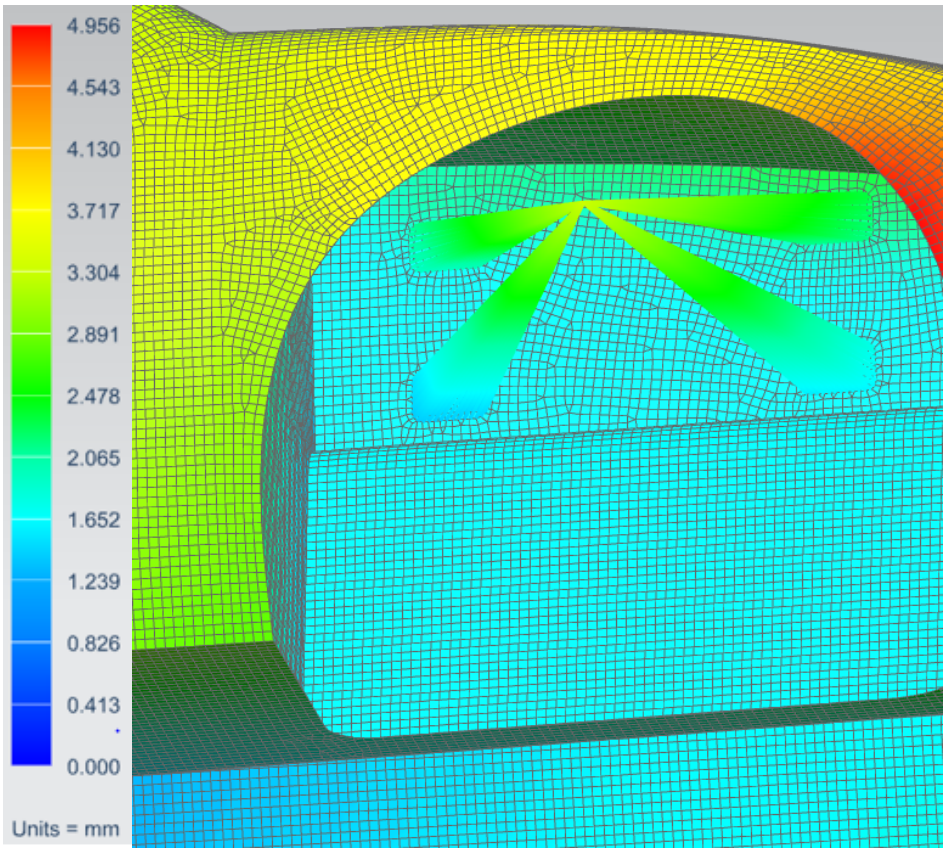

Figure 4.21: Close-up deflection result of front suspension mount of chassis with composite honeycomb and foam core

The effect of the composite honeycomb and foam core on the Von Mises ply stress experienced by the chassis was also investigated. Figure 2.22 shows that a maximum Von Mises ply stress of 77.43 MPa was experienced by the chassis, a decrease in the subjected maximum stress of 25.46 MPa than experienced by the previous model shown in Figure 4.19. This is a 24.7 % reduction in the experienced stress of the chassis. Implementing a honeycomb core in particular areas of the chassis results in such a high increase in the torsional stiffness, a 15.5 % increase, and significant reduction in the maximum ply stress, a 24.7 % reduction, of the chassis. The addition of the aluminium honeycomb core reduced the mass of the vehicle to 40.05 kg, a decrease of 2.40 kg when compared to the mass of the model in section 4.1.4. This is attributed to the addition of the aluminium honeycomb core, which has a lower mass than the polyurethane foam core for the same volume.

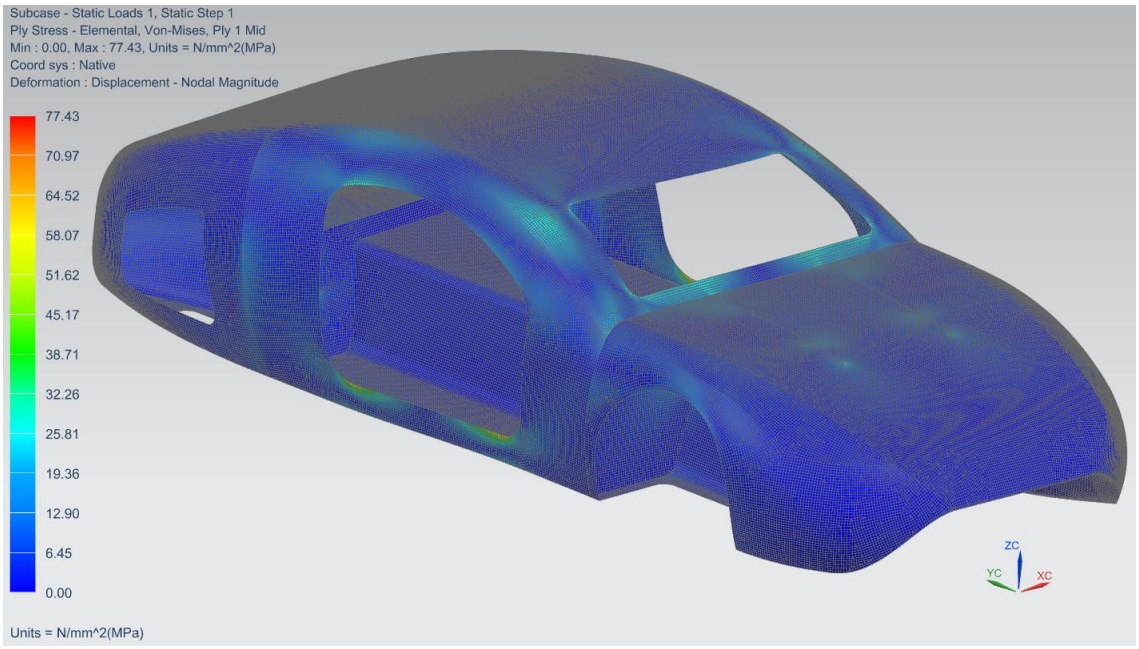

Figure 4.22: Ply tress of chassis with composite honeycomb and foam core

4.1.6 Summary of Torsional Stiffness Model Results

Table 4.6 comprises of a summary of the torsional stiffness finite element analysis results from section 4.1.

Table 4.6: Summary of Finite Element Analysis Results

Analysis	Maximum Deflection (mm)	Deflection at Front Suspension Ends (mm)	Torsional Stiffness (Nm/deg)	Maximum Ply Stress (MPa)	Mass (kg)
Preliminary Model	7.16	5.37	2745	120.55	43.41
Layup and Rear Geometry Modification Model	8.05	5.37	2745	145.54	43.87
Door Recess Effect on Torsional Stiffness Model	3.51	2.50	5899	136.71	44.84
Door Recess Geometry Modification Model	6.24	4.16	3546	102.89	42.45
Honeycomb Core Layup Modification Model	4.96	3.60	4097	77.43	40.05

Table 4.6 shows that the finite element analysis preliminary model, details of which are given in section 4.1.1, resulted in an inadequate torsional stiffness value. As specified by the methodology

in Figure 3.1 modifications needed to be made to the model and an iterative finite element process followed until the required torsional stiffness value is attained. To reduce the mass of the chassis, and improve accessibility of suspension members, the rear support plate was altered, and rear suspension access hatches were created, details of which are given in section 4.1.2. The inner structure core thickness was also increased, the consequence of which was a significant increase in mass. The modifications resulted in the torsional stiffness being the same as in the preliminary model results. The decrease in the structure's moment of area by creating rear suspension access hatches to reduce mass initiated an attempt to increase the structures moment of area by reducing the size of component recesses on the chassis. In an unrealistic scenario, the door recesses were enclosed to negate their effect on the torsional stiffness. Under the same loading conditions, the torsional stiffness increased substantially, exceeding the required 4000 Nm/deg, however, the vehicle doors will not be a rigid connection as modelled in this simulation. To increase the moment of area, and thereby the torsional stiffness, of the chassis the size of the door recesses, and consequently the height of the chassis, were reduced. This resulted in the torsional stiffness increasing significantly, but not sufficiently to satisfy the failure criterion, and the mass decreasing significantly. To further increase the torsional stiffness an aluminium honeycomb core was implemented to capitalise on its superior stiffness properties when compared to a foam core. Because aluminium honeycomb cannot be applied at areas of high curvature a layup comprising of a combination of the aluminium honeycomb and foam cores was created, details of which are given in section 4.1.5. The composite honeycomb and foam core resulted in the torsional stiffness surpassing the required value and satisfying the failure criterion and further decreased the mass of the chassis.

4.2 Principal Stress Analysis

The torsional stiffness models have resulted in a suitable geometry and layup being generated, however, it has not considered whether the material would be able to withstand the stresses present. To determine this, it is important to determine the maximum normal stress induced in the structure. There can be a vast number of planes passing through the given areas of a structure, each with its own normal stress value. There will be one plane on which the normal stress is a maximum. This is known as the maximum principal stress. Principal stresses are the components of the stress tensor when the basis is altered in such a way that the shear components become zero. This means that the maximum principal stress is greater in magnitude than the maximum normal stress and is particularly important to consider regarding composite materials, where the direction of the stress is imperative when determining an appropriate laminate layup orientation. The maximum principal ply stress, Figure 4.23, was determined from the simulation and model set up used in section 4.1.5 because this model exhibited a sufficient torsional stiffness value.

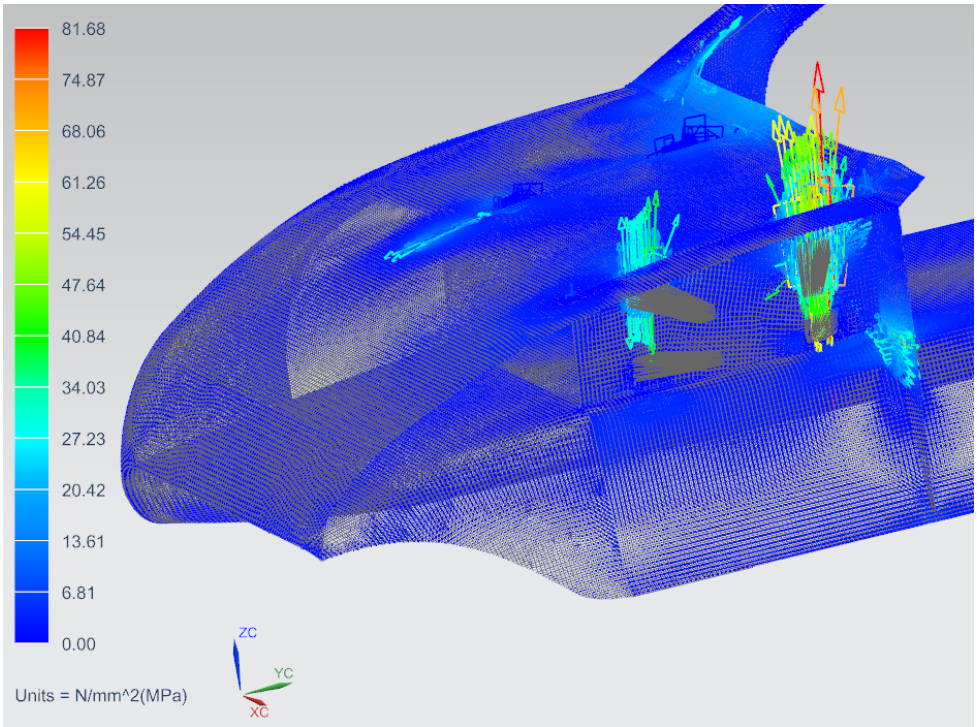

Figure 4.23: Static structural maximum principal ply stress

Figure 4.23 illustrates a maximum principal ply stress in the vertical, ZC axis in Figure 4.23, direction of 81.68 MPa. This is expected because the loads applied to the suspension mounts were vertical. The maximum principal stress is present at the front suspension mounts, where 'hardpoints' would need to be constructed to account for this stress concentration. The material layup at the front suspension mounts has two layers of 2x2 twill reinforcement on either side of the core orientated at zero/ninety degrees to the horizontal, XC direction. This means that the fibres are orientated in the ZC and XC directions and that the maximum principal ply stress is in the direction of the fibres, loading them in tension. It must be noted that although much greater than the stress experienced by most the chassis, the maximum principal stress is still below that of the tensile strength, 464.4 MPa, of the face material. This shows that the chassis can withstand the stresses imparted on it by the suspension.

4.3 Vertical Bending Model

To validate the literature that suggests a chassis with sufficient torsional stiffness would have sufficient bending stiffness, a vertical bending model was developed. Vertical bending arises from the squatting or diving of a vehicle under deceleration and acceleration respectively, detailed in section 2.4.2. The vertical bending analysis models the chassis as a simply supported beam, with the rear suspension mounting locations modelled as pin supports, only allowing rotation about their own axis, and the front suspension mounting locations modelled as a roller support, that only allows translation along the length of the chassis and rotation about its own axis. Regarding chassis vertical bending, the deflection ratio is important to consider as a failure criterion (Wong,

2001). The deflection ratio should be limited to 1/360th of the length of the vehicle. This suggests that, the maximum vertical deflection of the chassis, which is 4426 mm in length, should not exceed 12.29 mm. This maximum deflection occurs at the midspan of the chassis where the load is applied.

For this simulation, the same layup and model was used as in sections 4.1.5 and 4.2. The load is applied to the chassis centre over an area on the driver and passenger side to evenly distribute the load. This vehicle is intended to be designed to accommodate low speed endurance racing. This means that the vehicle will not accelerate/decelerate at a fast rate, such as that of a formula 1 vehicle which can be as much as 2g, and the resulting loads from acceleration/deceleration are lower in magnitude. This results in the chassis only requiring to withstand a bending load not exceeding 1g in the vertical direction (Singh, 2010). A load of 1250 N was applied to driver and passenger centres in the downward direction to simulate the squatting of the vehicle. Figure 4.24 illustrates the deflection result of the vertical bending chassis squatting model.

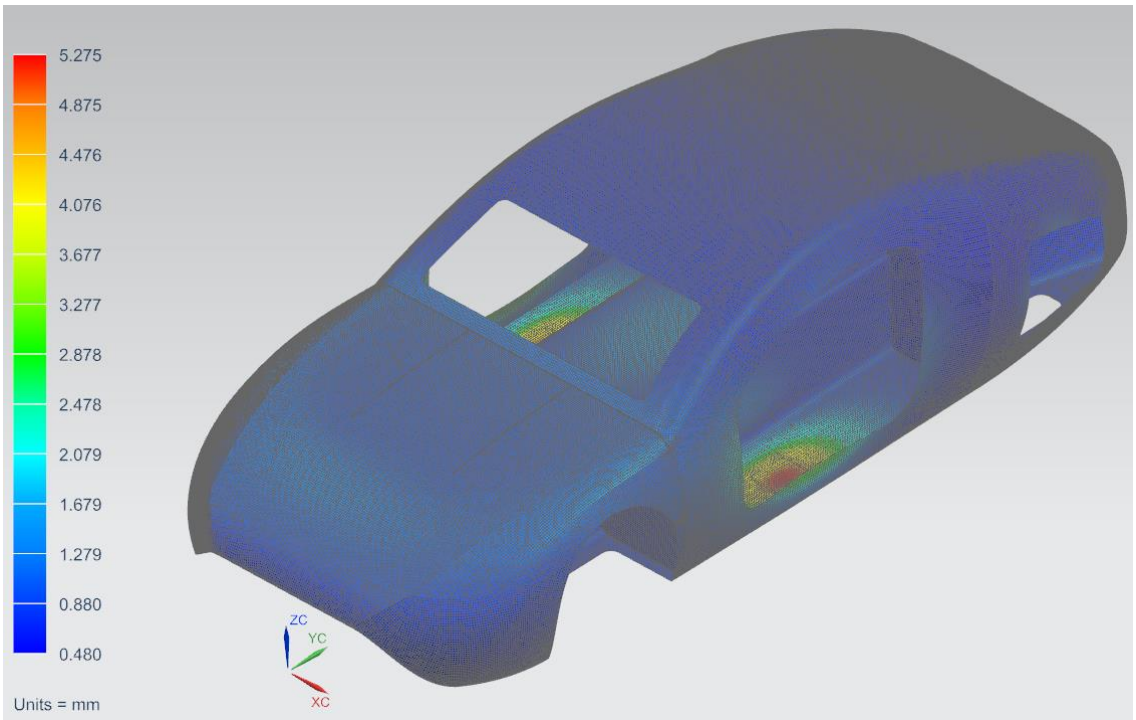

Figure 4.24: Deflection result of the vertical bending chassis squatting model

Figure 4.24 shows a maximum deflection of 5.28 mm at the areas at the driver and passenger centres where the load was applied, which is below that of the maximum allowable vertical deflection of 12.29 mm of the chassis centre where the load is applied. However, this result only yields the vertical deflection of the vehicle when squatting and the diving case must also be considered. For the diving case, the same loading conditions and constraints were used as with the squatting case, but the load was applied vertically upwards. Figure 4.25 illustrates the vertical deflection result under the diving case.

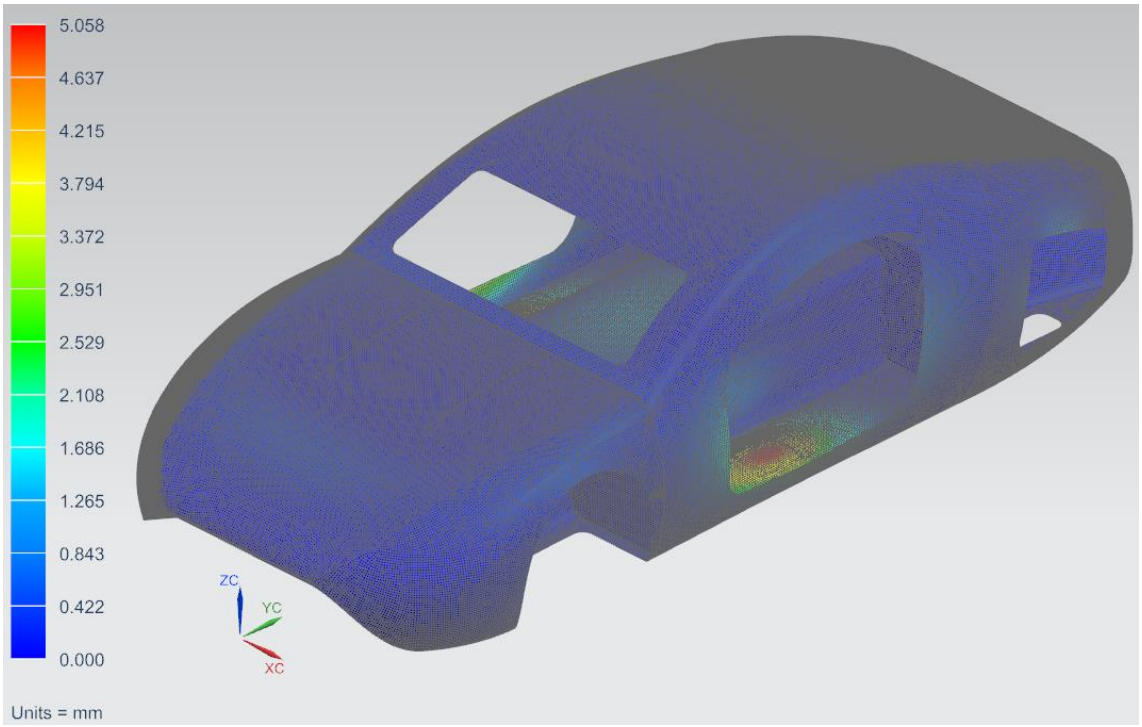

Figure 4.25: Deflection of the vertical bending chassis diving model

Figure 4.25 shows a maximum deflection of 5.06 mm at the driver and passenger loading areas, which is below that of the maximum allowable vertical deflection of 12.29 mm. Therefore, since the chassis does not deflect more than the maximum allowable deflection in either case, it exhibits sufficient bending stiffness regarding the vertical bending failure case. This verifies that a chassis with sufficient torsional stiffness will have sufficient bending stiffness.

4.4 Lateral Bending Model

Lateral bending loads occur because of the centrifugal forces that arise during cornering and side winds to some extent. Lateral loads act along the length of the chassis and are opposed by the traction of the tires. The lateral bending case was analysed to verify that the torsional load case is the most severe load case regarding chassis design, and would only need to be considered when designing a chassis. For this simulation, the front and rear suspension mounts were clamped, as in the vertical bending case, however, only rotation in the ZC direction was allowed, and the chassis was modelled as a simply supported beam. The layup literature suggests that the critical lateral acceleration should not exceed 1g (Carrol, 2003), which translates to a load of an approximate magnitude of 2500 N. This load was equally applied to each side of the chassis, the driver and passenger doors respectively, illustrated by the red arrows in Figure 4.26, to simulate the lateral force that would arise from cornering sharply at high speed.

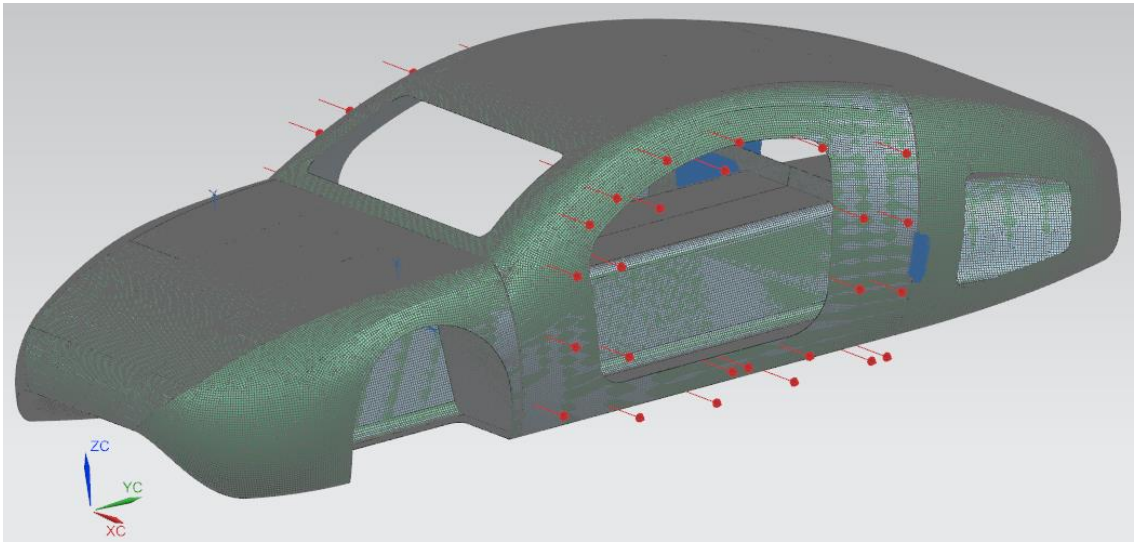

Figure 4.26: Lateral bending model force application

Regarding lateral bending, the maximum stress experienced by the chassis was analysed. This was decided to compare the maximum stress experienced by the torsional loading case and the maximum stress experienced by the lateral bending case. Figure 2.27 illustrates the maximum stress experienced by the chassis under the lateral bending load case.

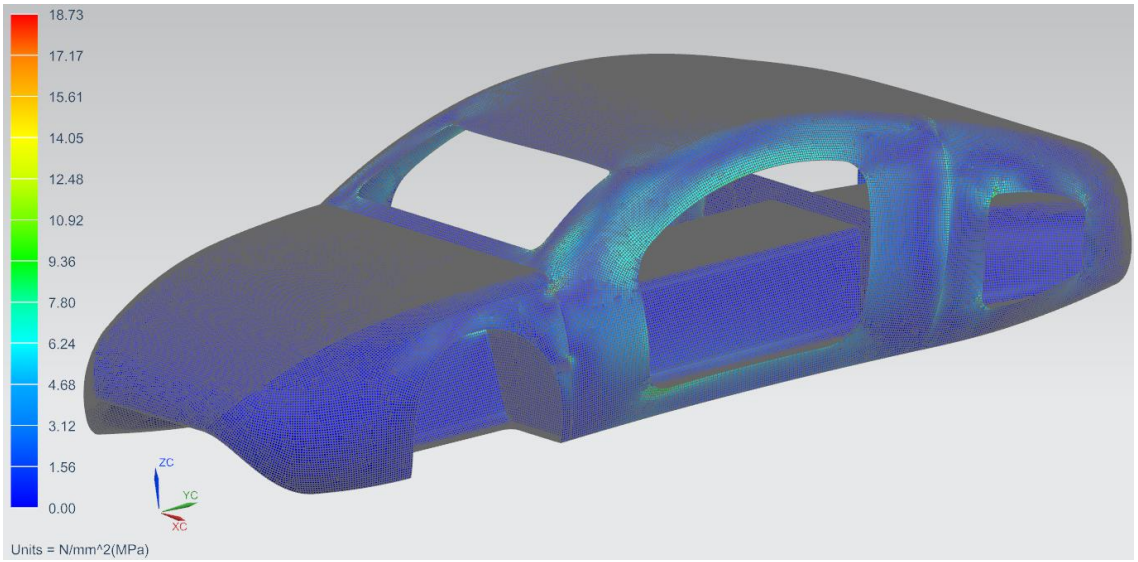

Figure 4.27: Lateral bending case maximum stress

Figure 2.27 shows a maximum bending stress of 18.73 MPa. This stress was located at the front suspension mounts and below that of the maximum ply stress of 77.43 MPa present in the torsional stiffness model in section 4.1.5. This verifies that the torsional load case is the most severe. It is interesting to note that the lateral bending stress is more than 75.8 percent less than the maximum stress experienced under the torsional load case, further verifying the importance and severity of the torsional stiffness parameter in chassis design.

Chapter 5. Flexural Bending Test

A flexural material bending test is used to determine the flexural modulus and the flexural bending strength of a material. Unlike a tensile test, a flexural test does not measure fundamental material properties, as flexural strength and stiffness are not basic material properties. Flexural properties are the combined attributes of a material's basic stress states, namely tension, compression, and shear, where a flexural test induces all three simultaneously (Hodgkinson, 2000). The first of these that reach its limiting value dictates the material failure type. The flexural strength is defined as the maximum stress, compressive or tensile, that the outermost fibre of the specimen can withstand. The flexural modulus is determined from the slope of the stress versus strain deflection curve that is plotted as a result of the flexural bending test. Flexural strength and modulus are used to evaluate a material's ability to resist bending. A flexural bend test was used to verify the lateral bending analyses results obtained in section 4.4 by verifying the assumed linear condition of the model. The stresses experienced by the chassis under the lateral bending loading conditions are bending stresses. To determine if these stresses exceed the maximum bending stress of the sandwich structure, a flexural bending test was conducted on the proposed sandwich structure layup present at the front suspension mounts, the region of the highest stress of the lateral bending model. A comparison of the maximum lateral bending stress and the peak flexural bending stress of the front suspension mount sandwich structure was conducted. In addition, a comparison of the simulation material properties and physical material properties was conducted. This was achieved by simulating the flexural bending tests by modelling the specimens in *Siemens NX Nastran*. The flexural bending stress from the finite element analysis of the specimens was compared to that of the flexural bending stress exhibited by the physical specimens under the same midspan deflection.

5.1 Flexural Bending Test Types

The most common flexural bending test types are the three and four-point flexural bending tests. A three-point flexural bending test consists of the specimen simply supported horizontally at two ends, with the force applied at the top surface of the rectangular specimen at its centre at a single point, as shown in Figure 5.1. A four-point flexural bending test consists of the same simply supported beam set up as with the three-point bending test, however, the force is applied through two points, each equal distance from the adjacent support point, with the distance between them being half the distance between the supports as shown in Figure 5.2. The major distance between the two tests is the location of the maximum bending moment and maximum flexural stress. The four-point configuration results in the bending moment being constant between the applied force members and the maximum flexural stress being uniform between the applied force members. The three-point bending test results in the maximum flexural stress being present directly beneath

the applied force member. Another difference is that the resultant vertical shear force is present throughout the beam, except beneath the applied force, in the three-point bending test whereas the region between the applied force members in the four-point bending test has no resultant vertical shear (O'Brien, 1991). The three-point bending test is used for testing a specific region of a specimen, whereas, the four-point bending test is well suited for testing a large region or area of a specimen, which determines the defects of the specimen better than a three-point bending test. However, relatively minor differences in test results have been demonstrated between the two tests (Hodgkinson, 2000). Due to limitations of the apparatus available, only a three-point flexural test can be conducted.

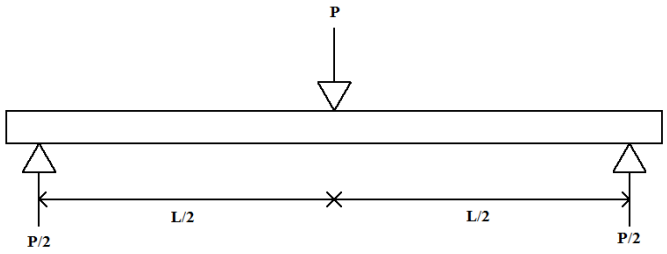

Figure 5.1: Three-point flexural bending test

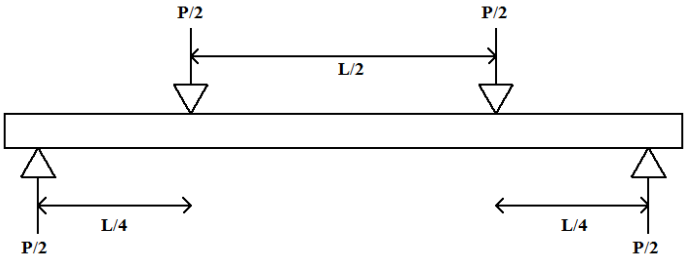

Figure 5.2: Four-point flexural bending test

5.2 Flexural Properties Testing Procedure

The shear stress component acting on the specimen is minimised to simplify the stress state in the specimen. This is achieved by making the span between the supports (L) long relative to the thickness of the specimen (h). This is achieved by designing specimens with span to thickness ratios (L/h) of 32:1 and 16:1, and in some cases 64:1 (Hodgkinson, 2000). This is done because the specimen length does not affect the shear stress while the bending moment is directly proportional to the specimen length. It is important to note that flexural properties may vary depending on which specimen of the surface is in compression, as no laminate is perfectly symmetric. Multidirectional laminates, with a moderate number of layers, may result in deviations of the flexural properties. This is because the ply-stacking sequence may affect the flexural properties and may not correlate with the extensional modulus. Flexural properties may also differ with varying specimen thickness, conditioning and/or environmental conditions, and rate of straining. Beam theory is used to calculate the flexural properties, although the specimens ingeneral may be described as plates; however, the

differences are only significant for laminates containing numerous plies in the ± 45º orientation. These deviations are less significant with decreasing width.

The test specimens were prepared by a hand layup process with vacuum bagging. The 2x2 twill weave carbon fibre reinforcement material was cut into appropriate sheet sizes in preparation of the alternating 0º/90º and ±45º laminate orientations. Due to a lack of availability, the flexural properties of the aluminium honeycomb core sandwich structure used in section 4.1.5 for the torsional stiffness model could not form part of this research. The M60 foam core was cut into similar sizes to the carbon fibre sheets for each different core thickness. This was done so that the test specimens would be cut from large sandwich panels as opposed to laying each test specimen individually. The flat surface was wiped with a releasing agent and formed the bottom of the vacuum chamber on which the sandwich panels were laid up on. The releasing agent inhibits the sandwich panels from bonding with the surface and allows them to be removed with relative ease. A medium hardness two-part epoxy resin, mixed in the ratio of 1:5 as per the manufacturer instructions, was used as the matrix material of the panels. Some of this resin was mixed with filler material and used to coat the foam cores, as illustrated in Appendix B Figure B.1 image (a). This creates a film on the core surface which inhibited the foam core from absorbing resin. The carbon fibre sheets and foam cores were then placed one by one in the required stacking sequence, with each layer being saturated with resin before the next layer being placed. Each sandwich panel was covered with peel-ply, Figure B.1 image (b), which inhibits the panels from bonding with the bleeder material, breather material and vacuum bag. Next followed the addition of the bleeder material, which absorbs excess resin that is extracted from the vacuum bag process, and the breather material, which is used to create a channel from the vacuum nozzle to each sandwich panel to allow suction to reach each panel evenly. The vacuum bag material was then placed over all the sandwich panels and vacuum nozzle and sealed to the flat surface, shown in Figure B.1 image (c). This creates the vacuum chamber. The vacuum was then switched on and allowed to operate for approximately four hours to ensure that all excess resin was extracted. The sandwich panels were then left to cure for twelve hours and demoulded the next day. Once demoulded the required specimens were cut from the sandwich panels and filed to the correct size. A span to thickness ratio of 16:1 was decided upon to conform to *ASTM* D-7264 standards (ASTM, 2017).

The specimens were tested on a Instron 5500 test machine. The test bench, to which the span supports are attached, was fixed to the machine. The specimens were placed on the bench and the load was applied by the machine. Figure 5.3 shows the three-point test bending set up. The required support span was determined and set for each layup group. Loading noses may be fixed, rotatable or rolling, with fixed or rolling noses typically used for composite material testing. The nose and supports are cylindrical, with a minimum radius of approximately 3 mm,

and must be free of any surface irregularities, such as sharp edges and indentations, as to ensure that uniform contact of the supports and nose with the specimen across its width is achieved. Three-point bending test method according to *ASTM* D-7264 (ASTM, 2017) was used to determine the flexural properties of the composite sandwich structures. The force was applied to the specimens by the machine crosshead at a rate of 1 mm/min. A failed specimen is shown in Figure 5.4 by the face fracture failure mode. Six specimens were tested for each layup group and the force versus deflection curves were generated.

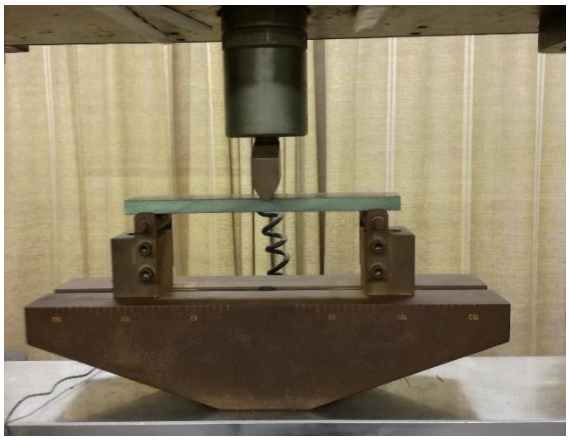

Figure 5.3: Three-point flexural bending test set up

Figure 5.4: Failed specimen (face fracture failure mode)

5.3 Flexural Properties

For a three-point flexural bending test, when a sandwich structure specimen is subjected to a flexural test and modelled as a simply supported beam loaded at the midpoint, the maximum bending stress occurs at the outer surface at the mid-span. This stress may be calculated at any point given by equation 5.1:

$$\sigma = \frac{3PL}{2bh^2} \tag{5.1}$$

where the maximum bending stress on the outer surface, σ (MPa), is directly proportional to the product of the applied load, P (N), and the support span, L (mm), and inversely proportional to the product of the specimen width, b (mm), and the square of the specimen thickness, h (mm).

This stress is equal to the flexural strength of the material corresponding to the peak applied force prior to failure. The maximum flexural bending stress can be determined for any given strain

using the force-deflection curve generated from the experiment by letting the load P in equation 5.1 equal the applied force read from the force-deflection curve at the deflection corresponding to the desired strain. The maximum strain at the outer surface also occurs at the mid-span and is given by equation 5.2:

$$\varepsilon = \frac{6\delta h}{L^2} \tag{5.2}$$

where the maximum strain on the outer surface, ε, is directly proportional to the product of the mid-span deflection, δ (mm), and the specimen thickness, h (mm), and inversely proportional to the square of the support span, L (mm).

The flexural chord modulus of elasticity is the ratio of the change in stress to the change in strain between two points on the stress-strain curve, and is given by equation 5.3:

$$E_f^{chord} = \frac{\delta\sigma}{\delta\varepsilon} \tag{5.3}$$

where the flexural chord modulus of elasticity, E_f^{chord} (MPa) is given by the change in flexural stress between the predetermined strain points, $\delta\sigma$ (MPa), over the change in strain, $\delta\varepsilon$.

5.4 Flexural Bending Test Results

Different test specimens comprising of different layups were manufactured and subjected to a flexural bend test. The first layup comprised of the same orientation and stacking sequence as the torsional stiffness model, in section 4.1.5, front suspension mount. This was decided because the simulation results suggest that the maximum stress occurs at this region. This is expected because the suspension arms transfer the operating loads to the chassis through the mounting locations. The next two specimen groups were compared to one another to verify the effect of the core thickness on sandwich panels. The same reinforcement orientation and number of layers was used in each of these cases, with different core thickness being used. Table 5.1 summarises the results of the flexural bend test for each specimen. Of the six specimens from each different layup, the three from each specimen group that exhibited the best correlation were selected and the others regarded as outliers.

Table 5.1: Flexural test results

Layup	Specimen	Span Length (mm)	Peak Load, P, (N)	Peak Mid-Span Deflection, δ, (mm)
[0º/90º; ±45º; 0º/90º;	1	186.40	874.7	5.542
10mm core; 0º/90º;	2	186.40	881.6	5.932
±45º; 0º/90º]	3	186.40	830.5	5.730
	Average	186.40	862.3	5.735
[±45º; 5mm core;	1	92.00	287.2	6.774
0º/90º]	2	92.00	295.6	6.871
	3	92.00	294.0	8.013
	Average	92.00	292.3	7.219
[±45º; 10mm core;	1	171.20	291.2	6.401
0º/90º]	2	171.20	286.2	6.212
	3	171.20	278.0	6.404
	Average	171.20	285.1	6.339

Table 5.1 shows that the layers of reinforcement material influence the peak load of the structure. This is evident because the test specimen with three layers of reinforcement material on each side of the core material fractured under an average peak load far greater than that of the average peak loads of the other sandwich structures. The test specimens that each had one layer of reinforcement material on either side of the core failed under a lower average peak load. Theory suggests that the average mid-span deflection will decrease with increasing core thickness, because the stiffness of composite sandwich panels increases with core thickness, however, the different span lengths mean that the midspan deflection and peak loads of the different specimen layups cannot be compared directly. The flexural properties provide a means of directly comparing the results of the different specimens. The flexural properties, given by the equations in section 5.3, are summarised in Table 5.2. Sample calculations for these properties are detailed in Appendix A.

Table 5.2: Test specimen flexural properties

Layup	[0°/90°; ±45°; 0°/90°; 10mm core; 0°/90°; ±45°; 0°/90°]	[±45°; 5mm core; 0°/90°]	[±45°; 10mm core; 0°/90°]
Specimen Thickness, h, (mm)	11.65	5.75	10.70
Span, L, (mm)	186.40	92.00	171.20
Width, b, (mm)	40	30	30
Average Peak Load, P, (N)	862.3	292.3	285.1
Average Peak Flexural Stress (MPa)	44.41	40.67	21.32
Specimen Failure Mode and Region	Compression under loading nose	Compression under loading nose	Core shear under loading nose
Average Mid-Span Deflection, δ, (mm)	5.735	7.219	6.339
Maximum Strain ε, (mm)	0.01154	0.02943	0.01389
Flexural Chord Modulus, E_f^{chord}, (MPa)	3848.4	1382.15	1536.90

Table 5.2 indicates an average peak flexural stress of 44.41 MPa for the test specimens that correspond to the model suspension mount layup. This maximum flexural stress is 137.1 % higher than the peak bending stress of 18.73 MPa experienced by the lateral bending model in section 4.4. This indicates that the stress does not exceed the maximum allowable stress of the sandwich structure.

The 5 mm core specimens and multiple reinforcement material 10 mm core specimens each failed at the surface in contact with the loading nose. This is the surface that is loaded in compression. This was expected because composite materials are stronger in tension than in compression, indicating that the surface experiencing compression loading would fail at the surface where the loading nose is applied. Literature suggests that composite sandwich structure stiffness increases with increasing core thickness. The results illustrated in Table 5.2 verify the theory that stiffness and core thickness are directly proportional because as the specimen core thickness increased, from 5 mm to 10 mm, with the same reinforcement material orientation and number of layers, the flexural stiffness increased from 1382.15 MPa to 1536.90 MPa. The average peak flexural stress decreased with increasing core thickness, shown in Table 5.2, due to stress being a material property and not a geometry property. This indicates that the bending behaviour of the composite sandwich structures is governed by the reinforcement material. The 10 mm core specimens exhibited an average peak flexural stress of 21.32 MPa whilst the 5 mm core specimens exhibited an average peak flexural stress of 40.67 MPa. The 10 mm core flexural stress is lower because

the specimens failed under the core shear failure mode. This is because the layers and orientation of the reinforcement material remained constant between the 5 mm and 10 mm core specimens, resulting in the likelihood of the core shear failure mode increasing with the increase in core thickness. The increased stiffness of the thicker core resulted in the 10 mm core specimens exhibiting a decreased average mid-span deflection. This resulted in most of the stress not being absorbed by the reinforcement material. Since the shear strength of the core material is relatively low, the sandwich structure failed at a lower flexural stress.

A simulation of the flexural test was conducted in *Siemens NX Nastran*. This was done to verify the simulation material properties. A strong correlation between the physical flexural test and simulation results would suggest a strong correlation between the simulation material properties and tested material properties, verifying the accuracy of the computational analyses conducted in Chapter 4. A simple bending test model for each sandwich structure layup was developed to simulate the flexural bending test that was conducted. The flexural bend stress of the experimental and simulation specimens was compared for the same midspan deflection. This was done by plotting the curve of midspan deflection versus flexural bend stress of the experimental and simulation specimens.

Figure 5.3 illustrates the graph of the midspan deflection versus flexural bend stress of the 5 mm core thickness specimens with one layer of reinforcement material on either side of the core. The simulation specimens curve shows a linear relationship between the midspan deflection and the flexural bend stress. The experimental specimens curve illustrates a linear region from 1 mm to 2 mm midspan deflection. This would indicate the elastic region of the specimens. At approximately 2 mm midspan deflection the curve begins to deviate from the linear simulation specimens curve, indicating that plastic deformation of the specimens has initiated, and the specimens have surpassed their elastic limit.

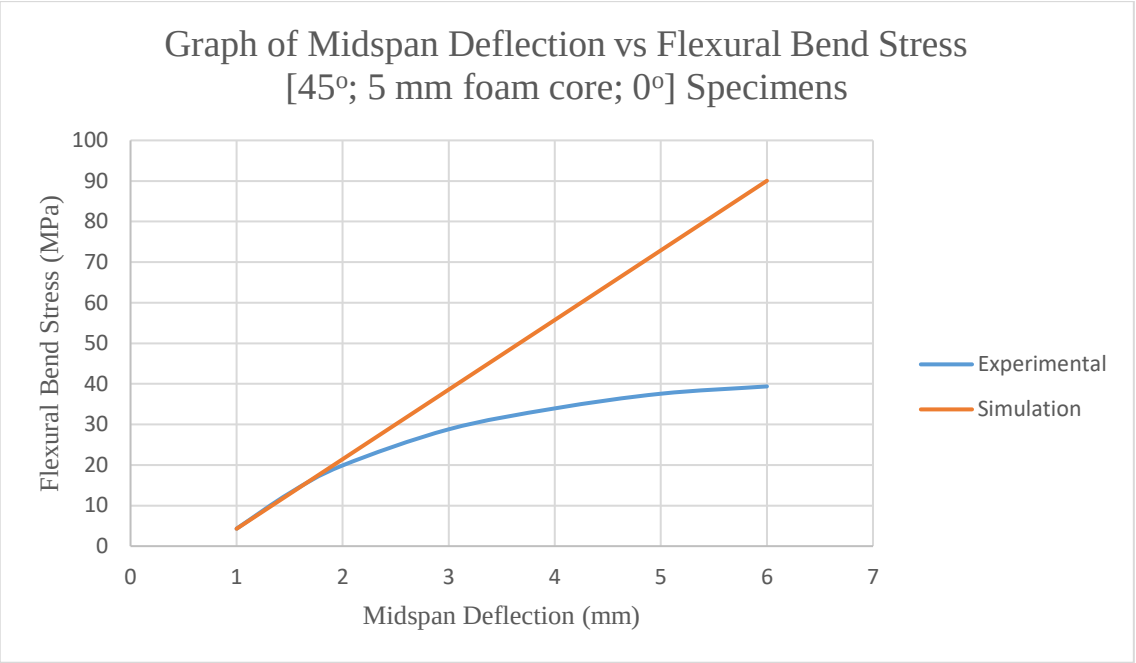

Figure 5.3: Graph of Midspan Deflection vs Flexural Bend Stress of [45º; 5 mm foam core; 0º] Specimens

Figure 5.4 illustrates the graph of the midspan deflection versus flexural bend stress of the 10 mm core thickness specimens with one layer of reinforcement material on either side of the core. The simulation specimens again illustrated a linear relationship between the midspan deflection and the flexural bend stress. The experimental specimens curve shows a linear relationship between 1.5 mm and 3.5 mm midspan deflection, whilst the specimens are within the elastic region, and once the elastic yield is surpassed an exponential relationship is illustrated.

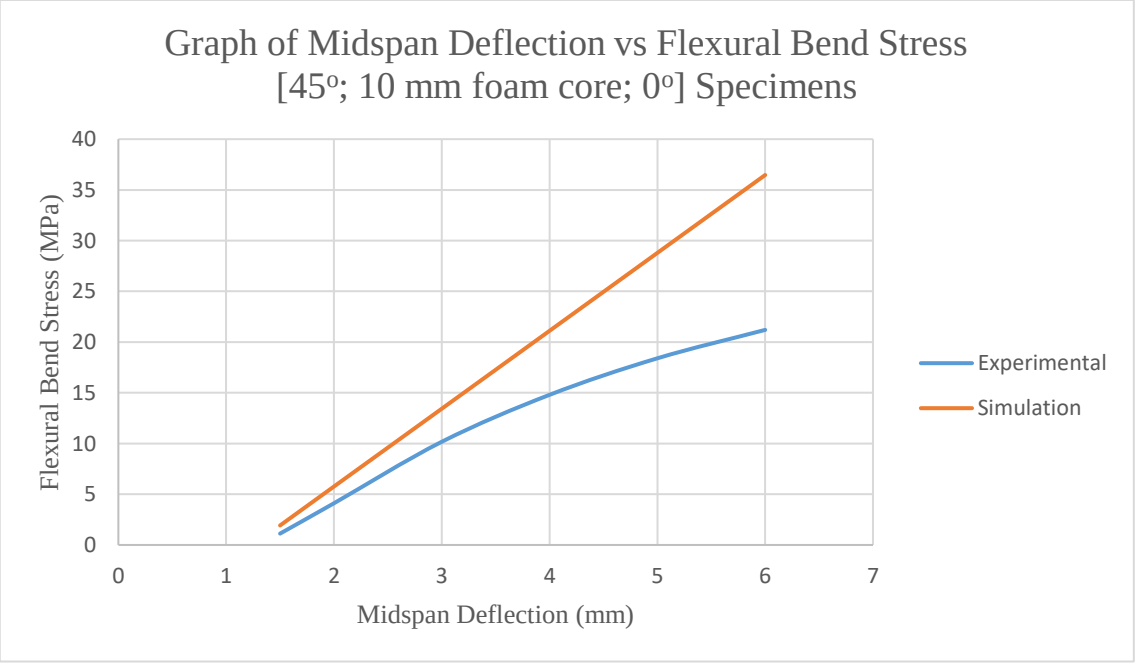

Figure 5.4: Graph of Midspan Deflection vs Flexural Bend Stress of [45º; 10 mm foam core; 0º] Specimens

Figure 5.5 illustrates the graph of the midspan deflection versus flexural bend stress of the 10 mm core thickness specimens with three layers of reinforcement material on either side of the core. The simulation specimens again illustrated a linear relationship between the midspan deflection and the flexural bend stress. The experimental specimens curve shows a linear relationship between 0.5 mm and 4 mm midspan deflection, whilst the specimens are within the elastic region, and once the elastic yield is surpassed an exponential relationship is illustrated.

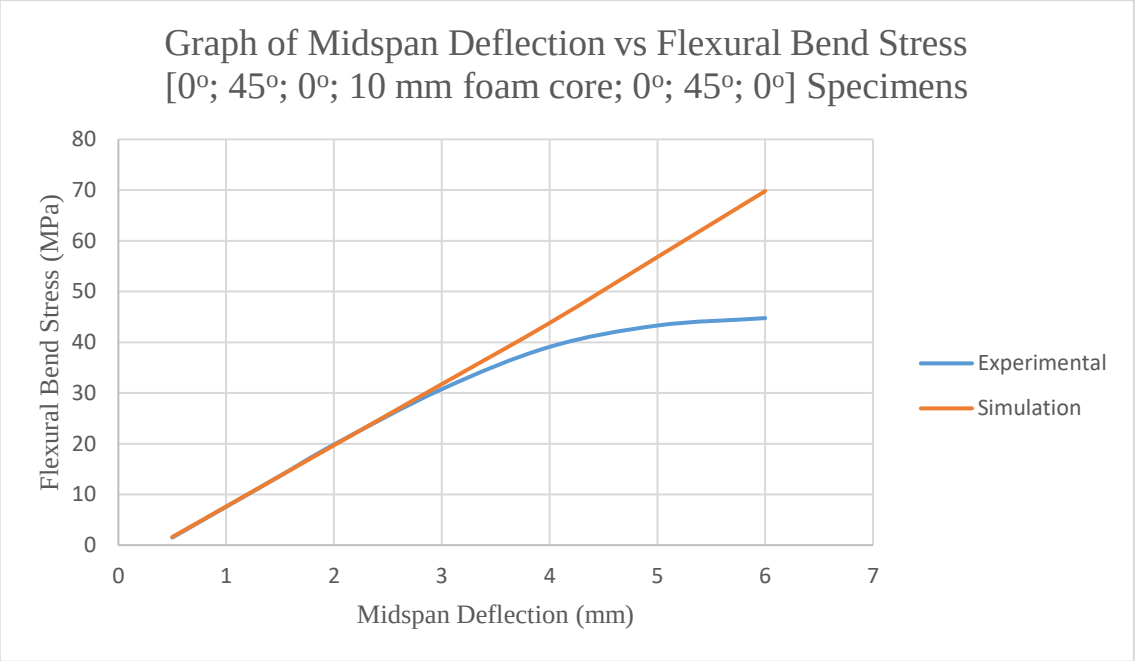

Figure 5.5: Graph of Midspan Deflection vs Flexural Bend Stress of [0°; 45°; 0°; 10 mm foam core; 0°; 45°; 0°] Specimens

A linear static model was developed for the analysis of the flexural bend test specimens but, as indicated by the experimental curve, the relationship between the midspan deflection and flexural bend stress is non-linear once plastic deformation has occurred. The experimental specimens with three layers of reinforcement material on either side of the core exhibited an extended elastic region, Figure 5.5, when compared to the elastic regions of the specimens with a single layer of reinforcement material on either side of the core, Figure 5.3 and Figure 5.4. This indicates that the reinforcement material allows the structure to elastically deform more before reaching its elastic limit, before plastic deformation begins. This is favourable because this allows the structure to deform and flex more and retain its original geometry. The results of the comparison of the simulated and experimental results indicate that the material properties and structural responses within the linear model represent the material responses accurately within the linear loading region. Similarly, to most engineering designs, the design limit can be set to the elastic region, allowing for a simplified (linear) simulation to be conducted.

Chapter 6. Conclusions

The aim of this research was to develop a design methodology of a composite monocoque chassis, through finite element analysis. The prominent key performance indicator regarding chassis design is torsional stiffness, the ability of the chassis to resist twisting. A preliminary model geometry was developed from the selection of the most suitable conceptual design. A torsional stiffness model was used to simulate the torsional loads acting on the chassis. An initial layup was developed from previous UKZN solar vehicle knowledge. The vertical deflection of the suspension mount ends resulted in an inadequate torsional stiffness value. The geometry and layup was modified with the intention of increasing the torsional stiffness. The first modification was the addition of rear suspension access hatches, alteration of the rear support plate, and increased inner structure core thickness. The resultant torsional stiffness was inadequate and it was concluded that the door recesses had a considerable influence on the torsional stiffness because of its effect on the moment of area. The size of the door recesses was reduced to improve the chassis ability to resist twisting. This increased the torsional stiffness significantly. A final modification was the addition of an aluminium honeycomb core. The honeycomb significantly increased the torsional stiffness to 4097 Nm/deg. In conclusion the chassis geometry, laminate layup orientation and core material significantly affect the torsional stiffness.

To verify the significance of the torsional stiffness parameter, lateral and vertical bending stiffness models were analysed. The vertical bending analysis resulted in a maximum mid-span deflection of 5.275 mm, which is 57.1 % below the maximum allowable mid-span deflection of 12.29 mm, determined from the span-deflection ratio. The lateral bending model resulted in a maximum stress of 18.73 MPa, which is 75.8 % below the 77.43 MPa experienced by the torsional stiffness model. The lateral and vertical bending stiffness analyses' results verify the torsional stiffness as the most significant key performance indicator regarding chassis design.

An analysis of the suspension mounting locations was conducted to ensure the maximum principal stress does not exceed the maximum allowable stress of the reinforcement material. The maximum principal stress of 81.68 MPa did not exceed the yield strength of the reinforcement material of 464.4 MPa. The direction of the maximum principal stress corresponded with the direction of the reinforcement material fibres, indicating that the applied loads from the front suspension will be transmitted along the reinforcement material fibres.

Flexural bending tests were conducted on various laminate sandwich structures used in the finite element analysis to confirm the simulation material properties. The peak load and mid-span deflection of each specimen was recorded to determine the maximum flexural stress and flexural modulus of elasticity. It was noticed that in each case, the specimen failed under the loading nose

on the surface in contact with the loading nose. The flexural stress at specific midspan deflections was compared, under the same loading conditions, to that of the bending stress exhibited by a flexural bend test model finite element analysis conducted in *Siemen's NX Nastran*. Graphs of the stress versus midspan deflection were plotted for each specimen layup type and the curves of the simulated and experimental results were compared. In each laminate sandwich structure case, the simulation curve exhibited a linear relationship between the midspan deflection and flexural bend stress, as expected for a linear FEA model, and the experimental curve exhibited a linear relationship until the elastic limit of the specimens were reached. Thereafter the curve exhibits an exponential relationship as plastic deformation occurs until the specimen failure. These results indicate that it is accurate to assume a linear relationship for the purposes of the model as long as the material response does not exceed the linear stress region. This simplifies the analysis time and material characterisation required.

Through an iterative finite element analysis, a methodology to designing a composite monocoque chassis, which is detailed in section 3.1, was developed. Once a suitable geometry was developed, a torsional stiffness model was analysed with the intention of attaining a suitable torsional stiffness parameter. The torsional stiffness of a chassis is largely dependent on chassis geometry and layup orientation. The geometry of the model and laminate sandwich structures are altered until a model that exhibited a suitable torsional stiffness value. A final check should be conducted to ensure the model meets the requirements of other failure criteria, however, results have shown that an adequate torsional stiffness will likely result in a structurally sound design in terms of other deflection modes.

References

Abrams, R., 2008. *Formula SAE Race Car Analysis: Simulation & Testing of the Engine as a Structural Member,* Ontario: The University of Western Ontario.

Alexander, R., 1999. *Basics of Composite Construction.* USA: EAA's Sport Aviation Magazine.

Allwood, J. M., 2009. *University of Cambridge, Department of Engineering.* [Online] Available at: http://www.lcmp.eng.cam.ac.uk/wellformed/incremental-sheet-forming [Accessed 28 February 2016].

AMT Composites, 2017. *amt composites.* [Online] Available at: http://www..co.za/products[Accessed 25 Janruary 2017].

Ashby, M. F., 2005. *Materials Selection in Mechanical Design.* 3rd ed. Oxford: Elsevier Butterworth-Heinemann.

Ashby, M. F., 2011. *Materials Selection in Mechanical Design.* 4th ed. Amsterdam: Elsevier Ltd.

ASTM, 2017. *ASTM International.* [Online] Available at: https://www.astm.org/Standards/D7264.htm[Accessed 26 June 2017].

Azzi, V. D. & Tsai, S. W., 1965. Anisotropic Strength of Composites. *Experimental Mechanics,* 5(9), pp. 283-288.

Barbero, E. J., 2011. *Introduction to Composite Materials Design.* 2nd ed. London: CRC Press, Taylor and Francis Group.

Bitzer, T. N., 1997. *Honeycomb Technology: Materials, Design, Manufacturing, Applications and Testing.* 1st ed. Dublin: Chapman and Hall.

Bolles, B., 2010. *Advanced Racecar Chassis Technology.* 1st ed. New York: Penguin Group.

Broad, M. & Gilbert, T., 2009. *Design, Development and Analysis of the NCSHFH 09 Chassis,* Raleigh: North Carolina State University, SAE Technical Paper.

Bunsell, A. R. & Renard, J., 2005. *Fundamentals of Fibre Reinforced Composite Materials.* 1st ed. Bristol: IOP Publishing Ltd.

Camanho, P. P., 2002. *Failure Criteria for Carbon-Reinforced Polymer Composites,* Porto: University of Porto Faculty of Engineering.

Carrol, D. R., 2003. *The Winning Solar Car.* 1st ed. Warrendale, Pa: SAE International.

Chen, P. E., 1971. Strength properties of discontinuous fiber composites. *Polymer Engineering & Science,* 11(1), pp. 51-56.

Crocombe, A., Sampe, E. & Somiotti, A., 2010. *Chassis Torsional Stiffness: Analysis of the Influence on Vehicle Dynamics.* Detroit, Michigan, USA, SAE International.

Davies, G., 2012. *Materials for Automobile Bodies.* Oxford: Elsevier.

Denny, J. A., Govender, S., Moodley, J. & Ngema, B., 2015. *Group 19: 2015 Design and Research Project 2,* Durban: University of Kwa-Zulu Natal.

Eurenius, C. et al., 2013. *Analysis of Composite Chassis,* Göteborg: Chalmers University of Technology.

Fibremax Composites, 2014. *Fibremax Composites.* [Online] Available at: http://www.fibremaxcomposites.com/shop/index_files/yarntownomenclature.html [Accessed 26 February 2016].

Genta, G. & Morello, L., 2009. *The Automotive Chassis.* 1st ed. Torino: Springer Science + Business.

Gibson, R. F., 2015. *Principles of Composite Material Mechanics.* 4th ed. Bocca Raton: Taylor & Francis Group.

Goerge, A. & Riley, W., 2002. *Design, Analysis and Testing of a Formula SAE Car Chassis,* New York: Cornell University, SAE Technical Paper.

GT-R Life, 2012. *GT-R Life: Ferrari F70 carbon fiber Monocoque chassis.* [Online] Available at: http://www.gtrlife.com/forums/topic/75748-ferrari-f70-carbon-fiber-monocoque-chassis/[Accessed 16 February 2016].

Happian-Smith, J., 2001. *An Introduction to Modern Vehicle Design.* 1st ed. Oxford: Butterworth-Heinemann.

Hexcel Composites, 1997. *Sandwich Panel Fabrication Technology,* Dexford: Hexcel Composites.

Hexcel, 2015. *Hexcel Honeycomb Cell Configurations.* [Online] Available at: http://www.hexcel.com/Products/Aerospace/AHoneycomb-Cell[Accessed 26 February 2016].

Hexweb, 2000. *Hexweb Honeycomb Manual,* Duxford: Hexcel Composites.

Hibbeler, R., 2008. *Mechanics of Materials.* 1st ed. Upper Saddle River, USA: Pearson Prentice Hall.

Hodgkinson, J. M., 2000. *Mechanical Testing of Advanced Fibre Composites.* 1st ed. Boston: Woodhead Publishing Limited.

Hoffman, O., 1967. The Brittle Strength of Orthotropic Materials. *Journal of Composite Materials,* 1(2), pp. 200-206.

J Composites, 2012. *J Composites.* [Online] Available at: http://www.jcomposites.eu/en/j-boats/j-composites/[Accessed 22 March 2016].

Jiang, L., Wang, G., Gong, G. & Zhang, R., 2012. *Lightweight Design for a FSC Car Based on Modal and Stiffness Analysis.* Beijing, Springer.

Law, E., Raju, S. & Thompsom, L., 1998. *Design of a Wnston Cup Chassis for Torsional Stiffness.* Dearborn, Michigan, USA, Motorsports Engineering Conference and Exposition.

Lee, S. M., 1993. *Handbook of Composite Reinforcements.* 1st ed. Palo Alto: VCH Publishers.

Liu, Q. et al., 2013. Lightweight design of carbon twill weave fabric composite body structure for electric vehicle. *Composite Structures,* Volume 97, pp. 231-238.

Mallick, P. K., 1997. *Composites Engineering Handbook.* 1st ed. Michigan: Marcel Dekker, Inc..

Mallick, P. K., 1997. *Composites Engineering Handbook.* Michigan: Marcel Dekker Inc..

Mat, M. H., Redzi, A. & Ghani, A. B., 2012. *Design and Analysis of 'Eco' Car Chassis.* Kuching, Sarawak, Elsevier Ltd, pp. 1756-1760.

Mazumdar, S. K., 2002. *Composites Manufacturing Materials, Production, and Process Engineering.* 1st ed. Washington: Taylor and Francis.

McLaren, 2016. *1981 Formula 1 McLaren MP4/1.* [Online] Available at: http://www.mclaren.com/formula1/heritage/cars/1981-formula-1-mclaren-mp4-1/[Accessed 20 February 2016].

Messiry, M. & Deeb, R., 2016. Engineering Fibre Volume Fraction of Natural Fibre Staple-Spun Yarn Reinforced Composite. *Journal of Textile Science & Engineering,* 6(5), pp. 1-2.

Milliken, W. F. & Milliken, D. L., 1994. *Race Car Vehicle Dynamics.* 1st ed. Warrendale: Society of Automotive Engineers.

O'Brien, T. K., 1991. *Composite Materials: Fatigue and Fracture.* 3rd ed. Philadelphia: ASTM.

Reddy, N. Y. & Kumar, V. S., 2013. Study of Defferent Parameters on the Chassis Space Frame for the Sports Car by Using FEA. *IOSR Journal of Mechanical and Civil Engineering,* 9(1), pp. 1-3.

Rugdeo, S. et al., 2014. *Ukzn Solar Car First Semester Report,* Durban: University of Kwa-Zulu Natal.

Savage, G., 2008. *Speautomotive.com.* [Online] Available at: http://www.speautomotive.com/SPEA_CD/SPEA2008/pdf/k/K3.pdf[Accessed 21 February 2016].

Singh, R., 2010. *Structural Performance Analysis of Formula SAE Car,* Rajpura: Chitkara Institute of Engineering and Technology.

Solar Team Eindhoven, 2015. *Stella Lux The Energy Positive Family Car.* [Online] Available at: http://www.solarteameindhoven.nl/stella-lux/[Accessed 21 February 2016].

Sovran, G., 1978. *Aerodynamic Drag Mechanisms of Bluff Bodies and Road Vehicles.* 1st ed. New York: Springer.

Thiede, P., 2000. *Aerodynamic Drag Reduction Technologies.* Potsdam, Springer.

Thompson, L. L., Lampert, J. K. & Law, H., 1998. Design of a Twist Fixture to Measure the Torsional Stiffness of a Winston Cup Chassis. *SAE International,* 1(1), pp. 1-2.

Thompson, L. L., Lampert, J. K. & Law, H. E., 1998. Design of a Twist Fixture to Measure the Torsional Stiffness of a Winston Cup Chassis. *SAE International,* 1(1), pp. 1-2.

Thomsen, O. T., Bozhevolnaya, E. & Lyckegaard, A., 2005. *Sandwich Structures 7: Advancing with Sandwich Structures and Materials.* Aalborg, Springer.

Tsai, S. W. & Wu, E. M., 1971. A General Theory of Strength for Anisotropic Materials. *Journal of Composite Materials,* 5(1), pp. 58-80.

Velie, H. D., 2016. *Chassis Torsional Rigidity Analysis for a Formula SAE Racecar,* Ann Arbor: Dept. of Mechanicla Engineering, University of Michigan.

Walker, A., 2012. *3D CAD Browser.* [Online] Available at: http://www.3dcadbrowser.com/download.aspx?3dmodel=55511[Accessed 12 February 2016].

Wallace, L. E., 1998. *From Engineering Science to Big Science.* 1st ed. Washington, D.C.: NASA History office.

Wanberg, J., 2009. *Composite Materials Fabrication Handbook #1, Composite Garage Series.* 1st ed. Stillwater: Wolfgang Publications Inc..

Wanberg, J., 2010. *Composite Materials Fabrication Handbook #2, Composite Garage Series.* 1st ed. Stillwater: Wolfgang Publications Inc..

Wong, J. Y., 2001. *Theory of Ground Vehicles.* 3rd ed. New York: John Wiley and Sons, Inc..

World Solar Challenge, 2015. *Bridgestone World Solar Challenge.* [Online] Available at: http://wsc.bridgestone/[Accessed 20 February 2016].

Youwheel, 2016. *Car Body Torsional Rigidity - A Comprehensive List.* [Online] Available at: http://blogs.youwheel.com/2014/04/25/car-body-torsional-rigidity-a-comprehensive-list/ [Accessed 28 June 2016].

APPENDIX A. Torsional Stiffness and Flexural Properties Sample Calculations

Torsional Stiffness Calculation

The overall chassis torsional stiffness, K_T, is given by equation 2.2, details of which are specified in section 2.4.2 and directly proportional to the product of the applied force, *F*, and the wheel track, *B*, and inversely proportional to the sum of the angular deflections of the driver, φ_d, and passenger, φ_p, wheels. The models in each simulation in Chapter 4 have the same wheel track and applied force. Details of the applied force magnitude are specified on section 3.5.

B = 1.3 m

F = 2000 N

$$K_T = \frac{T}{\varphi} = \frac{FB}{\varphi_p + \varphi_d} \tag{2.2}$$

The vertical deflection of the preliminary model, shown in Figure 4.6 in section 4.1.1, is converted to an angular deflection by equations 2.3 and 2.4 respectively. Since the chassis is longitudinally symmetrical the deflection of the driver and passenger front suspension ends are identical.

$v_d = v_p$ = 5.373 mm

$$\varphi_d = tan^{-1}\left(\frac{v_d}{B/_2}\right) \tag{2.3}$$

$$\varphi_d = tan^{-1}\left(\frac{5.37 \text{ x } 10^{-3}}{1.3/_2}\right)$$

$$\varphi_d = 0.4736\ deg$$

Similarly:

$$\varphi_p = tan^{-1}\left(\frac{v_p}{B/_2}\right) \tag{2.4}$$

$$\varphi_p = tan^{-1}\left(\frac{5.37 \text{ x } 10^{-3}}{1.3/_2}\right)$$

$$\varphi_p = 0.4736\ deg$$

The Torsional Stiffness, K_T, is given by:

$$K_T = \frac{(2000)(1.3)}{0.4736 + 0.4736}$$

$$\boldsymbol{K_T = 2745\ Nm/deg}$$

Flexural Properties Calculations

The peak load result for each specimen from the flexural bend tests was substituted into equation 5.1 to obtain the maximum flexural bending stress of each specimen. The sample calculation below uses the results from one of the specimens with three layers of reinforcement material on either side of a 10 mm foam core. The specimen span, *L*, width, *b*, and thickness, *h*, were measured for each specimen. The peak load, *P*, and the midspan deflection, δ, were recorded from the results of the flexural bending test.

P = 862.3 N

L = 186.40 mm

b = 40 mm

h = 11.65 mm

δ = 5.735 mm

The maximum flexural bending stress is given by the result of substituting the above values into equation 5.1.

$$\sigma = \frac{3PL}{2bh^2} \tag{5.1}$$

$$\sigma = \frac{3(862.3)(186.40)}{2(40)(11.65)^2}$$

$$\boldsymbol{\sigma = 44.41\ MPa}$$

The maximum strain at the outer surface occurs at the midspan and is calculated by equation 5.2. The flexural chord modulus of elasticity is the ratio of the change in flexural bending stress, σ, to the change in strain, ε, between two points on the stress-strain curve, and is given by equation 5.3.

$$\varepsilon = \frac{6\delta h}{L^2} \tag{5.2}$$

$$\varepsilon = \frac{6(5.735)(11.65)}{(186.40)^2}$$

$$\boldsymbol{\varepsilon = 0.01154}$$

$$E_f^{chord} = \frac{\delta\sigma}{\delta\varepsilon} \tag{5.3}$$

$$E_f^{chord} = \frac{44.41}{0.01154}$$

$$\boldsymbol{E_f^{chord} = 3848.40\ MPa}$$

APPENDIX B. Flexural Bending Test Specimen Preparation and Testing Procedure

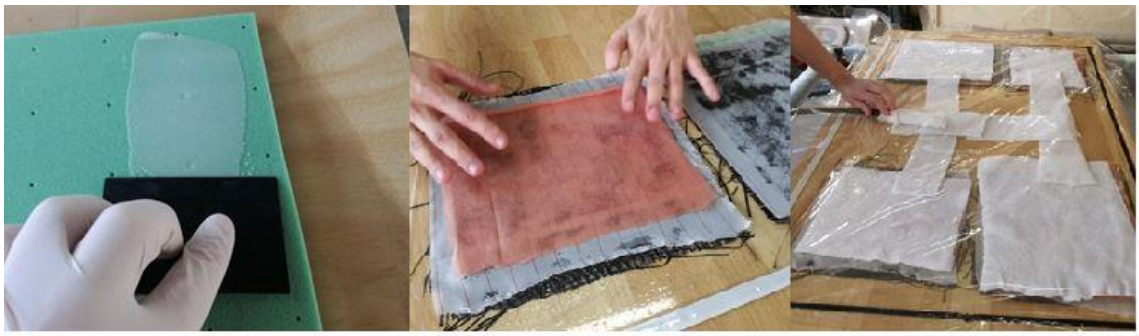

Figure B.1: Test specimen preparation

The testing procedure was as follows:

1. Prepare a minimum of 5 test specimens for each test condition, using the thickness of the specimens to set the span of the testing apparatus using the span to thickness ratio of 16:1.
2. Align the loading nose and supports such that the axes of the cylindrical surfaces are parallel, positioning the loading nose midway between the supports.
3. Apply the force to the specimen at the specified crosshead rate. Measure and record the force and deflection magnitudes at a rate such that a minimum of 50 data points comprises the force deflection curve.
4. To obtain valid flexural strength data it is necessary that the specimen fails at either of its outer surfaces, without succumbing to shear failure or crushing failure under a support or loading nose. Surface failure may be a crack on the surface loaded in tension or local buckling on the surface loaded in compression. Record the failure mode, region, and location of failure for each specimen.